1 2  9 0

UNIVERSIDADE D
COIMBRA

Mariana Fragata Miranda

Characterisation of Natural Killer T cell phenotype and function in alfa-Galactosidase A Deficiency

Dissertação no âmbito do Mestrado em Investigação Biomédica, no ramo de Infeção e Imunidade, orientada pela Professora Doutora Maria de Fátima Matos Almeida Henriques de Macedo e coorientada pela Professora Doutora Teresa Maria Fonseca Oliveira Gonçalves, e apresentada à Faculdade de Medicina da Universidade de Coimbra.

Setembro de 2023

Faculdade de Medicina da Universidade de Coimbra

Characterisation of Natural Killer T cell phenotype and function in alfa-Galactosidase A Deficiency

Mariana Fragata Miranda

Dissertação no âmbito do Mestrado em Investigação Biomédica, no ramo de Infeção e Imunidade, orientada pela Professora Doutora Maria de Fátima Matos Almeida Henriques de Macedo e coorientada pela Professora Doutora Teresa Maria Fonseca Oliveira Gonçalves, e apresentada à Faculdade de Medicina da Universidade de Coimbra.

Setembro de 2023

Esta tese é dedicada a ti, Zezinho.

Obrigada por toda a força que me deste, mesmo quando já não estavas cá.

És a estrela mais brilhante que existe no céu.

Da tua donzela, obrigada por me fazeres sempre rir.

<3

Agradecimentos

Este ano foi sem dúvida difícil, com muitos altos e baixos, não só a nível académico, mas também a nível pessoal. Mas não seria possível chegar aqui sem algumas pessoas, que me ajudaram e acreditaram que eu conseguia. Algumas delas fizeram, sem dúvida, com que eu nunca desistisse. Assim, não poderia deixar de agradecer:

À minha orientadora, Fátima Macedo, pela confiança depositada em mim ao me ter aceite para integrar este projeto e por me fazer aprender a valorizar o meu trabalho.

À minha coorientadora, Prof. Teresa Gonçalves que aceitou, sem hesitação, desempenhar este papel. Obrigada por todo o apoio e ensinamentos durante as aulas.

Ao meu coordenador de mestrado, Prof. Henrique Girão, por todo o apoio e ajuda. Obrigada por todos os ensinamentos, tanto teóricos, como da vida. É uma pessoa especial e que irá ficar para sempre comigo.

À Inês Mondragão por toda a paciência e disponibilidade e por todos os desabafos. Um especial obrigada à Sofia Borges, por me ter acompanhado, ajudado e ensinado na fase inicial. Aos restantes membros do CAGE, em especial à Liliana e à Carolina, pela companhia, disponibilidade e por todas as conversas terapêuticas, que eu bem precisava. A todas as pessoas do Lab 120, em especial à Diana, Lua e Xaninha, por toda ajuda durante este ano (salvaram-me muitas vezes, meninas!) e ao Bruno miguxo por todos os cafezinhos e por me tentar meter um pouco de juízo na cabeça. À D. Teresa por melhorar sempre o meu dia com a sua alegria.

À Catarina Meireles e à Emília Cardoso, da Plataforma de Citometria Translacional (TraCy) do i3S, pela formação e auxílio na utilização dos citómetros. Obrigada por todo o apoio necessário durante este ano, sem vocês não teria sido possível.

À Gabriela M. Almeida, da Unidade de Proteção de Dados do i3S, por toda ajuda no preenchimento dos documentos a submeter à Proteção de Dados do Centro Hospitalar Universitário de São João (CHUSJ). Ao Prof. João Paulo Oliveira, médico e investigador do CHUSJ, envolvido no recrutamento de doentes Fabry para este projeto. Ao Departamento de Imunohemoterapia do CHUSJ e aos seus dadores, pelo fornecimento de Buffy Coats. Ao National Institute of Health Tetramer Core Facility (NIH, USA), por ceder os tetrâmeros CD1d-PBS57 e MR1 5-OP-RU.

À Fundação para a Ciência e a Tecnologia (FCT), I.P., pelo financiamento deste trabalho no âmbito do projeto 2022.01788.PTDC.

E agora, o MAIOR OBRIGADA vai para as pessoas que estiveram lá sempre quando eu mais precisei, tanto presencialmente, como à distância de uma chamada:

À minha mãe, por fazer tudo por mim e por acreditar que eu vou sempre sempre dar o meu melhor. Ao meu pai, babado, que vai a tudo o que eu participo e me leva para todo o lado. Obrigada do fundo do coração. Ao meu Trident (AKA, irmão), por todas as risadas, por todos os olhares cúmplices, por me aturares mesmo quando estou mais resmungona (a verdade é que também és um chato). Nunca cresças. Obrigada a vocês os três, que me aturaram todos os dias durante este ano, que sei que também foi difícil para vocês.

Aos meus avós, por me apoiarem sempre e (mesmo às vezes não percebendo tão bem o meu trabalho), torcerem sempre por mim.

À minha madrinha, por todo o apoio que sempre me deu, por me fazer sempre pensar no lado positivo das coisas e por saber que posso sempre contar com ela.

Ao meu tio e João, por nunca duvidarem de mim e me fazerem sempre dar o meu melhor. Aos meus primos, Afonso e Zezinho, por todas as gargalhadas juntos e parvoíces que fazíamos com os avós.

Aos meus amigos, Miss, Tats, Diogo, Leninha, Rui, Rita(s), Bea, Johnny, Gabi, Rafa, por terem sempre um tempinho para mim, por estarem sempre lá para mim quando eu preciso, seja para dar gargalhadas, chorar, passear, comer (e beber eheheh).

ADORO-VOS.

A ti, husbando, (last but not least) sem dúvida que foste o meu grande pilar durante este ano (e sempre). Obrigada por me compreenderes e nunca me julgares. Obrigada por me apoiares, qualquer que seja a minha decisão. Obrigada por me ajudares a relaxar quando não sei como o fazer. You are my safe space. Amo-te.

Resumo

A doença de Fabry é uma doença lisossomal de sobrecarga, ligada ao cromossoma X, causada pela deficiência da enzima alfa-Galactosidase A (α-Gal A), que leva à acumulação do lípido globotriosilceramida (Gb3). A apresentação clínica da doença de Fabry é altamente heterogénea e está relacionada com a atividade da α-Gal A, sendo que os casos mais graves não apresentam atividade da enzima. Ainda não é possível prever a progressão da gravidade da doença e identificar quais os doentes que devem ser tratados e quando deve ser iniciado o tratamento. Foi demonstrado que o modelo de ratinho da doença de Fabry tem uma frequência reduzida de um tipo específico de células T, as células Natural Killer T invariantes (iNKT). Ao contrário das células T convencionais, as células iNKT são células T restritas a CD1d, com um TCR semi-invariante, que reconhece lípidos e produzem rapidamente citocinas quando estimuladas. O Gb3, entre outros lípidos, pode impedir a ativação das células iNKT. Em estudos anteriores feitos com humanos, não foram observadas alterações na percentagem de células iNKT em doentes com doença de Fabry atípica (início tardio) com a variante cardíaca, apesar de haver variação no subset de células iNKT $CD4^+$.

Apenas foram analisadas as células iNKT dos doentes de início tardio e existe heterogeneidade nesta doença. Para além disso, pouco se sabe sobre o fenótipo das células iNKT nestes doentes. Assim, este estudo teve como objetivos definir as condições experimentais, incluindo a definição dos marcadores e diversos painéis de citometria de fluxo para analisar o fenótipo e a função das células iNKT em doentes com doença de Fabry e caraterizar a frequência e o fenótipo das células iNKT nestes doentes, especialmente nos doentes com a apresentação clássica da doença (início precoce). A primeira tarefa consistiu em construir um painel de citometria de fluxo e definir/ otimizar as condições experimentais necessárias. As células iNKT foram identificadas utilizando anti-CD3 e um tetrâmero CD1d ligado a lípidos. O fenótipo celular foi estudado utilizando anti-CD4, anti-CD8α e anti-CD8β, bem como marcadores de ativação (ICOS) e exaustão (PD-1 e TIM-3). Foram feitas titulações para cada anticorpo/ reagente. Tentámos identificar uma subpopulação de células iNKT citotóxicas circulantes, recentemente descrita na literatura. Surpreendentemente, os resultados não foram reprodutíveis, uma vez que a população circulante não foi obtida, pondo em causa a existência desta população.

Após a validação das condições experimentais, foram analisadas células iNKT de quatro controlos saudáveis e de três doentes com doença de Fabry. Dois dos doentes apresentavam a variante clássica da doença, enquanto o terceiro doente apresentava a variante cardíaca de início tardio. Foi analisada a frequência de diferentes populações de leucócitos, subsets de células iNKT e o fenótipo das células iNKT de doentes com doença de Fabry, incluindo a expressão dos dímeros CD8, CD8αα e CD8αβ, nas células iNKT. As análises foram sempre comparadas com as células T convencionais ($CD3^+$). Nos doentes observou-se uma tendência para um aumento da percentagem de monócitos em relação aos indivíduos saudáveis, embora não fosse estatisticamente significativa. Esta alteração está de acordo com a literatura. Surpreendentemente, não foram observadas variações entre doentes e controlos no que diz respeito às percentagens de células B e T. No entanto, foram observadas diferenças na percentagem de leucócitos entre o doente Fabry em tratamento e os não tratados. Tal como esperado, a frequência de células iNKT não apresentou variação estatisticamente significativa entre os doentes e controlos. Embora não tenham sido observadas diferenças estatisticamente significativas entre os subsets CD4 e CD8 de iNKT dos controlos e dos doentes, os doentes Fabry apresentavam uma tendência para a redução

do subset $CD8^+$ iNKT, assim como para o aumento do subset DN iNKT. Os dadores saudáveis e os doentes Fabry não apresentaram qualquer variação relativamente aos dímeros CD8 das células iNKT. No entanto, foi observado que, em ambos os grupos, mais de 90% das células iNKT expressam CD8αα, enquanto mais de 82% das células $CD3^+$ expressam CD8αβ. Não há muita informação disponível sobre a expressão destes dímeros nas células iNKT, embora a expressão mais elevada de CD8αα nas células iNKT também tenha sido obtida em quatro indivíduos saudáveis num estudo anterior. Relativamente ao fenótipo das células iNKT, os doentes Fabry apresentaram uma tendência para expressar mais PD-1 (63,8 ± 17,2 %) em comparação com os controlos (41,2 ± 24,6 %), mas esta diferença não foi estatisticamente significativa. Esta tendência também foi observada na expressão de ICOS, apesar de não ser estatisticamente significativa. A expressão de CD161 e TIM-3 nas células iNKT não apresentou diferenças entre os controlos e os doentes Fabry. No geral, não foram observadas diferenças significativas entre os doentes Fabry com diferentes fenótipos da doença. Com este estudo, foram definidas as condições necessárias para estudar as células iNKT. Devido ao número reduzido de doentes com doença de Fabry e de controlos saudáveis analisados, ainda não é possível concluir acerca das diferenças na percentagem de leucócitos, incluindo as células iNKT, e no fenótipo das células iNKT nos doentes Fabry.

Palavras-Chave: Doença de Fabry; Células Natural Killer T invariantes; Citometria de fluxo; Doenças Lisossomais de Sobrecarga; Biomarcadores

Abstract

Fabry disease is an X-linked lysosomal storage disease caused by deficiency of the enzyme alpha-Galactosidase A (α-Gal A) which leads to the accumulation of the lipid globotriosylceramide (Gb3). The clinical outcome of Fabry disease is highly heterogeneous and it is related to the α-Gal A activity, with more severe cases presenting no activity. An unmet need for this condition is to predict the progression of disease severity and to identify which patients should be treated and when treatment should start. It was demonstrated that the mouse model of Fabry disease has a reduced frequency of a specific type of T cells, the invariant Natural Killer T (iNKT) cells. Contrary to conventional T cells, iNKT are CD1d-restricted T cells, with a semi-invariant TCR, that recognise lipids and rapidly produce cytokines when stimulated. Gb3, among other lipids, can prevent iNKT cell activation. In humans, previous studies have found no alterations in iNKT cell percentage in patients with late onset Fabry disease patients with the cardiac variant, despite alteration in the $CD4^+$ iNKT cell subset.

Only the late onset patients' iNKT cells have been analysed in the past and there is heterogeneity of this disease. Furthermore, little is known about iNKT cell phenotype in these patients. Hence, the aims of this study were to set up experimental conditions, including the definition of the markers and diverse flow cytometry panels to analyse the phenotype and function of iNKT cells in Fabry disease patients and to characterize iNKT cell frequency and phenotype in these patients, especially patients with the classical disease presentation. The first task was to construct a flow cytometry panel and define/optimise the required experimental conditions. iNKT cells were identified using anti-CD3 and a lipid loaded CD1d tetramer. Cell phenotype was unravelled by using anti-CD4, anti-CD8α and anti-CD8β as well as activation (ICOS) and exhaustion (PD-1 and TIM-3) markers. Titrations were done for each antibody/reagent. We attempted to identify a circulating cytotoxic iNKT cell subpopulation, recently described in the literature. Surprisingly, the results were not reproducible since the circulating population was not obtained, questioning the existence of this population.

After validation of the experimental set up, iNKT cells from four healthy controls and three Fabry disease patients were studied. Two of the patients presented the classical variant of the disease whereas the other presented the late onset cardiac variant. The frequency of different leukocyte populations, iNKT cell subsets and iNKT cell phenotype of Fabry disease patients were analysed, including the expression of CD8 dimers CD8αα and CD8αβ in iNKT cells. The analyses were always compared to conventional T cells ($CD3^+$). Patients presented a tendency to have a higher percentage of monocytes compared to healthy subjects, although not statistically significant. This alteration is in accordance with the literature. Surprisingly, no variations were observed between patients and controls regarding B cell and T cell percentages. On the other hand, differences regarding the leukocyte percentage were observed between the treated Fabry disease patient and non-treated patients. As expected, iNKT cell frequency showed no statistical variation between the two groups. Although no statistically significant differences were observed between controls and patients' CD4 and CD8 iNKT subsets, a reduction in the Fabry disease patients' $CD8^+$ iNKT subset, as well as a bias towards the increase of DN iNKT subset were observed. Healthy donors and Fabry disease patients presented no variation regarding iNKT cells CD8 dimers. However, it was observed that in both groups more than 90% of iNKT cells express CD8αα whereas more than 82% of $CD3^+$ cells express CD8αβ. Little is known about the expression of these dimers in iNKT cells, albeit the higher expression of CD8αα in iNKT cells was also obtained in in four

healthy subjects from a previous study. Regarding iNKT cell phenotype, Fabry disease patients' iNKT cells presented a tendency to express more PD-1 (63.8 ± 17.2 %) compared to controls (41.2 ± 24.6 %) but it wasn't statistically significative. This tendency was also observed in ICOS expression, in spite of not being statistically significative. CD161 and TIM-3 expression in iNKT cells presented no differences between controls and Fabry disease patients. Overall, no significant differences were observed among the Fabry disease patients presenting different disease phenotypes. With this study, the necessary conditions to study iNKT cells were defined. Due to the low number of Fabry disease patients and healthy controls analysed, it is still early to conclude about differences in leukocyte percentage, including iNKT cells, and iNKT cell phenotype in Fabry disease patients.

Keywords: Fabry disease; Invariant Natural Killer T cells; Flow Cytometry; Lysosomal Storage Disease; Biomarkers

Table of contents

List of Figures

List of Tables

List of Abbreviations

5-OP-RU. *5-(2-oxopropylideneamino)-6-D-ribitylaminouracil*

6-FP. *6-formyl pterin*

AF. *Alexa Fluor*

AP. *Adaptor protein complex*

APC. *Allophycocyanin*

APCs. *Antigen presenting cells*

BB. *Brilliant Blue, Brilliant Blue*

BFA. *Brefeldin A*

BSA. *Bovine serum albumin*

BV. *Brilliant Violet*

CCR. *C-C chemokine receptor*

CD. *Cluster-of-differentiation*

CHUSJ. *Centro Hospitalar Universitário de São João*

CXCR. *C-X-C chemokine receptor*

Cy. *Cyanine*

DAMPs. *Damage-associated molecular patterns*

DN. *Double negative*

DP. *Double positive*

EDTA. *Ethylenediamine tetraacetic acid*

ER. *Endoplasmic reticulum*

ERT. *Enzyme Replacement Therapy*

FITC. *Fluorescein*

FMO. *Fluorescence Minus One*

FSC. *Forward scatter*

GalCer. *Galactosylceramide*

Gb3. *Globotriaosylceramide*

GLA. *Galactosidase Alpha*

GSL. *Glycosphingolipids*

HGMD. *Human Gene Mutation Database*

HIV. *Human immunodeficiency virus*

ICOS. *Inducible T-cell Costimulator*

iFBS. *inactivated Fetal Bovine Serum*

IFN-γ. *Interferon-gamma*

IL. *Interleukin*

iNKT cells. *invariant Natural Killer T cells*

$iNKT_{FH}$ cells. *Follicular helper invariant Natural Killer T cells*

KO. *Knock out*

LPT. Lipid transfer proteins

LSDs. *Lysosomal storage diseases*

lyso-Gb3. *Globotriaosylsphingosine*

MACS. *Magnetic-activated cell sorting*

MAIT cells. *Mucosal-associated Invariant T cells*

MFI. *Median Fluorescence Intensity*

MHC. *Major Histocompatibility Complex*

MR1. *MHC class I related-1 molecule*

MTP. *Microsomal triglyceride transfer protein*

NF-κB. *Nuclear factor kappa Beta*

NK cells. *Natural Killer cells*

NKT cells. *Natural Killer T cells*

PBMCs. *Peripheral blood mononuclear cells*

PBS. *Phosphate-buffered saline*

PBS-57. *α-GalCer analog*

PC. *Phosphatidylcholine*

PD-1. *Programmed Death Receptor-1*

PE. *Phycoerythrin*

PE-Cy5. *Phycoerythrin-Cy5*

PerCP. *Peridinin chlorophyll protein*

PerCP-Cy5.5. *Peridinin chlorophyll-Cy5.5*

PFA. *Paraformaldehyde*

PHA. *Phytohemagglutinin*

PI. *Phosphatidylinositol*

PLZF. *Promyelotic leukemia zinc finger*

PMA. *Phorbol myristate acetate*

PRRs. *Pattern recognition receptors*

RBC. *Red Blood Cells*

RT. *Room temperature*

r-α-Gal A. Recombinant α-galactosidase A

SD. *Standard Deviation*

SI. *Staining index*

SLs. *Sphingolipids*

SSC. *Side scatter*

TCR. *T cell receptor*

Th. *T helper*

TIM-3. *T-cell immunoglobulin mucin-3*

TLRs. *Toll-like receptors*

TNF-α. Tumor necrosis factor alpha

T_{reg} cells. *Regulatory T cells*

TSH. Thyroid stimulating hormone

α-Gal A. *α-Galactosidase A*

α-GalCer. *α-galactosylceramide*

β_2M. *β2-microglobulin*

1. The lysosome

The lysosome, discovered in 1955 by De Duve et al., is an acidic membrane-bound organelle often described as the recycling compartment of the cell[1]. It is the major intracellular site of enzymatic degradation for most macromolecules due to containing a wide range of acid hydrolases[2–4].

The lysosomal hydrolases are only capable to function as a result of the acidic pH of the lysosome, which is maintained through the action of an H^+-ATPase, which pumps protons to the lysosome[5].

Macromolecular substrates are delivered differently to the lysosome depending on their origin: 1) Extracellular substrates are delivered through the fusion of the lysosome with late endosomes, via the endocytic pathway; 2) Intracellular substrates are transported by the fusion of autophagosomes with lysosomes, via the autophagic pathway[6–8]. Besides late endosomes and autophagosomes, lysosomes are also able to fuse with the plasma membrane, making it possible to secrete lysosomal content and translocate components of the lysosomal membrane to the plasma membrane (**Figure 1**)[7,9].

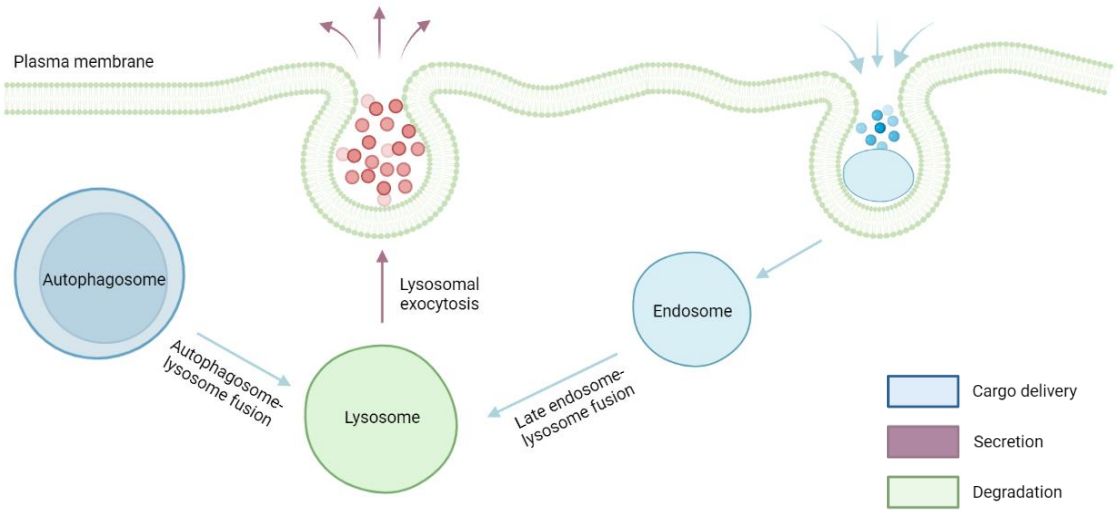

Figure 1. The lysosome and cellular clearance. The figure illustrates the three main aspects involved in lysosome-mediated cellular clearance: cargo targeting to lysosomes, substrate degradation, and secretion. Extracellular substrates are delivered through the fusion of the lysosome with late endosomes, via the endocytic pathway (cargo delivery). Intracellular substrates are transported by the fusion of autophagosomes with lysosomes, via the autophagic pathway (cargo delivery). Lysosomes are also able to fuse with the plasma membrane, making it possible to secrete lysosomal content and translocate components of the lysosomal membrane to the plasma membrane (secretion). Different colours represent the different processes: blue (cargo delivery), dark pink (secretion) and green (degradation). This figure was created with *BioRender.com*.

Lysosomes are not only a catabolic organelle, but they are also involved in vital cellular functions, such as vesicle trafficking, signalling, nutrient sensing, cellular growth, plasma membrane repair, cholesterol homeostasis, and cell death[5,7,10]. Notably, the lysosome plays a key role in antigen presentation (particularly through antigen processing) and phagocytosis[5,11]. Thus, this organelle is essential for the maintenance of cellular homeostasis.

1.1 Lysosomal storage diseases

Lysosome disfunction can result in impaired lysosomal degradation of macromolecules and consequent accumulation of storage material, which is the hallmark of lysosomal storage diseases (LSDs). These disorders constitute a heterogeneous group of metabolic disorders.

LSDs can occur due to mutations in genes encoding lysosomal hydrolases and proteins responsible for vesicular trafficking, lipid transportation and lysosomal biogenesis. These defects can result in the disruption of the lysosomal function, leading to accumulation of non-degraded substrates in lysosomes and endosomes. As a consequence, the lysosomal homeostasis is disturbed which has important implications in protein degradation, autophagy and metabolic stress[12]. The progressive build-up of substrates within the lysosome ultimately leads to impaired cellular and organ function. As a consequence, LSDs typically aggravate over time and often result in premature mortality[2,5,13].

LSDs are commonly classified based on the accumulated material type. The main categories include sphingolipidoses (accumulation of sphingolipids), mucopolysaccharidoses (accumulation of glycosaminoglycans), mucolipidoses (accumulation of glycolipids, glycosaminoglycans, and oligosaccharides) and glycoproteinoses (accumulation of glycoproteins)[4,5]. Patients with LSDs exhibit diverse clinical presentations, often presenting as a multisystemic disease with notable neurological involvement[12]. While there may be certain resemblances in the clinical phenotype among various lysosomal storage disorders, it is important to note that no two disorders share identical pathophysiology[2].

LSDs comprise over 70 diseases and, although individually rare, they have a collective incidence of 1 in 5,000 live births[2,13–15]. In the last study done regarding the Portuguese

population, this particular category of inborn errors of metabolism was observed to have a relatively higher overall prevalence rate, estimated to be 25 cases per 100,000 live births. Among these, the sphingolipidoses subclass is the most prevalent, followed by the mucopolysaccharidoses[16].

Available treatment strategies mitigate symptom severity and slow down disease progression rather than offer a complete cure. Enzyme replacement therapy is the standard therapeutic approach for the treatment of LSDs. Other therapies encompassing substrate reduction therapy, hematopoietic stem cell transplantation, gene therapy and use of molecular chaperones are used in few LSDs or are under clinical trials/ development[17,18].

Sphingolipids (SLs), which are crucial constituents of membranes and perform important functions in various signalling pathways, are involved in the pathology of several neurological and immune diseases[19,20]. Depending on the head groups, sphingolipids can be classified into phosphosphingolipids [e.g., sphingomyelin which is present in the myelin sheath that surrounds the axonal regions of neural cells] and glycosphingolipids (GSLs), which are more complex and possess ceramide molecules modified by the addition of sugar head groups[21]. Most SLs are catabolized in the lysosome through a single pathway, meaning that a deficiency in one of the proteins or enzymes involved lysosomal degradation will lead to the accumulation of SLs[22].

Most of the first described LSDs were sphingolipidoses, which include Fabry, Niemann-Pick, Gaucher, Tay-Sachs and Sandhoff diseases[4]. This type of LSDs is usually characterized by the accumulation of GSLs. Galactosylceramide (GalCer) and glucosylceramide (GlcCer) are the simplest GSLs, being GlcCer the most common and the precursor of the more complex GSLs[23,24]. Numerous diseases result from abnormalities in GSLs catabolism[22,25]. The enzymatic defects responsible for the various sphingolipidoses and the major SL(s) that accumulate, as well as the mutated genes, are described in **Table 1**[25].

Table 1. Sphingolipidoses: defective enzyme, mutated gene and major accumulating SL(s).

	Disease	Defective enzyme	Mutated gene	Major accumulating SL(s)
	GM1-Gangliosidosis	β-galactosidase	GLB1	GM1 ganglioside
GM2-Gangliosidosis	Tay-Sachs disease	β-hexosaminidase A	HEXA	GM2 ganglioside and lyso-GM2
	Sandhoff disease	β-hexosaminidase A and B	GM2A	GM2 gangliosideand GA2 ganglioside
	Fabry disease	α-galactosidase A	GLA	Globotriaosylceramide (Gb3) and globotriaosylsphingosine (lyso-Gb3, deacylated form)
	Metachromatic Leukodystrophy	Arylsulfatase A	ASA	Sulfatide
	Krabbe disease	Galactosylceramidase	GALC	Psychosine
	Gaucher disease	Glucosylceramidase	GBA1	Glucocerebroside and glucosylsphingosine
	Niemann-Pick disease types A and B	Sphingomyelinase	SMPD1	Shingomyelin
	Farber disease	Ceramidase	ASAH1	Ceramide

The sphingolipidosis Fabry disease is one of the main characters of this study, which is presented in the following section.

1.1.1 Fabry Disease

Fabry disease was first described in 1989 by William Anderson (surgeon) and Johannes Fabry (dermatologist) as an association of "*angiokeratoma corporis diffusum*" (skin lesions) with the risk of developing renal failure[26,27]. Also known as Anderson-Fabry disease or α-Galactosidase A (α-Gal A) deficiency, it is the second most common disorder among all LSDs [OMIM number: 301500][28,29].

α-Gal A deficiency is an inherited X-linked genetic disorder, caused by mutations in the Galactosidase Alpha (GLA) gene. The GLA gene, localized in a region of the long arm of the X chromosome (Xq22), is responsible for the production of the lysosomal hydrolase α-Gal A which is involved in the catabolism of glycosphingolipids. Due to mutations in the GLA gene, there is a deficiency in the activity of α-Gal A, leading to accumulation of the lipid globotriaosylceramide (Gb3), although other lipids, as globotriaosylsphingosine (lyso-Gb3, deacylated form), are also detected[30,31].

Subsequent accumulation of Gb3 and other glycosphingolipids occurs in lysosomes of deficient cells and body fluids. The deposits of lipids occur more prominently in the lysosomes of endothelial, perithelial, and smooth muscle cells found in blood vessels. Additionally, deposition occurs in ganglion cells as well as in various cell types in the heart, kidneys, eyes, and other tissues throughout the body[30,32].

Φ Clinical Manifestations and Frequency

There are two main variants of Fabry disease, depending on the onset of the disease and α-Gal A activity of the patient: the classic form, also called the "severe" or early-onset form, and the late-onset form[32]. The rate of progression of Fabry disease depends on the level of residual enzymatic activity, i.e. a lower α-Gal A activity corresponds to an earlier disease manifestation and a faster development[28].

Patients with the classic form of the disease have no residual α-Gal A activity and symptoms are often detected in childhood or adolescence (early-onset). The symptoms observed in childhood are not specific: pain in the extremities (acroparesthesias), unexplained fever, decreased sweating (hypohidrosis), and gastrointestinal issues. This makes it hard to diagnose the disease in this phase[32]. More distinct symptoms appear during late adolescence, including skin lesions (angiokeratoma) and corneal opacity[32]. Later in life, around 30-50 years old, renal and cardiac complications emerge, which results in a reduced life expectancy[32]. Cardiac involvement in Fabry disease can present as hypertrophic cardiomyopathy, valvular disease, conduction abnormalities, and arrhythmias[30,32]. Besides this, cerebrovascular problems also arise in Fabry disease patients[32]. The quality of life of these patients is significantly impacted by acroparesthesias (chronic or episodic pain of varying duration), a neuropathy affecting

small nerve fibres, which also contributes to reduced sensitivity to temperature and heat pain. These skin lesions result from vascular dysfunction and tend to increase in number and size over time[30,32]. Gastrointestinal manifestations primarily manifest as diarrhea and abdominal pain. Respiratory problems, bone deformities, lymphadenopathy, anemia, and delayed growth are also reported manifestations[32].

On the other hand, late-onset Fabry disease patients present variants of the disease in which angiokeratoma, corneal opacities, and acroparesthesias are not exhibited. As the name suggests, these variants manifest later in life, like the cardiac variant with isolated cardiac dysfunction and cases where only the kidneys are affected[30]. In these cases, there is typically a significant residual activity of α-Gal A enzyme[30].

Nonetheless, the impact of the disease can differ between women and men, because the condition is inherited in an X-linked manner, meaning that men only have one copy of the X chromosome, while women have two copies[30]. Men inherit the disease when they receive the affected X chromosome from their mothers, being the clinical manifestation related to the variant they possess[30]. Although Fabry disease used to be referred to as an X-linked recessive disorder, Wang et al. (2007) reported that women with Fabry disease who are heterozygous (only one X chromosome carries the GLA gene mutation) experience severe life-threatening conditions that require medical intervention and treatment[33]. Consequently, referring to these women as carriers undermines the gravity of the disease in this group of patients[30,32–34]. Albeit little is known about the impact of Fabry disease in pregnancy, it has been reported that there are increased pregnancy complications in Fabry disease women when compared to the general population of women[35,36].

In summary, Fabry disease patients, depending on the variant, can suffer from a multisystem disease, experiencing progressive renal insufficiency, requiring dialysis, along with cardiomyopathy that can lead to potentially life-threatening cardiac arrhythmias. Gastrointestinal pain, recurrent strokes and neuropathic pain in the extremities are also common symptoms, sometimes leading to Fabry crises (**Figure 2**)[37,38]. However, women tend to have more variable clinical manifestations of Fabry disease than men, due to the random inactivation of one of the X chromosomes in each cell during early embryogenesis[39].

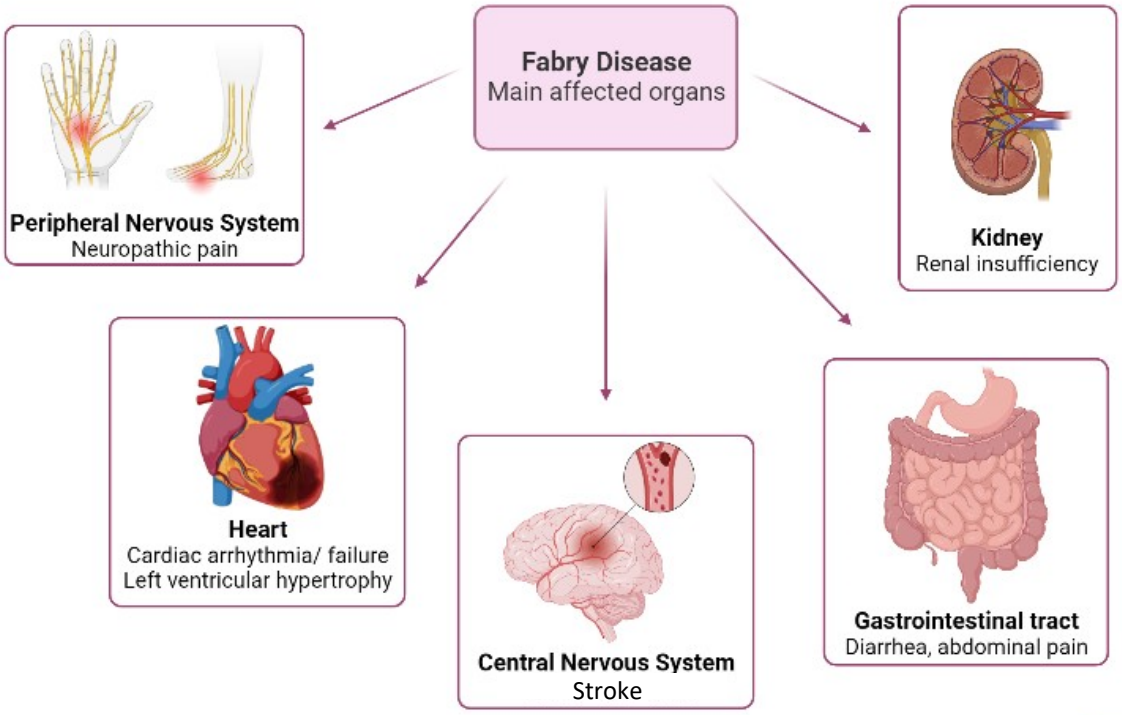

Figure 2. Fabry disease is a multisystemic disease. Main affected organs by Fabry disease are represented: heart, kidney, nervous system (peripheral and central), gastrointestinal tract. This figure was created with *BioRender.com*.

Anderson-Fabry disease is a pan-ethnic disorder and, since it is a rare and an under-diagnosed condition, it is difficult to determine an accurate disease frequency[32,37]. Fabry disease affects both men and women, occurring in approximately 1 in 40 000 to 1 in 117 000 individuals, even though higher incidences have been reported in males[37]. The prevalence of this LSD in white male populations possesses a wide range, approximately 1 in 17 000 to 1 in 117 000. Around 1 in 22 000 to 1 in 40,000 males present classic Fabry disease mutations whereas 1 in 1000 to 1 in 3000 males show atypical presentation. Atypical variants in females have an incidence of 1 in 6000 to 1 in 40 000[37,40].

Φ Diagnosis and Treatment

Angiokeratoma and corneal dystrophy usually lead to the clinical suspicion of Fabry disease, especially when there are Fabry disease patients in the family[30]. The diagnosis of the disease is made by resorting to biochemical and genetic tests. Men and women are evaluated differently when it comes to diagnosing Fabry disease, but genetic confirmatory

testing is mandatory in both[41]. In males, the diagnostic is based on the evaluation of α-Gal A activity in the circulating leukocytes, which is very low or absent in classical phenotype (α-Gal A activity < 1% suggests a diagnosis of classical Fabry disease)[32,37,41]. However, in the case of an invariant phenotype , the values of α-Gal A activity can be less than 25–30% of the mean normal level[42]. In these cases, the specific mutation responsible for the disease needs to be investigated through molecular diagnosis[30]. Due to X-chromosome random inactivation, women often present α-Gal A activities within the normal range, making the biochemical diagnosis inadequate for ruling out the presence of Fabry disease in females[32,37]. Consequently, the molecular diagnosis becomes crucial in identifying female Fabry disease patients. The molecular diagnosis is done by gene sequencing, allowing for the identification of a specific mutation in the GLA gene[32,37,43].

According to the *Human Gene Mutation Database* (HGMD), there are 980 mutations recorded for the GLA gene causing α-Gal A deficiency (accessed 7th July 2023). Diagnosing and treating certain cases of Fabry disease becomes challenging due to the presence of genetic variants with unknown significance and newly identified mutations[44]. However, most patients carry family-specific ("private") mutations, due to X-linked inheritance[37]. Studies on sequence conservation are being undertaken to identify the key residues for protein function, so that it is possible to establish a correlation between genotype and phenotype in Fabry disease[45].

The current treatment options approved for Fabry disease are the enzyme replacement therapy (ERT) with recombinant α-galactosidase A (r-α-Gal A), available for medical use since 2001, and the chaperone migalastat, which was recently approved[46–48].

ERT is a burdensome lifelong intravenous treatment given every 2 weeks with recombinant enzymes available: agalsidase-alfa (0.2 mg/kg body weight) or agalsidase-beta (1 mg/kg body weight)[37]. There are differences in the glycosylation pattern but it has been shown that both enzymes have similar efficiency[49,50]. In spite of existing an extensive literature published about ERT, there are still many unresolved issues, such as the best timing to initiate therapy, the optimal dose and the clinical implications of using anti-drug antibodies[47]. It is known that this therapy with r-α-Gal A may slow down the disease progression, but most patients still develop cardiac, renal, and cerebral complications.

Chaperone therapy with migalastat is administered orally (123 mg every other day) in Fabry disease patients with migalastat-amenable (responsive to migalastat) GLA mutations (i.e., GLA variants that despite abnormal folding, still possess some catalytic activity). Migalastat binds to the active site of α-Gal A, correcting its misfolding and facilitating the traffic to the lysosome[37,51]. Although an improvement of cardiac problems is observed and renal function remains stable, different amenable-mutations may have diverse clinical outcomes of the treatment, making it ineffective for some patients[51]. Furthermore, it still remains unclear if this chaperone therapy should be used in obese Fabry disease patients as it's dose is independent of the weight[37,51].

ERT and migalastat may lead to an improvement of the disease burden, enabling cellular clearance of Gb3, by exogenous administration of the enzyme or its stabilization with a chaperone, respectively[37]. However, they are not able to fully revert Fabry disease pathology and its clinical manifestations[31].

Unfortunately, women with Fabry disease, despite manifestations of the disease, are often left untreated, even though it is important to have an early initiation of therapy for it to be successful in both males and females[37,52].

ERT and chaperone therapy cost thousands of euros/ year per patient, making it a health economic burden, since it generally is a lifelong therapy. Besides this, there's a need for the development of criteria that consider the therapy initiation as well as its discontinuation[37]. As a result, there are currently new treatments in (pre)clinical trials assessing the efficacy of second-generation enzyme replacement therapies (Pegunigalsidase-alfa, Moss-aGal), substrate reduction therapies (Venglustat and Lucerastat), as well as mRNA- and gene-based therapies[46].

2. The immune system in Fabry Disease

Lysosomes are involved in several immune processes, such as phagocytosis, antigen processing and presentation by antigen presenting cells (APCs), secretion of perforins by cytotoxic T cells, and release of pro-inflammatory mediators by mast cells. Consequently, the immune system is dysregulated by diseases where the function of the lysosome is affected[53–55]. In fact, the presence of unmetabolized glycolipids in lysosomes triggers the activation of harmful cascades, particularly those related to inflammation. This can be

explained due to the fact that lysosomal deposits may act as damage-associated molecular patterns (DAMPs; i.e., molecules of endogenous origin released by injured or dying cells that are recognized by pattern recognition receptors (PRRs) on immune cells, such as toll-like receptors (TLRs), triggering an inflammatory response) or induce the production of DAMPs by injured cells, leading to subsequent pro-inflammatory activity[56]. In LSDs, since the stimulus, i.e. accumulated substrates in the lysosome, cannot be eliminated, the inflammatory response is constantly being activated, becoming a chronic process[53].

Fabry disease is characterised by the accumulation of Gb3 in several organs, which may trigger the dysregulation observed in innate immunity in Fabry disease, inducing over secretion of pro-inflammatory cytokines [30,57]. For instance, Biancini et al. have reported that the high levels of urinary Gb3 correlate with the increased plasma interleukin-6 (IL-6) levels[58]. Furthermore, it has been demonstrated that peripheral blood mononuclear cells (PBMCs) present significantly increased production of pro-inflammatory cytokines [e.g., interferon-gamma (IFN-γ), tumor necrosis factor alpha (TNF-α), IL-6 and IL-1β] in patients with α-Gal A deficiency[58–60].

Chronic inflammation causes organ damage, emphasizing the need for enzyme replacement therapy early in patients' lives. Renal and heart fibrosis (i.e. excessive growth, hardening, and scarring of different tissues, caused by the accumulation of extracellular matrix components, consequence of chronic inflammatory reactions[61]), as well as organ deformation and oxidative stress, have been described in Fabry disease patients[53,62–65]. A study demonstrated that lyso-Gb3 is able to induce inflammatory response, by activating the NOTCH1 signalling pathway (NOTCH1 is a cell-surface receptor whose pathway influences cell fate[66]), which activates the nuclear factor kappa Beta (NF-κB) pathway[67]. This leads to the production of pro-inflammatory cytokines, subsequently inducing local and systemic inflammatory responses[67,68]. Besides this, De Francesco et al. demonstrated that blockade of TLR4 prevents the Gb3-mediated cytokine production[60]. Nitta et al. showed that TLR4 is positively regulated by Gb3[69]. Together these studies suggest that Gb3 may bind to TLR4, playing a role in organ inflammation and damage[54,70]. Fabry disease has also been associated with disturbances in leukocytes and excessive expression of immune molecules[29,71,72].

Martinez et al. showed that 57% of the Fabry patients studied possessed reactivity to at least one autoantigen, being anti-phospholipid autoantibodies detected in 45% of them[73].

Some studies also described overt thyroid disease [abnormal levels of both thyroid stimulating hormone (TSH) and thyroid hormone] in Fabry disease patients[74–76].

Since ERT consists of infused recombinant proteins, humoral response, including anti-drug antibodies, develops in Fabry disease patients: males with the classical disease have higher risk of developing this response, enhancing disease progression and worsening clinical outcome[77].

In summary, the immune system is dysregulated in Fabry disease, being chronic inflammation the main disturbance, and there are even correlations between autoimmune diseases and this LSD. The accumulation of lipids is the main cause for this dysregulation, since they can act as antigens and regulate immunity by activating lipid-reactive T cells[78]. Lipid antigens and lipid-reactive T cells are going to be described in the following sections.

2.1 Lipid antigen presentation

T lymphocytes, which are part of the adaptive immune response along with B lymphocytes, are known to recognise protein antigens that are bound to Major Histocompatibility Complex (MHC) class I or II molecules (i.e., MHC I molecules present to cluster-of-differentiation (CD) 8^+ T cells and MHC II to $CD4^+$ T cells) at the surface of APCs. This antigen exposure at the cell surface allows T cell receptor (TCR) engagement and subsequent T cell activation[79]. Nonetheless, in 1989, Porcelli et al. described a different type of T cells that weren't MHC-restricted, but CD1-restricted T cells[80]. Although the antigen of these cells wasn't identified at the time, in 1994, Beckman et al. were able to established that CD1-restricted T cells recognised lipids instead of peptide antigens[81]. In **Figure 3**, a comparative illustration of MHC- and CD1-restricted T cells is represented.

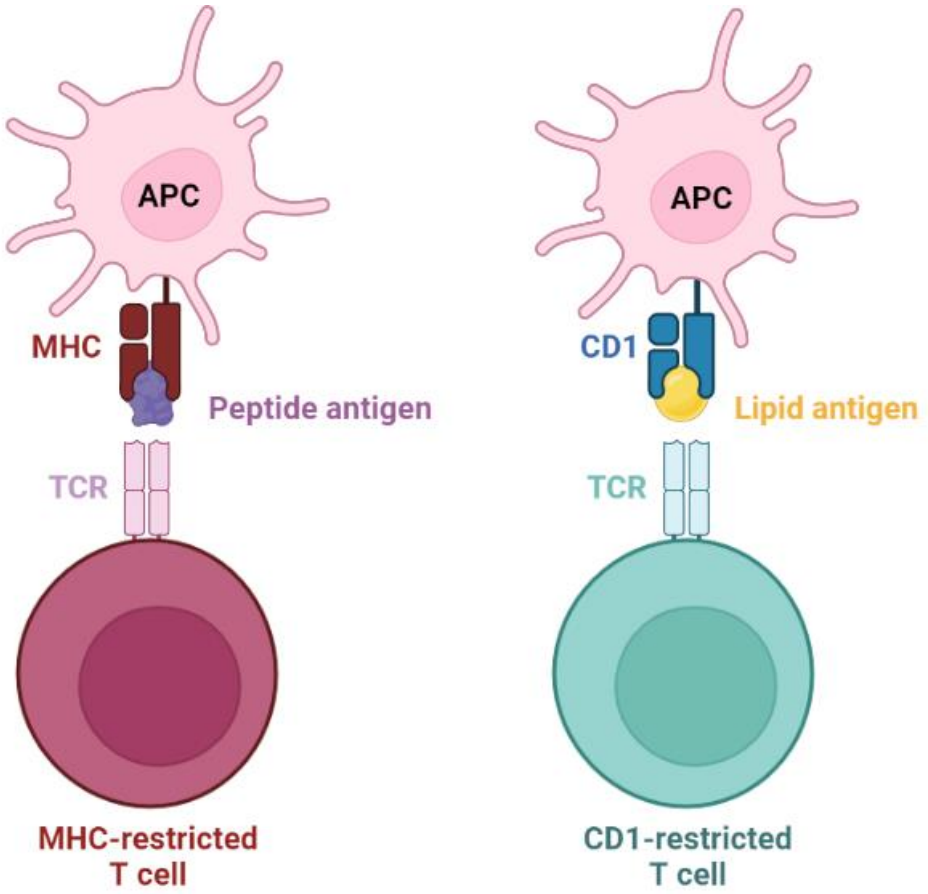

Figure 3. Mediated antigen presentation by MHC and CD1 to T cells. MHC molecules present peptide antigens (left) whereas CD1 molecules present lipid antigens (right) to T cells. This figure was created with *BioRender.com*.

Since then, many exogenous and endogenous lipids have been described as being recognised by CD1-restricted T cells[82].

2.1.1 CD1 molecules

CD1 molecules enable the recognition of lipids and glycolipids by T lymphocytes (**Figure 3- right**). The CD1 family are members of the non-classical MHC class I related proteins, which are not encoded by the MHC but are MHC-like molecules[83].

Φ CD1 expression

Human CD1 molecules were first described as being encoded in a locus on chromosome 1[84]. It is known that this chromosomal segment encodes five CD1 isoforms: CD1a, CD1b, CD1c, CD1d and CD1e[85]. Based on sequence homologies, the CD1 molecules can be

divided into three groups: group 1, containing CD1a, CD1b and CD1c, group 2, only consisting of CD1d, and group 3, only comprising CD1e[86,87]. Interestingly, mice lack group 1 CD1 genes and just possess one isoform (CD1d) which is codified by two genes in chromosome 3[88].

Group 1 CD1 molecules are predominantly expressed on thymocytes and professional APCs (i.e., dendritic cells and macrophages). Additionally, CD1a is found on Langerhans cells, and CD1c is expressed in a subset of B cells[86,89]. On the other hand, group 2 CD1 molecule, which contains the only CD1 isoform shared between humans and mice, presents a broader distribution, being present in hematopoietic and non-hematopoietic cells. CD1d is highly expressed by cortical thymocytes, but its expression is reduced in medullary thymocytes. In hematopoietic cells, the highest CD1d expression is usually observed in leukocytes such as monocytes, dendritic cells or B cells[90]. Circulating activated T cells also express CD1d[91]. Additionally, CD1d can be found in non-hematopoietic cells in various tissues, including the skin, liver, pancreas, endometrium, breast, kidney, testis, gut, bile duct epithelium, epididymis, and conjunctiva[86]. Studies have also unveiled the expression of CD1d in adipocytes, which determines the adipose tissue inflammation and insulin resistance in obesity[92–94].

Lastly, CD1e (group 3 CD1 molecule) is expressed on dendritic cells. CD1e molecules participate in lipid antigen presentation, but they don't interact with the TCR, due to their absence on the plasma membrane, contrary to group 1 and 2 CD1 molecules[95]. Instead, they serve as a lipid transfer proteins (LPT)[86,96]. By binding to lipids in lysosomes and facilitating the processing of complex glycolipids, it enhances the editing of lipid antigens: CD1e promotes lipid loading and unloading in CD1d, and influences lipid presentation by CD1b and CD1c[95].

Φ Structural features

All CD1 proteins consist of a heavy chain with three extracellular domains (α1, α2, and α3), a transmembrane domain, and an intracellular tail. The extracellular domains, α1 and α2, have two anti-parallel α-helices on the top of six β-strands[97]. The α3 domain interacts with the light chain, β2-microglobulin (β_2M), forming a heterodimer[97,98]. The first crystal structure of CD1 is represented in **Figure 4**[99].

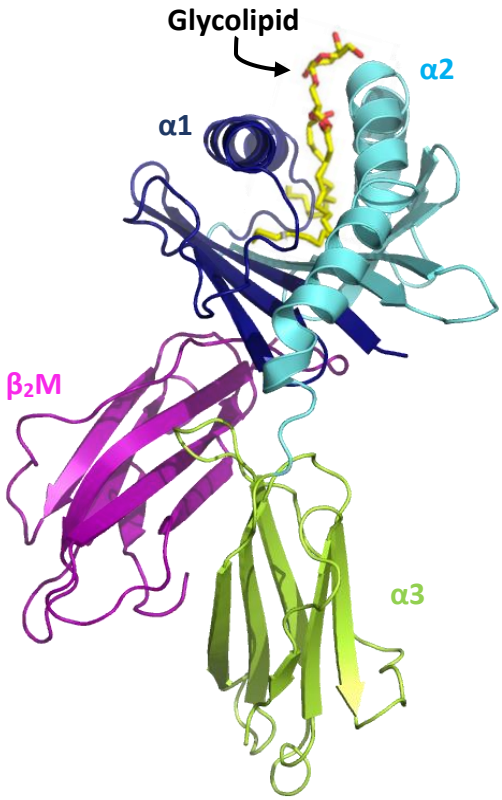

Figure 4. Mouse CD1 structure. CD1 heavy chain (α1-blue; α2- cyan; α3- lime green), β2M (magenta) and glycolipid (yellow) are represented. Structure extracted from PDB (PDB:1CD1). Obtained using PyMol program (The PyMOL Molecular Graphics System, Version 2.5.2, Schrödinger, LLC).

CD1 molecules possess structural similarities with MHC class I, including their association with β_2M, and exhibit functional traits akin to MHC class II molecules, such as their potential association and trafficking with the invariant chain[82,86,100,101].

On the other hand, their most outstanding difference from other MHC and MHC-like molecules lies in the composition of the groove where the antigen is presented: CD1 molecules groove is composed of hydrophobic residues that can exclusively accommodate lipid chains or highly hydrophobic amino acid side chains[99]. In CD1 molecules, the groove consists of two large pockets (A' and F'), except in humans' CD1b. In CD1b, there is an additional smaller C' pocket, between A' and F', as well as a T' tunnel located in front of the C' pocket. CD1 isoforms exhibit differences in the size, shape, and number of their pockets, enabling them to accommodate lipids with varying lengths of fatty acid chains (**Figure 5**)[102]. CD1a have the smallest groove, facilitating the binding of small lipids. CD1b is the isoform that is capable of binding larger lipids. CD1c and human CD1d possess intermediate binding grooves. CD1e possesses a larger groove[102–104]. These

differences in groove characteristics among the CD1 isoforms play a crucial role in the antigen-presenting function, allowing them to bind and present a wide variety of lipid antigens to T cells, thereby influencing immune responses[83,102].

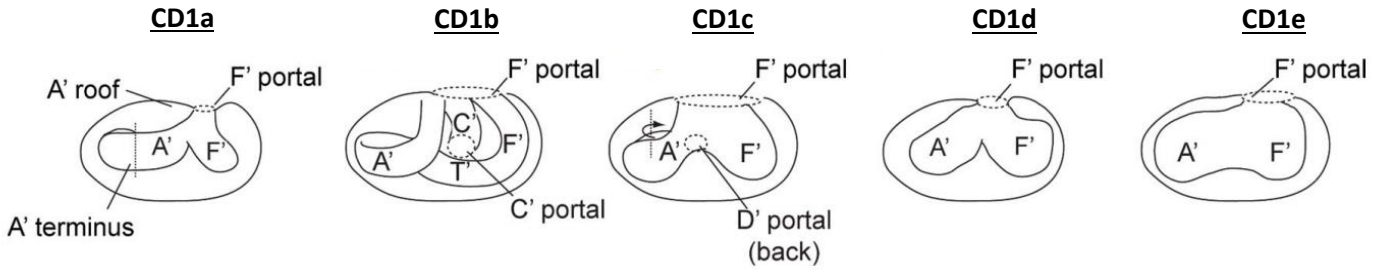

Figure 5. Representation of CD1 isoforms grooves. Each CD1 isoform possesses a distinct antigen-binding groove with unique capacities. The groove architecture among CD1 isoforms varies significantly. Adapted from Dalam et al.[100].

Φ CD1 synthesis and trafficking

The knowledge of how CD1 molecules are synthetised and trafficked is important in order to understand how lipid antigens are presented by these molecules to T cells. CD1 proteins are synthetised in the endoplasmic reticulum (ER), followed by glycosylation, which enables the binding of calnexin, calreticulin, and thiol oxidoreductase ERp57. This bound promotes the right folding of the protein, being CD1 α chain bound in a non-covalent form to β_2M[90,98]. Microsomal triglyceride transfer protein (MTP) is also an ER protein that plays a crucial role in CD1 assembly[105]. Some studies have showed that when this ER lipid transfer protein is absent, there is a severe decrease in lipid antigen presentation by CD1a-CD1d molecules[106–108]. During assembly, CD1 molecules don't present empty pockets, being associated with lipids from the ER. These lipids can be loaded by MTP, which stabilises CD1 proteins[83,108,109]. Besides stabilisation, MTP is also important for recycling CD1 molecules from the lysosome to the plasma membrane[110].

The cellular trafficking of CD1 molecules is represented in **Figure 6**. When CD1 molecules are correctly assembled, they move on with their maturation in the Golgi complex. Here, they complete the glycosylation process and then, they are presented in the plasma membrane, via the secretory pathway, except CD1e. This CD1 isoform is not present on the plasma membrane, as stated above, and it functions as a LTP: loads and

unloads lipids in CD1d and influences lipid presentation by CD1b and CD1c[95]. After the glycosylation process, CD1e migrates to the late endosome and, subsequently, to the lysosome, where it undergoes cleavage into a more stable soluble form[111]. When in the lysosome, CD1e is involved in lipid loading on CD1b and CD1c[95,96].

When present in the plasma membrane, CD1 molecules are recycled via the endosomal pathway, actively searching for lipid antigens. Human and murine CD1 molecules, except CD1a, are internalised due to the interaction between the tyrosine motifs in their cytoplasmic tails and the adaptor protein complex (AP)-2. Afterwards, CD1b and mouse CD1d interact with AP-3, which leads these molecules to the late endosomes and lysosomes. Nevertheless, CD1c and human CD1d don't associate with AP-3 to reach late endosomes[112]. Studies with mouse CD1d lacking the cytoplasmic tail (prevents internalisation for recycling) showed that these molecules were present in lysosomes, which suggests an alternative pathway for direct sorting[113]. The mechanism involves mouse CD1d association with the invariant chain and MHC class II in the ER, leading to its direct transport to MHC class II compartments or lysosomes[100]. This mechanism can be the used by human CD1d molecules. CD1a lacks tyrosine motif on its tail and so, it cannot interact with AP-2. This CD1 isoform seems to function as a cell surface molecule, exchanging lipids without internalisation or by accessing early endosomes[114,115]. Once internalised, different CD1 molecules follow separate pathways with distinct outcomes: CD1a primarily localizes in early endosomes, while CD1b traffics to lysosomes; CD1c and human CD1d share similar trafficking pathways, being localized in late endosomes; Notably, the trafficking pathway of mouse CD1d resembles the one used by human CD1b[103,116]. Furthermore, it was demonstrated that pH influences the localization of CD1d at the plasma membrane[117].

In endocytic compartments, CD1 molecules load with lipid antigens and return to the plasma membrane to stimulate T cells. The localization of lipid antigens in specific organelles is determined by their biochemical characteristics, such as lipid length, saturation, and headgroups, suggesting that the distinct pathways of CD1 isoforms are crucial for encountering various types of lipid antigens[82].

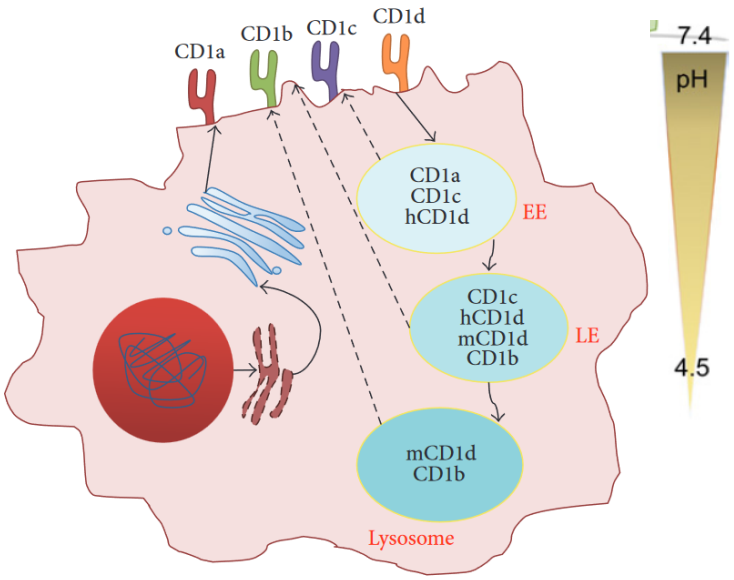

Figure 6. Cellular trafficking of CD1 molecules with the lysosome. CD1 molecules undergo cellular trafficking following their synthesis. Initially, they combine with β2-microglobulin in the endoplasmic reticulum. Subsequently, they move to the Golgi complex network, where glycosylation takes place, and from there, they proceed to the plasma membrane (indicated by solid arrows). At the plasma membrane, CD1 molecules are taken up by the endocytic pathway, which is the primary site for loading. Differences in pH are involved in the processes of protein conformation as well as antigen loading. Notably, different CD1 isoforms are found in distinct endocytic compartments. Once loaded, the CD1 molecules travel back to the plasma membrane, where they activate T cells (shown by dashed arrows). Early endosome (EE); late endosome (LE); human CD1d (hCD1d); mouse CD1d (mCD1d). Adapted from Pereira et al. and Teyton, Luc[80,102].

Summarily, CD1a, b, c and d (group 1 and group 2 CD1 molecules) present lipid antigens to lipid-specific T cells, while CD1e is involved in loading lipids in other CD1 molecules. Notably, all these molecules undergo trafficking through the endo-lysosomal compartments, making them susceptible to defects in LSDs.

2.1.2 Lipid antigens

Lipid antigens are recognised by CD1-restricted T cells[78,90]. These antigens can be classified as self- or nonself-antigens, depending on their origin: they are called self-antigens when produced within the body, and nonself-antigens, when they derive from external microbial or environmental sources[118]. Contrary to peptide antigens, lipid-specific T cells exhibit considerable self-reactivity[119,120]. Lipid antigens can also be categorized according to their synthesis place: endogenous antigens, produced in the same APC, and exogenous antigens, synthesized in other cells and transferred to an APC[87].

The glycosphingolipid α-galactosylceramide (α-GalCer) was the first lipid antigen identified, after being isolated from a marine sponge compound[121]. A few years later, α-GalCer was demonstrated to activate CD1d-restricted T cells[122]. Other self-origin glycosphingolipids, such as GM1, sulfatide, and GD3, were identified as lipid antigens as well[87]. Phosphatidylinositol (PI), phosphatidylcholine (PC), lyso-PC, and phosphatidylethanolamine (PE) are also antigenic lipids to CD1-restricted T cells. The majority of nonself-lipid antigens were isolated from mycobacteria[123].

The CD1 family has the ability to bind and exhibit a wide variety of diverse lipids. Certain CD1 isotypes, like CD1b and CD1c, can specifically present certain unique mycobacterial antigens. On the other hand, more common lipids like self and nonself glycosphingolipids and phosphoglycerolipids can be presented by most CD1 isoforms, being recognition specificity controlled by the CD1-restricted T cell[97]. For instance, sulfatide can be identified by all antigen-presenting CD1 isoforms and it can stimulate CD1a-, b-, c-, and d- restricted T cells[87]. An overview of some CD1-presented lipids is represented in **Table 2**.

Table 2. Antigenic lipids of self and nonself origin. CD1 restriction is specified for each antigen. Adapted from De Libero et al., Zajonc et al., and Pereira et al.[87,97,104].

Antigen	Origin	Restriction
Cardiolipin	Self	mCD1d
PE	Cypress plant; self	CD1a; mCD1d
PC	Cypress plant; self	CD1a; hCD1d; CD1c
Lyso-PC	Self	m/hCD1d; CD1a
PI	*M. tuberculosis*; self	mCD1d
Lyso-Sph	Self	hCD1d
Sulfatide	Self	CD1a; CD1b; CD1c; m/hCD1d
α-GalCer	Self	m/hCD1d
β-GlcCer	Self	mCD1d
β-GlcSph	Self	mCD1d
iGb3	Self	mCD1d
GD3	Self	mCD1d
GM1	Self	CD1b
Triacylglyceride	Self	CD1a
Dideoximycobactin	*M. tuberculosis*	CD1a
PIM_6	*M. tuberculosis*	CD1b; CD1e
GMM	*M. tuberculosis*	CD1b

Mycolic acid	*M. tuberculosis*	CD1b
MPM	*M. tuberculosis*	CD1c
LPG	*L. donovani*	mCD1d

Abbreviations: mCD1d- mouse CD1d; hCD1d- human CD1d; PE-phosphatidylethanolamine; PC-phosphatidylcholine; PI-phosphatidylinositol; Sph- sphingomyelin; GalCer- Galactosylceramide; GlcCer-glucosylceramide; GlcSph-glucosylsphingosine; iGb3- isoglobotriaosylceramide; GD3- GSL-1-glycosphingolipid 1; PIM-phosphatidylinositol mannose; GMM- Glucose monomycolate; MPM- mannosyl phosphomycoketide; LPG: lipophosphoglycan; *M. tuberculosis- Mycobacterium tuberculosis; L. donovani- Leishmania donovani.*

Although many lipids can be CD1 ligands, not all of them are T cell antigens. Some self-antigens interact with CD1 proteins to stabilize them as they migrate to the cell surface. The lipids bound to CD1 can be exchanged at the plasma membrane or during the trafficking of CD1 along endosomal compartments. The process of lipid loading on CD1 involves various LTPs, including the saposins, GM2 activator protein, MTP, apolipoprotein E and fatty acid amide hydrolase[97,108,109]. Low pH also induces conformational alterations that allow the lipid loading[124,125].

Among CD1-binding lipids that do not trigger an immune response, some molecules possess inhibitory properties. For instance, the glycosphingolipid Gb3 was described as an inhibitor of a subset of CD1d-restricted T cells, called invariant Natural Killer T cells, by binding to CD1d[126]. This inhibition occurs due to direct competition between Gb3 and these T cells subset antigens for CD1d binding[104,126]. This CD1d-restricted T cell population is one of the main focus of this project and will be described in the following section.

2.1.3 *CD1-restricted T cells*

CD1-restricted T cells are part of the group of "unconventional" T cells, which do not recognise peptides antigens bound to MHC. These T cells often operate rapidly and coordinate other immune cells[127,128].

Group 1 CD1-restricted T cells express various α β or γ δ TCRs[87]. After recognising self- or nonself-lipids antigens, they go through clonal expansion in the periphery, resulting in a delayed effector response, resembling an adaptive-like immune response, which is analogous to MHC-restricted T cells[128]. Group 2 CD1-restricted T cells are also known as natural killer T (NKT) cells, because of expressing simultaneously a TCR and

natural killer (NK) cells markers[104,129]. CD1d are divided into two groups: type 1 and type 2 NKT cells[130]. These groups will be discussed below. In **Table 3**, Group 1 and 2 CD1-restricted T cells are compared.

Table 3. Comparison between different types of CD1-restricted T cells. Modified from Godfrey et al.[131].

	CD1a	CD1b	CD1c	CD1d	
				Type I NKT cells	Type II NKT cells
TCR	αβ and γδ	Aβ	αβ and γδ	Vα24Jα18; Vβ11	αβ and γδ
Phenotype	CD4+, CD8+, DN	CD4+, CD8+, DN	CD4+, CD8+, DN	CD4+, CD8+, DN	CD4+, DN (mouse)
Main lipid antigens	Sulfatide	Sulfatide, GM1, mycolic acid	Sulfatide	iGb3; α-GalCer and analogs	Sulfatide; lysophosphatidylcholine

2.1.3.1 Group 1 CD1-restricted T cells

Group 1 CD1-restricted T cells haven't been analysed as intensively as NKT cells. Regarding the expression of CD4 and CD8, these cells can be CD4 positive ($CD4^+$), $CD8^+$ or double negative (DN), i.e., negative for CD4 and CD8[119]. According to their phenotype, this group of T cells releases different types of cytokines that are typical of T helper (Th) 1, Th2 and Th17 cells[87]. Studies performed *in vitro* showed that, after recognising lipid antigens, group 1 CD1-restricted T cells exhibit cytolytic activity and produce significant amounts of cytokines like IFN-γ and TNF-α (Th1 phenotype). Such cytokines possess potent antiviral effects, controlling virus infections[130,132]. Interestingly, self-reactive CD1b-restricted T cells can recruit neutrophils due to their ability of adopting Th17 cells characteristics[133]. Group 1 CD1-restricted T cells also induce TNF-α dependent dendritic cell maturation[134]. Stimulation of PRRs enhances the autoreactivity of group 1 CD1-restricted T cells[135], which can happen through viruses[130,136]. Furthermore, CD1a-, b- and c- restricted T cells are involved in several pathways of the immune response: they are increased during *M. tuberculosis* infections; they have been

implicated in autoimmune diseases[87,137]; they have been associated with allergies to pollen[86]. Moreover, these T cells can present a naïve, memory or effector phenotype[87].

2.1.3.2 CD1d restricted T cells

Humans and mice have CD1d-restricted T cells, which are the most intensively studied CD1-restricted T cells. Also called NKT cells, CD1d-restricted T cells can be divided in two different populations based on their TCR properties. Type 1 NKT cells or invariant NKT (iNKT) cells express a semi-invariant αβ TCR: humans express an invariant Vα24-Jα18 chain paired with a Vβ11 chain[138] whereas in mice an invariant Vα14-Jα18 chain is paired with one of three β chains (Vβ8.2, Vβ2 or Vβ7)[139,140]. Type 2 NKT cells, however, exhibit a preference for certain Vα and Vβ chains, being more variable than type 1 NKT cells TCRs[140,141].

Type 1 and type 2 NKT cells express surface markers of NK cells including CD161 (NK1.1 in mice), CD54 and NKG2D molecules. These markers are not always co-expressed, making it possible to define different subpopulations[87,104,129].

Φ Type 1 NKT cells or "Classical" NKT cells

Contrary to conventional T cells, iNKT cells exhibit innate-like functions. After expanding and maturing in thymus, iNKT cells can be stimulated by innate signals, responding within hours, instead of days. On the other hand, they are also able to respond to specific antigens that engage their TCR. These characteristics place iNKT cells at the crossroads between innate and adaptive immune responses[104]. iNKT cells recognize glycolipid antigens from various sources, including microbial and environmental, when presented by CD1d[142].

iNKT cells are greatly stimulated by α-GalCer (**Figure 7**). They are easily identified in tissues by antibodies against the semi-invariant TCR or by CD1d tetramers loaded with the glycolipid antigen α-GalCer or its analogue, PBS-57[104,130,143]. The frequency of iNKT cells is different between mice and humans. In mice, iNKT cells are more abundant in the liver and adipose tissue, while their presence is relatively lower in the thymus, spleen, bone marrow, peripheral blood, and lymph nodes. In humans, iNKT cells are more frequent in the adipose tissue, followed by the liver, and are found at lower percentages

in the spleen, peripheral blood, lymph nodes, bone marrow, and thymus[144]. iNKT cells percentage in PBMCs is very variable, ranging from 0.001% to over 3%, even though this range is usually between 0.01% and 0.1%, with no differences between gender[104,144,145].

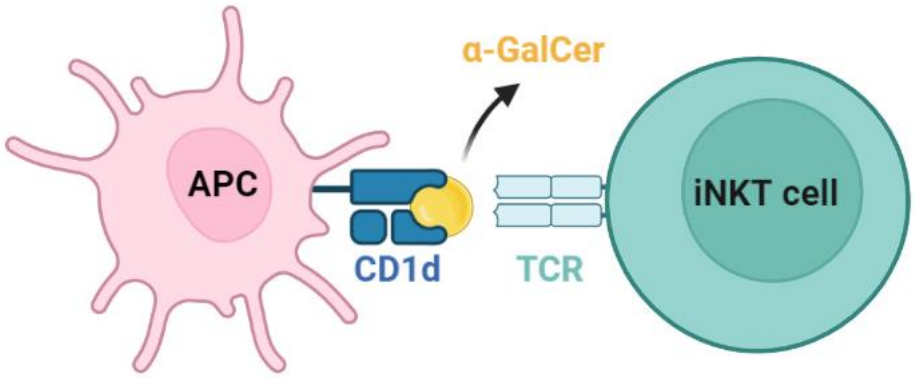

Figure 7. α-GalCer presentation by CD1d molecule on the surface of an APC to an iNKT cell. This figure was created with *BioRender.com*.

iNKT cells can be divided into different subsets according to their CD4 and C8 expression: in humans, they can be $CD4^+$, $CD8^+$ or DN and a very small double positive (DP) subset has also been observed[146,147], while mice iNKT cells are exclusively $CD4^+$ or DN cells[148,149]. Human iNKT cells are generally described by their expression of CD4 ($CD4^+$ or $CD4^-$ subsets). Different subsets frequencies vary significantly between individuals, with $CD4^+$ and DN cells being the most common: $CD4^+$ ranges between 17% and 53% and DN between 19% and 63% of total iNKT cells[146,150–160]. $CD8^+$ iNKT cells are present at a lower frequency, representing 5 to 25% of the iNKT cell population[146,151,152,154,157,158]. Human $CD4^+$ and $CD8^+$ iNKT cells frequencies can be altered in certain conditions. In human immunodeficiency virus (HIV) infection and kidney transplants without rejection, the percentage of iNKT $CD4^+$ cells is decreased[153,157]. Conversely, if kidney transplants are rejected, the frequency of iNKT $CD4^+$ subset increases, as well as in refractory celiac disease, and *Mycobacterium tuberculosis* infection[150,153,157]. Moreover, the percentage of iNKT $CD4^+$ subset tends to increase with age[155,158]. Concerning the frequency of iNKT DN subset, it was shown to be decreased during *Mycobacterium leprae* infection and in hepatocellular carcinoma[151,154]. Regarding the frequency of iNKT $CD8^+$ subset, it is increased in HIV infection but decreases in metastatic uveal melanoma[151,157].

Mice iNKT cells display heterogeneity in both phenotype and function. Murine iNKT cells differentiate into at least three distinct functional populations, depending on the transcription factor expressed (T-bet, GATA3 or RORγt) and cytokines produced. iNKT1 population expresses T-bet and produces IFN-γ and some IL-4, whereas iNKT2 subset is GATA-3^{+} and produces IL-4. iNKT17 population expresses RORγt and produces IL-17. iNKT1, iNKT2 and iNKT17 display a Th1, Th2 or Th17 cytokine profile, respectively[149,161]. Moreover, all iNKT cells (including human iNKT cells) require zinc finger transcription factor promyelotic leukemia zinc finger (PLZF) expression to mature[162,163]. Besides this, the three distinct thymic subpopulations express different levels of PLZF, being highly expressed in iNKT2, intermediately expressed in iNKT17 and low expression is observed in iNKT1[161,164]. Additionally, there are other described murine iNKT subsets, including follicular helper iNKT (iNKT$_{FH}$) which assist B cells[165,166], and iNKT10 cells that play crucial roles in the homeostasis of adipose tissue[167].

Human iNKT cells have also been categorised into Th-cell subsets, based on their cytokine secretion (**Figure 8**). Stimulated Th1-like iNKT cells produce Th1-associated cytokines (e.g., IFN-γ and TNF-α)[147,168,169]. Th1-like iNKT cells are predominantly DN iNKT cells and exhibit a higher expression of NKG2D, when compared to CD4^{+} iNKT cells[168]. Contrarily to Th1-like iNKT cells, Th2 like iNKT cell subsets are predominantly CD4^{+} iNKT cells and secrete IL-4, IL-13 and IFN-γ when activated[145,147,168]. CD8^{+} iNKT cells produce predominantly IFN-γ[170]. Proinflammatory cytokines like IL-17, IL-21, and IL-22 are secreted by human Th17-like iNKT cells upon stimulation[171]. Additionally, regulatory T cells (T$_{reg}$)-like iNKT cells that express FOXP3 are able to produce IL-10, an immunosuppressive cytokine, and T$_{FH}$-like iNKT cells secrete IL-21 when activated[171,172].

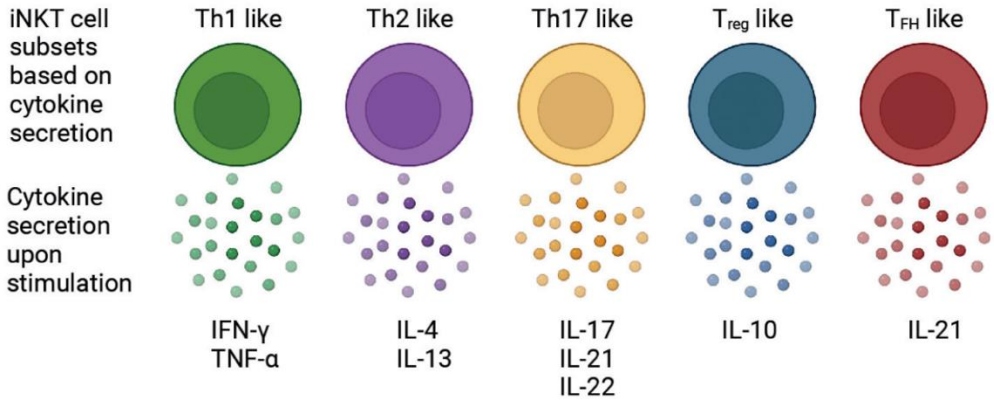

Figure 8. Th-iNKT cell subsets based on their cytokine secretion. When iNKT cells are stimulated, they secrete various cytokines, that depend on the iNKT cell subtype. Adapted from Look et al.[143].

In spite of exhibiting a common expression profile for several chemokine receptors, iNKT cells subsets can also present variations in their chemokine receptor expression (chemokines regulate leukocyte migration). Specifically, $CD4^+$ iNKT cells mainly express C-C chemokine receptor type 4 (CCR4), while $CD8^+$ and DN iNKT cell subsets predominantly express CCR1, CCR6 and C-X-C chemokine receptor type 6 (CXCR6)[173,174]. These observations suggest a distinct tissue distribution pattern among different iNKT cells subsets: for instance, CXCR6 is involved in distributing, in an homeostatic manner, iNKT cells to the lung and the liver[175,176]. Tian et al. showed that iNKT cells expressing CD62L (a ligand involved trafficking T cells to secondary lymphoid organs) have anti-tumour activity and prolonged persistence *in vivo*[177].

Like conventional T cells, iNKT cells undergo functional exhaustion, by expressing higher levels Programmed Death Receptor-1 (PD-1) and T-cell immunoglobulin mucin-3 (TIM-3)[178–180].

Recently, Cui et al. discovered that, both humans and mice, possess a circulating population of $CD244^+CXCR6^+$ iNKT cells with augmented cytotoxic properties, producing higher levels of IFN-γ than the $CD244^-CXCR6^-$ iNKT cells[181]. Surprisingly, this cytotoxic iNKT cells subset lacks CD4 expression, which may explain why CD4- iNKT cell population possesses an enhanced cytotoxic function[181]. A representative example of some markers that can be expressed on the surface of iNKT cells is illustrated in **Figure 9**.

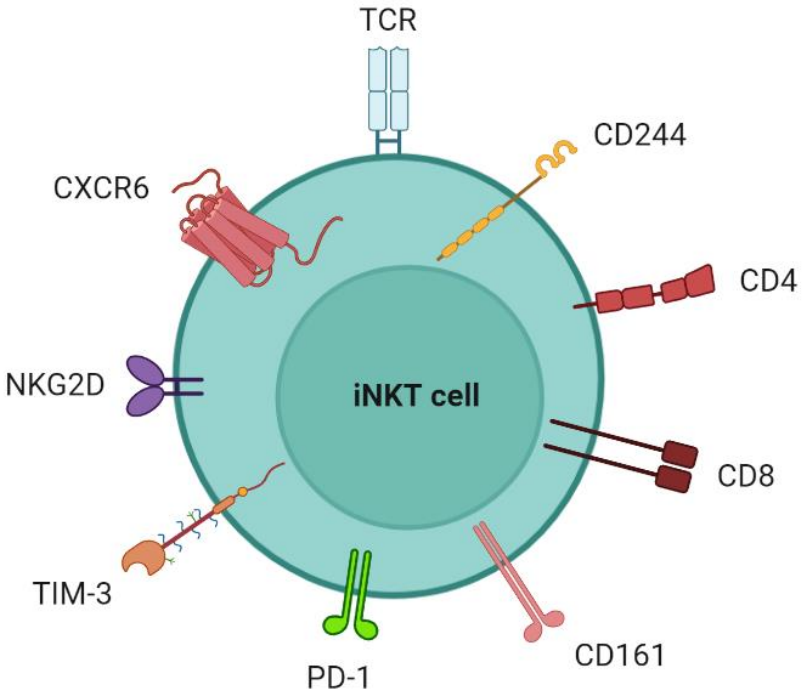

Figure 9. Cell surface markers expressed in iNKT cells. Note that some markers may not be co-expressed. This figure was created with *BioRender.com*.

iNKT cells are crucial, for instance, to initiate immune responses at an early stage by activating and recruiting APCs, which subsequently guide the adaptive immune response, providing protection against infections and tumor development[130,145].

Φ Type 2 NKT cells or "Non-classical" NKT cells

Type 2 NKT cells exhibit greater TCR sequence variability and are not stimulated by α-GalCer. Instead, they recognise antigens like sulfatide and PC[131]. Non-classical NKT cells are more abundant in humans than iNKT cells, displaying characteristics of both conventional iNKT and T cells and influencing the outcome of persistent viral infections. They have been associated with functions such as suppressing autoimmunity and inhibiting tumor rejection. Type 2 NKT cells present immunosuppressive roles in autoimmune diseases, inflammatory liver diseases, and cancer[182].

2.1.4 Mucosal-associated Invariant T cells

Mucosal-associated Invariant T (MAIT) cells have the ability to detect antigens derived from vitamin B that are presented by the non-polymorphic MHC class I related-1 molecule (MR1)[183–185]. MAIT cells TCR and MR1 exhibit a high degree of conservation across various mammalian species, indicating their vital and conserved role in immune function[183]. Lately, MAIT cells have been widely studied and can act as a control in our research, since they constitute a substantial portion, up to 10%, of the T cells present in PBMCs, and present several similarities with iNKT cells (including an invariant TCR α chain), as they are also considered "unconventional" T cells[186–188].

2.1.5 *Invariant natural killer T cells in Fabry disease*

The enzyme α-Gal A is responsible for degrading Gb3, a glycolipid which has been shown to inhibit iNKT cells[126]. α-Gal A is also involved in the degradation of α-psychosine, an antigen found in mammalian tissues[189]. Hence, this enzyme has the role of breaking down antigenic (α-psychosine) and inhibitory (Gb3) lipids for iNKT cells. As consequence, a defect in α-Gal A results in the accumulation of both lipids within the cells.

Glycolipids behave as antigens of CD1-restricted T cells. By understanding this, it is possible to assume that the accumulation of Gb3 or lyso-Gb3 in Fabry disease patients, because of the deficiency in α-Gal A, will have a direct impact on the immune system. The accumulated glycolipids in this disease are recognised by APCs bearing CD1d molecule, which then are presented to NKT cells, and CD1d goes through lysosomal compartments where the accumulation occurs[82,116,182]. Besides this, in α-Gal A deficient cells there is also the accumulation of the lipid antigens α-GalCer and α-GalSph, which are iNKT cell antigens[189].

α-GalCer is a lipid presented by CD1d-bearing APCs, whose loading is influenced by the access to a functional lysosomal compartment. Several studies have demonstrated that that APCs from mouse models of Fabry disease and other LSDs have decreased capacity of presenting lipid antigens[190]. Surprisingly, this reduced capacity was not observed in human patients[116]. The differences in CD1d lipid antigen presentation between mice and humans could be attributed to variations in intracellular trafficking and lysosomal

function. For instance, mouse CD1d mainly recycles to the lysosome, while human CD1d is found in late endocytic compartments[116].

Furthermore, in Fabry disease animal model (α-Gal A deficient/ knock out (KO) mice), it was shown that the total iNKT cell frequency is decreased, as well as the $CD4^+$ iNKT cells subset[190–194]. In other LSDs, this reduced total number of iNKT cells is also observed, which may suggest that it is a consequence of a general lysosomal dysfunction[190,192]. The decrease in iNKT cell numbers could be attributed to the accumulation of non-antigenic lipids interfering with CD1d antigen presentation to iNKT cells. Gb3, among other lipids, can bind to CD1d and prevent iNKT cell activation[126,195,196]. On the other hand, iNKT cells may become over-stimulated in α-Gal A KO mice due to the presence of lipid antigens α-GalCer and α-GalSph in α-Gal A deficient cells, leading to their exhaustion[189,193]. It is important to note that both phenomena can be occurring in parallel in α-Gal A KO mice, depending on the balance between Gb3, α-GalCer and α-GalSph levels in different organs. Importantly, treating adult α-Gal A KO mice with ERT prevented the decrease in splenic iNKT cell number[191].

When compared to α-Gal A KO mice, little is known about iNKT cells in Fabry disease patients. iNKT cells and lipid antigen presentation have already been studied in late onset Fabry disease patients (patients with residual α -Gal A enzyme activity)[116,197]. In these patients' blood, iNKT cell frequency and CD1d lipid antigen presentation is similar to healthy subjects. Nevertheless, late onset patients have a decreased percentage of $CD4^+$ iNKT cells, similar to α-Gal A KO mice, and an increase in DN iNKT cells frequency[197]. It is known that occurs downregulation of CD4 expression in iNKT cells upon cell activation[198], which supports the hypothesis that the accumulation of self-lipid antigens can lead to the activation of iNKT cells in α-Gal A deficiency. In terms of cytokine profile, these late onset Fabry patients showed a significant reduction in the production of IL-4 by iNKT cells subsets, but no important alterations in the production of IFN-γ. This suggests a bias towards a pro-inflammatory phenotype of iNKT cells in Fabry disease[197].

Although there are some data regarding iNKT cells in late onset Fabry disease patients, classical patients, with more severe α-Gal A deficiency, haven't been analysed yet.

Hypothesis and aims

We hypothesize that the progressive accumulation of lipids in a-Gal A deficiency leads to iNKT cell frequency, phenotypic and functional alterations.

The specific aims of this thesis project were:

1) To set up experimental conditions, including the definition of the markers to analyse the phenotype and function of iNKT cells;

2) To characterize iNKT cell frequency and phenotype in Fabry disease patients.

Experimental set up had to be optimised before performing it with the Fabry disease patients and healthy subjects' blood samples.

Experimental analyses were performed using Buffy Coats from healthy subjects and peripheral blood samples from Fabry disease patients. PBMCs from healthy donors were isolated and used for: 1) the titration of antibodies, tetramers and fixable viability dye (some antibodies and CD1d loaded tetramers were also titrated using the iNKT cell line); 2) the optimisation of anti-iNKT MicroBeads volume. PBMCs from control subjects and Fabry disease patients were isolated and used for flow cytometry analyses, to study the iNKT cell population.

1) Ethics statement

Fabry disease patients were recruited from *Centro Hospitalar Universitário de São João* (CHUSJ), Porto, Portugal. Informed consent was obtained from all Fabry disease patients in accordance with the Helsinki declaration. The study was approved by CHUSJ Ethical Committee and Data Protection Officer.

2) Biological samples

Three Fabry disease patients and four control subjects were analysed in this study. Two females (siblings) and one male composed the Fabry disease patients' group. In the control group, there were two females and two males. PBMCs from control subjects were isolated from Buffy Coats, kindly provided by *Banco de Sangue* from CHUSJ (Porto, Portugal). The Buffy Coat is a product from the blood processing, that contains most of the white blood cells and platelets. Fabry disease patients were recruited by their physician, Prof. João Paulo Oliveira from Hospital São João. The male patient was already under ERT, when the blood samples were acquired. The two female patients were not under any treatment. Blood samples from patients were collected in ethylenediamine tetraacetic acid (EDTA) containing tubes (two blood tubes ~9 mL each were collected per patient), when blood tests were made to the patients. The blood samples from Fabry

disease patients were collected from the Human Genetic Service at CHUSJ (Porto, Portugal).

3) Peripheral blood mononuclear cells isolation

Buffy Coats from healthy blood donors were collected from *Banco de Sangue* from CHUSJ (Porto, Portugal). Blood samples (blood tubes) from Fabry disease patients were acquired from the Human Genetic Service at CHUSJ (Porto, Portugal). PBMCs from the Buffy Coats and blood samples were isolated by density gradient centrifugation with Histopaque-1077® (Sigma-Aldrich), under sterile conditions. In the case of Buffy Coats, they were first diluted 1:1 with phosphate-buffered saline (PBS) 1x (Gibco) and, then, the diluted blood was gently layered in a 2:1 proportion with Histopaque-1077®. Blood from blood tubes (Fabry disease patient's blood samples) was not diluted and it was gently layered in a 1:1 proportion with Histopaque-1077®. Afterwards, diluted blood and whole blood were centrifuged at 400 x g, room temperature (RT), for 30 min, without brake. After centrifugation, PBMCs were collected from a visible ring, called "PBMCs layer", located between the plasma and Histopaque-1077® (**Figure 10**). PBMCs were washed with 10 mL of PBS 1X at 1300 rpm for 6 minutes. PBMCs were then incubated with 5 mL Red Blood Cells (RBC) lysis buffer 1X (BioLegend®) for 10 minutes, in order to lysate any remaining erythrocytes. PBMCs were counted in an optic microscope by using a Neubauer chamber and Trypan blue for exclusion of dead cells. The needed quantity of PBMCs was collected, according to the experiment performed. PBMCs were used for: titration of antibodies, tetramers and fixable viability dye (Buffy Coats from healthy donors); optimisation of anti-iNKT MicroBeads volume to use in patients (Buffy Coats from healthy donors); optimisation of protocols (Buffy Coats from healthy donors); flow cytometry analyses of peripheral blood iNKT cells (Fabry disease patients' blood samples and healthy subjects' Buffy Coats).

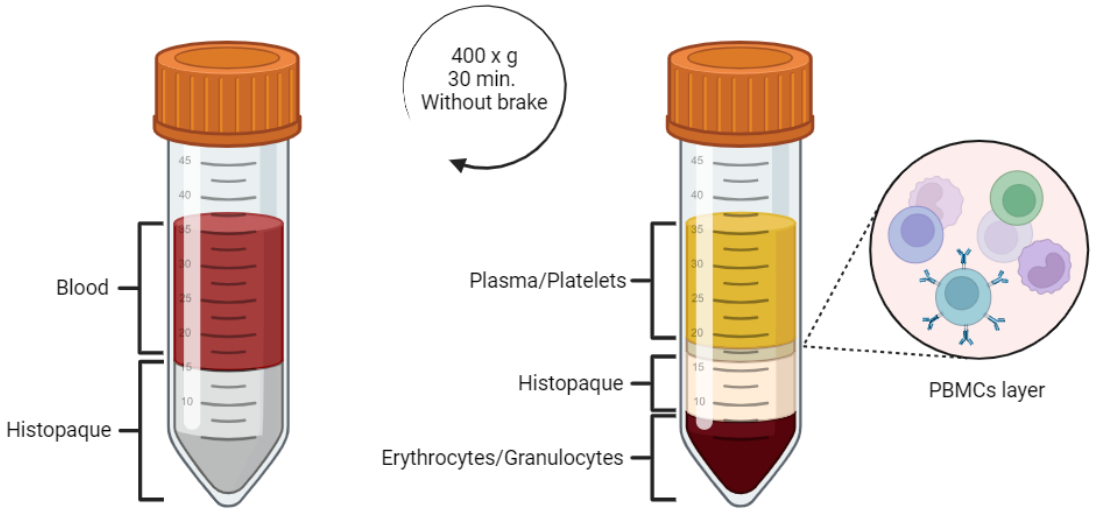

Figure 10. PBMC isolation using Histopaque 1077®. This figure was created with *BioRender.com*.

PBMCs isolated from Buffy Coats from healthy donors were also used as APCs in iNKT cell line re-stimulations. The iNKT cell line was used to titrate some antibodies and tetramers (described in **section 6) iNKT cell line culture and re-stimulation**). For iNKT cell re-stimulation, 25 mL of RPMI complete medium (RPMI 1640 1X GlutaMAX with Sodium Pyruvate 1X, Kanamycin Sulfate 1X, Non-Essential Amino Acids 1X, from Gibco) with 10% heat-inactivated Fetal Bovine Serum (iFBS) (with FBS from Gibco) were added to the PBMCs isolated from a Buffy Coat. PBMCs were irradiated with 40 Gy in a gamma irradiator (Gammacell 1000, Nordion). Irradiated PBMCs were centrifuged at 1300 rpm for 6 min and pellet was resuspended in 10 mL of RPMI complete medium with 10% iFBS. Cells were then counted in a Neubauer chamber.

4) Activation of T cells with phorbol myristate acetate and ionomycin

Upon isolation of the PBMCs from a Buffy Coat, activation of T cells with phorbol myristate acetate (PMA) and ionomycin was performed to titrate the antibodies anti-IL-4 and anti-IFN-γ. Cytokines are analysed intracellularly and this activation technique with PMA and ionomycin is better for the intracellular cytokine staining. PMA triggers the activation of protein kinase C, and when combined with the Ca^{2+} ionophore ionomycin, it initiates intracellular signalling pathways within T cells. This results in the release of

cytokines. Nevertheless, this stimulation is toxic and does not increase the number of viable cells. To inhibit cytokine secretion, Brefeldin A (BFA) is introduced as it obstructs the movement of proteins from the endoplasmic reticulum to the Golgi complex. This action amplifies the cytokine signal within the cell while minimizing background noise. The protocol followed was adapted from Foster et al[199]. Briefly, the PBMCs isolated from a Buffy Coat were washed with PBS 1X, counted and resuspended at 4 x10^6 cells/ mL in RPMI complete medium with 10% iFBS. 100 µL of the resuspended cells were plated in 96-well round-bottom plates and 100 µL of complete RPMI medium with 10% iFBS containing 50 ng/mL of PMA (Sigma), 2 µg/mL ionomycin (Sigma), and 20 µg/mL BFA (Sigma) was added to each well. Cells were incubated at 37 ºC, 5% CO_2 for 5 hours. The final concentrations of the reagents added were diminished to half, because 100 µL of complete medium was already present with cells in the wells (in the beginning, the double of the reagents concentration was added in order to get intended concentration). Besides the wells containing PMA/ionomycin for single staining (four dilutions of each antibody: 1:100 to 1:800), two control wells containing isolated PBMCs without stimuli were added (unstained and stained). 5 hours later, cells were recovered and subjected to intracellular staining.

5) Human iNKT cell enrichment from PBMCs

iNKT cells from Fabry disease patients and healthy subjects, as a rare population of cells, had to be enriched in a sample in order to study all the markers.

iNKT cells were isolated from PBMCs (isolated from Buffy Coats or blood tubes/ whole blood) by performing immunomagnetic labelling with anti-human iNKT MicroBeads (Miltenyi Biotec) using a Magnetic-activated cell sorting (MACS®) cell separation system (Miltenyi Biotec). This technique makes use of magnetic beads that are bound to an anti-human iNKT cell antibody which allows the positive selection of human iNKT cells based on the expression of the TCR α-chain Vα24-Jα18. A scheme of positive selection using MACS® cell separation system is represented in **Figure 11**.

Besides analysing iNKT cells from Fabry disease patients and healthy subjects, they were also compared to $CD3^+$ T cells (conventional T cells). This way, the positive fraction ($iNKT^+$) didn't have to have 100% purity of iNKT cells, but 0% of iNKT cells was wanted

in the negative fraction, so that iNKT cells weren't being lost. Following this line of thought, in order to optimise the amount of microbeads that were going to be used with patients and controls, half of the recommended amount of microbeads by the manufacturer was used.

The manufacturer's protocol was followed under sterile conditions. Briefly, isolated PBMCs from a Buffy Coat were washed with 5 mL of MACS Buffer (1x PBS, 2 mM EDTA, 0.5% Bovine serum albumin (BSA)), by centrifuging at 1800 rpm, for 5 minutes. The pellet was resuspended in MACS Buffer (400 µL per $100x10^6$ cells) and incubated with anti-human iNKT magnetic beads (50 µL per $100x10^6$ cells- the recommended amount was 100 µL per $100x10^6$ cells) on ice in the dark, for 20 min, occasionally shaking. With this incubation, anti-human iNKT cell antibodies present in the microbeads are able to bind to iNKT cells. Then, cells were washed twice with 5 mL of MACS Buffer.

According to the number of cells needed or available (in the case of Fabry disease patients, as the PBMCs were isolated from two blood tubes (whole blood) the number of PBMCs was lower), the type of columns for positive selection of cells varied: if less than 200×10^6 cells were to be obtained, MS columns were used; if more than 200×10^6 cells (and less than 2000×10^6 cells) were to be obtained, LS columns were used. Once the columns were chosen, they were placed in the magnetic support and respective separator (MiniMACS separator for MS columns and MidiMACS separator for LS columns). Labelled cells are kept from eluting because of the magnetic force existing between the beads and the magnetic support. Columns were pre-wetted with MACS Buffer: 0.5 mL for MS columns and 4 mL for LS columns. After washing 2X with MACS buffer, cells were resuspended in 0.5 mL of MACS buffer, if MS columns were used, or in 4 mL, if LS columns, and were applied to the column. The cells that bound to the beads (iNKT cells) remained in the column (positive fraction), while non-labelled cells were eluted (negative fraction). The columns were washed twice with MACS Buffer (0.5 mL for MS columns and 4 mL for LS columns). These washes elute cells that are not bound to the magnetic beads. The columns were then removed from the magnetic support and separator and placed in Falcon tubes. 1 mL (MS columns) or 5 mL (LS columns) of

MACS Buffer were loaded in the column and iNKT^{+} cells were eluted by using a syringe plunger.

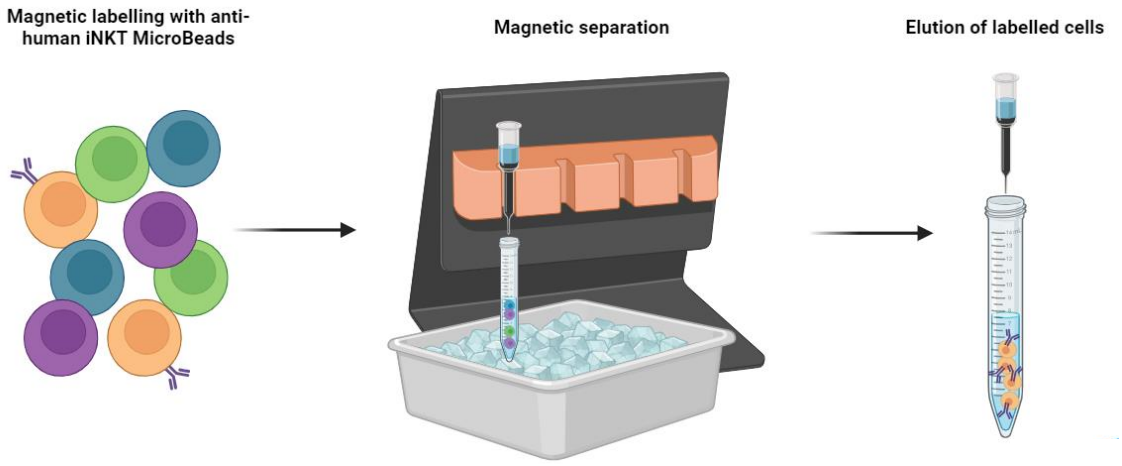

Figure 11. Separation of iNKT^{+} cells by positive selection using anti-human iNKT MicroBeads (Miltenyi Biotech) and (MACS®) cell separation system (Miltenyi Biotech). This figure was created with *BioRender.com*.

Cells from negative and positive fractions were counted in an optic microscope by using a Neubauer chamber and Trypan blue for exclusion of dead cells. 0.2x10^{6} to 1x10^{6} cells from the negative fraction were used for flow cytometry analyses. As the number of iNKT cells was usually low, all the cells from this fraction were used for flow cytometry analyses.

6) iNKT cell line culture and re-stimulation

iNKT cell line was used to titrate the antibodies anti-TIM-3 and anti-PD-1 and the CD1d tetramers. This cell line used was previously generated in our group[126]. After thawing, iNKT cells were cultured in 24 well plates with T cell medium: RPMI complete medium with 100 U/mL of recombinant IL-2 (kindly provided by the National Cancer Institute, USA) and 5% of human serum. iNKT cells were re-stimulated every 17-20 days, by adding 2x10^{6} of irradiated PBMCs (Section **3) Peripheral blood mononuclear cells isolation**) and 2 µg of phytohemagglutinin (PHA) (Thermo Fisher Scientific) per mL of T cell medium to 1x10^{6} iNKT cells. Two wells without iNKT cells were used as controls to confirm that the irradiated PBMCs were dead after 15 days. Every 3 or 4 days after the re-stimulation, and depending on the cell growth, cells had their medium refreshed or a split was done. In order to refresh the medium, 1 mL of culture medium was removed

from each well and replaced by 1 mL of T cell medium. Splits were performed by resuspending the cells and 1 mL was transferred to another well, then 1 mL of culture media was added to each well to make up the 2 mL total volume. The splits and medium refresh were done until days 17-20, time when iNKT cells were re-stimulated again.

When iNKT cells were growing well, some wells were resuspended and counted in order to perform flow cytometry to titrate the antibodies and tetramers.

7) Flow cytometry

iNKT cells were analysed by flow cytometry to investigate their frequency and phenotype. Before the acquisition of Fabry disease patients' blood samples to analyse iNKT cells, the antibodies, tetramers and fixable viability dye had to be titrated.

Before patients

Antibodies, tetramers and the fixable viability dye were usually first titrated using the dilutions 1:100, 1:200, 1:400 and 1:800 in $1x10^6$ PBMCs/ well. Nonetheless, the antibodies anti-PD-1 and anti-TIM-3 were titrated using the dilutions 1:20, 1:40, 1:80 and 1:160 and 1:50, 1:100 and 1:200, respectively. These two antibodies were first titrated using the iNKT cell line (since they are more expressed in iNKT cells than in conventional T cells[178–180]) and then the optimal concentration was tested in PBMCs. In the case of the BV421 tetramer, a higher dilution was tested, 1:1600 (besides 1:100-1:800). Cells were stained extracellularly with the dilutions mentioned above and for the antibodies against the cytokines (IL-4 and IFN-γ), they were stained intracellularly. The list of antibodies, tetramers and fixable viability dye titrated and tested is presented in **Table 4**.

Table 4. Antibodies, tetramers and fixable viability dye titrated before patients for staining experiments and respective information.

Antibody/ Tetramer/ Fixable viability dye	Cells tested	Clone	Dilutions tested	Fluorochrome	Supplier
Anti-human CD3	Isolated PBMCs	OKT3	1:100; 1:200; 1:400; 1:800	FITC	Biolegend
Anti-human CD3	Isolated PBMCs	OKT3	1:100; 1:200; 1:400; 1:800	PerCP-Cy5.5	Biolegend
Anti-human CD3	Isolated PBMCs	OKT3	1:100; 1:200; 1:400; 1:800	BB700	BD Biosciences
Human CD1d PBS-57 Tetramer	iNKT cell line and isolated PBMCs	----	1:100; 1:200; 1:400; 1:800; 1:1600	BV421	NIH
Human CD1d unloaded Tetramer	iNKT cell line and isolated PBMCs	----	1:100; 1:200; 1:400; 1:800; 1:1600	BV421	NIH
Human CD1d PBS-57 Tetramer	iNKT cell line and isolated PBMCs	----	1:100; 1:200; 1:400; 1:800	APC	NIH
Human CD1d unloaded Tetramer	iNKT cell line and isolated PBMCs	----	1:100; 1:200; 1:400; 1:800	APC	NIH
Anti-human CD4	Isolated PBMCs	RPA-T4	1:100; 1:200; 1:400; 1:800	PE-Cy7	Biolegend
Anti-human CD8α	Isolated PBMCs	HIT8a	1:100; 1:200; 1:400; 1:800	APC-Cy7	Biolegend
Anti-human CD8β	Isolated PBMCs	SIDI8BEE	1:100; 1:200; 1:400; 1:800	PE	Thermo Fisher
Anti-human CD244 (2B4)	Isolated PBMCs	K041E5	1:100; 1:200; 1:400; 1:800	APC	Biolegend
Anti-human CXCR6 (CD186)	Fresh iNKT cells and iNKT cell line	C1.7	1:50; 1:100; 1:200; 1:400; 1:800	PE-Cy5	Biolegend
Anti-human TIM-3 (CD366)	iNKT cell line and isolated PBMCs	F38-2E2	1:50; 1:100; 1:200	BV711	Biolegend

Anti-human PD-1 (CD279)	iNKT cell line and isolated PBMCs	EH12.2H7	1:20; 1:40; 1:80; 1:160	BV785	Biolegend
Anti-human ICOS (CD278)	Isolated PBMCs	C398.4A	1:100; 1:200; 1:400; 1:800	APC	Biolegend
Anti-human CD161	Isolated PBMCs	HP-3G10	1:100; 1:200; 1:400; 1:800	PE-Cy5	Biolegend
Anti-human IFN-γ	Activated PBMCs	4S.B3	1:100; 1:200; 1:400; 1:800	BV711	Biolegend
Anti-human IL-4	Activated PBMCs	8D4-8	1:100; 1:200; 1:400; 1:800	APC	Biolegend
Human MR1 5-OP-RU Tetramer	Isolated PBMCs	----	1:100; 1:200; 1:400; 1:800	AF488	NIH
Human MR1 6-FP Tetramer	Isolated PBMCs	----	1:100; 1:200; 1:400; 1:800	AF488	NIH
Human MR1 5-OP-RU Tetramer	Isolated PBMCs	----	1:100; 1:200; 1:400; 1:800	BV421	NIH
Human MR1 6-FP Tetramer	Isolated PBMCs	----	1:100; 1:200; 1:400; 1:800	BV421	NIH
Fixable Viability Dye	Isolated PBMCs	----	1:100; 1:200; 1:400; 1:800	Zombie Aqua	Biolegend

Abbreviations: APC – Allophycocyanin; BV – Brilliant Violet; Cy – Cyanine; FITC – Fluorescein; PE – Phycoerythrin; PerCP - Peridinin chlorophyll protein; PBS-57 – α-GalCer analog; AF- Alexa Fluor: BB- Brilliant Blue; 5-OP-RU: 5-(2-oxopropylideneamino)-6-D-ribitylaminouracil; 6-FP: 6-formyl pterin.

Cell acquisition was performed on the same day or the day after the staining and the cells were kept at 4 ºC until acquisition. For titrations in fresh PBMCs and iNKT cell line, around 50 000 cells were acquired. To check if the concentration of an antibody/ tetramer was optimal in fresh iNKT cells, the totality of the sample was acquired. Acquisition was performed in a Cytek Aurora cytometer (Cytek Biosciences) using the SpectroFlo® Software. All post-acquisition analyses were done using FlowJo™ software v10.9.0. In order to analyse the titrations, the Stain Index plugin from FlowJo™ software was used. Staining index (SI) measures the relative brightness of the fluorochrome by using the formula: $SI = \frac{\text{Median (Positive Cells)} - \text{Median (Negative Cells)}}{2 * \text{Standard Deviation (Negative Cells)}}$.

The higher the value of SI, the greater the separation of negative and positive populations, allowing a better definition of the positive cells for the marker in question. This helps choosing the optimal concentration of an antibody, tetramer and fixable viability dye.

Extracellular staining

Before extracellular staining, cells were initially washed once with PBS 1X and then resuspended in PBS 1X (nº of wells x 100 µL). 100 µL of PBS 1X containing $1x10^6$ isolated PBMCs from a Buffy Coat, were plated and stained per well in a round-bottomed 96-well plate. If the iNKT cell line was used, 100 µL of PBS 1X containing ~$0.2x10^6$ cells were stained per well.

After being added 100 µL of cells to the plate, cells were washed once with PBS 1X by centrifuging at 1200 rpm, for 2 minutes. Pellet was resuspended and 25 µL of antibodies (except anti-IL-4 and anti-IFN-γ) and tetramers diluted in FACS Buffer were added with the corresponding dilutions to each well (1 dilution = 1 well; 4 dilutions = 4 wells of the same antibody/ tetramer). Both PBMCs and iNKT cells from the cell line were incubated in the dark for 20 minutes at 4 °C. Cells were washed once with 100 µL of FACS Buffer (centrifuged at 1200 rpm, for 2 minutes). In the case of the fixable viability dye, cells were incubated in the dark for 30 min, at room temperature (manufacturer's instructions). After centrifuging, cells were resuspended in 200 µL of PBS 1% paraformaldehyde (PFA) and incubated in the dark for 15 minutes, at room temperature. After 15 minutes, plate was centrifuged at 1200 rpm, for 2 minutes, and pellet was washed once with 200 µL of FACS Buffer (centrifuged at 1200 rpm, for 2 minutes), resuspended in 200 µL of FACS Buffer, filtered, and transferred to FACS tubes.

A well containing unstained cells was used as a control in each experiment. The higher concentration of each antibody and tetramer that was titrated was used as single-stained control. Since the fixable viability dye was titrated in fresh PBMCs, half of the amount of PBMCs designated to the well of the single fixable viability dye were submitted to 65 ºC for 5 minutes in a heating block. This way it was possible to have dead and live cells in this single stain, which enabled a better separation of the negative and positive cells after the staining. The staining of the fixable viability dye is due to the reaction between the dye and cellular amino groups. The dye is not able to penetrate live cell membranes,

only cell surface proteins react with the dye, whereas on dead cells, it penetrates their membranes, staining intracellular amines, which results in a more intense fluorescence. Therefore, viable and non-viable cells are distinguished by their difference in fluorescence intensity.

Besides the singles and unstained, Fluorescence Minus One (FMOs) controls were done for the antibodies anti-PD-1 BV785 and anti-ICOS APC, which presented a stain that did not distinguish negative from positive populations. FMOs are samples stained with all the fluorophores in the panel, minus one of them, in this case, minus BV785 or APC, respectively. Hence, a more accurate gating control was done for these markers, because the widening of negative populations due to spillover spread is taken into account.

Intracellular staining

Antibodies against the cytokines IL-4 and IFN-γ were titrated in activated T cells (Section **4) Activation of T cells with phorbol myristate acetate and ionomycin**) from isolated PBMCs from a Buffy Coat.

After PMA and ionomycin activation, cells were centrifuged at 1300 rpm for 3 minutes, and supernatants were discarded. Cells were kept on ice in buffers with BFA (Sigma) at 10 μg/mL to prevent cytokine secretion, until the fixation step. Then, each well was washed with 150 μL of PBS 1X + BFA (centrifuged at 1300 rpm for 3 minutes). Resuspended pellet was incubated in 150 μL of PFA 2% for 10 minutes, at room temperature, in the dark (fixation step). The plate was centrifuged at 1300 rpm for 3 minutes and supernatants were discarded. A permeabilization solution, PBS Saponin (PBS 1X + 2% FBS + 1mM EDTA + 0.01% NaN3 + 0.5% Saponin), was added to each well and incubated in the dark for 5 minutes. After the incubation, the plate was centrifuged and pellet was resuspended. 25 μL of fluorochrome-labeled antibodies for intracellular cytokines (anti-IL-4 and anti-IFN-γ) diluted in FACS Buffer were added with the corresponding dilutions to each well. After incubation for 30 minutes, at 4 ºC, in the dark, the wells were washed with 200 μL of PBS Saponin, and cells were fixed with PFA 1%, as explained previously. Wells were washed once with 150 μL of FACS Buffer (centrifuged at 1300 rpm for 3 minutes) and resuspended in 200 μL of FACS Buffer, filtered, and transferred to FACS tubes.

Anti-CXCR6 was also titrated intracellularly to investigate if the antibody was working. iNKT cell line was used for this titration and iNKT cells were not stimulated prior staining. The protocol for intracellular staining was followed as mentioned above.

Reference controls

In Cytek Aurora cytometer, it is possible to re-use/ save the single-stained and unstained samples, which are called "reference controls". These controls provide the individual fluorescence spectra that is necessary to unmix the data (compensation).

Since the number of cells is limited with patients, reference controls (except the unstained sample, which needs to be done every experiment as a control) were acquired before the patients, using compensation beads (UltraComp eBeads™ Compensation Beads, Invitrogen™). These beads are microspheres coated with antibodies designed to identify antibody light chains specific to certain species, being crucial to guarantee their ability to attach to the species in which the antibody labelled with fluorochrome was developed. Compensation beads are a mixture of antibody-coated and uncoated compensation beads, allowing the detection of positive and negative signals, respectively, for the fluorochrome. However, for the fixable viability dye and CD1d PBS-57 tetramer BV421, compensation beads can't be used as they cannot bind. Instead, the single-stained for the fixable viability dye contained half live, half dead (by heat shock) PBMCs (isolated from a Buffy Coat) and the iNKT cell line was used for the single-stain of CD1d PBS-57 tetramer BV421 (enabling a higher percentage of positive iNKT cells compared to isolated PBMCs). These single-stained samples were done only after the optimal concentrations of each antibody, tetramer and fixable viability dye had been defined (**Table 5**).

The compensation beads were treated as if they were cells, to eliminate additional variabilities. First, the vial containing the beads was vortexed vigorously. Three drops of compensation beads were added per 1 mL of PBS. 100 µL of this mix were added per well in a round-bottomed 96-well plate, each well corresponding to a different antibody from **Table 5** (antibodies used with the patients). Afterwards, extracellular staining was performed as mentioned above: first by centrifuging the plate and then by adding the

optimal concentration of each antibody to the corresponding well. The rest of the protocol was followed.

These reference controls were done only once and have to be done every ~ 6 months (if parameters of the cytometer are changed) or every time a new antibody/ tetramer is purchased or used.

With patients

From the PBMCs isolated from Fabry disease patient's blood samples, three fractions were analysed by flow cytometry: PBMCs before enrichment (fresh PBMCs that did not go through anti-iNKT Microbeads enrichment), positive fraction (fraction enriched in iNKT cells after anti-iNKT Microbeads enrichment) and negative fraction (fraction without iNKT cells after anti-iNKT Microbeads enrichment). For these three different fractions, a different mix/ flow cytometry panel was done. A well containing unstained PBMCs before enrichment was used as negative control.

In **Table 5**, the antibodies, tetramers and fixable viability dye used to stain each fraction are represented.

Table 5. Antibodies, tetramers and fixable viability dye used with Fabry disease patients for staining experiments and respective information.

Fraction	Antibody/ Tetramer	Clone	Fluorochrome	Dilution	Brand
PBMCs before enrichment	Human CD1d PBS-57 Tetramer	-----	BV421	1:800	NIH
	Anti-human CD3	OKT3	BB700	1:100	BD Biosciences
	Anti-human CD19	HIB19	PE-Cy7	1.5:100	Thermo Fisher
	Anti-human CD14	OFC14D	PerCP	1:100	Biolegend
	Anti-human CD40	5C3	FITC	3:100	Biolegend

Positive Fraction	Anti-human CD86	BU63	APC	1:50	Biolegend
	Human CD1d PBS-57 Tetramer	-----	BV421	1:800	NIH
	Anti-human CD3	OKT3	BB700	1:100	BD Biosciences
	Anti-human CD4	RPA-T4	PE-Cy7	1:100	Biolegend
	Anti-human CD8α	HIT8a	APC-Cy7	1:100	Biolegend
	Anti-human CD8β	SIDI8BEE	PE	1:100	Thermo Fisher
	Anti-human TIM-3 (CD366)	F38-2E2	BV711	1:50	Biolegend
	Anti-human PD-1 (CD279)	EH12.2H7	BV785	1:40	Biolegend
	Anti-human ICOS (CD278)	C398.4A	APC	1:100	Biolegend
	Anti-human CD161	HP-3G10	PE-Cy5	1:100	Biolegend
Negative Fraction	Human CD1d PBS-57 Tetramer	-----	BV421	1:800	NIH
	Anti-human CD3	OKT3	BB700	1:100	BD Biosciences
Fixable Viability Dye			Zombie Aqua	1:400	Biolegend

Abbreviations: APC – Allophycocyanin; BV – Brilliant Violet; Cy – Cyanine; FITC – Fluorescein; PE – Phycoerythrin; PerCP - Peridinin chlorophyll protein; PBS-57 – αGal-Cer analog; BB- Brilliant Blue.

Once the optimal concentrations of each antibody, tetramer and fixable viability dye had been defined, they were used in Fabry disease patient's samples and healthy controls. Here, it was important to analyse the cell viability, which was done by staining the fixable viability dye in each fraction studied. After PBMCs isolation from the blood tubes (patients) or Buffy Coats (controls), $0.2x10^6$ PBMCs in 100 µL of PBS 1X were plated

in two wells of a round-bottomed 96-well plate: unstained sample and PBMCs before enrichment sample. After iNKT cell enrichment with anti-iNKT MicroBeads, $0.2x10^6$ cells (in 100 µL of PBS 1X) of the negative fraction and the totality of cells (in 100 µL of PBS 1X) obtained in the positive fraction were plated in the designated wells. Plate was centrifuged at 1200 rpm for 2 minutes and pellets were resuspended in 25 µL of fixable viability dye (with the double concentration: 1:200) diluted in PBS. After incubating in the dark for 15 minutes at room temperature, 25 µL of the mixes diluted in FACS Buffer were added to the corresponding wells, without washing. The antibodies, tetramers and fixable viability dye used are described in **Table 5**, with the corresponding fraction. The rest of the extracellular staining was followed as mention previously.

With patients, intracellular staining was not performed, since the cytokines were not analysed.

8) Statistical analysis

Statistical analyses were performed using GraphPad Prism software v8.0.1.

Mean and standard deviation values were calculated and statistical significance was assessed by paired T-Test with Welch's correction (for the comparison of the percentage of iNKT cells within different fractions using anti-iNKT MicroBeads) and unpaired T-Test with Welch's correction (for the rest of the experiments, when comparing healthy controls with patients). P-values below 0.05 were considered significant.

1. Preparation of the documents to submit to the *Centro Hospitalar Universitário de São João* Ethical Committtee and Data Protection Officcer

This work was funded by National Funds through FCT—*Fundação para a Ciência e a Tecnologia*, I.P., under the project 2022.01788.PTDC. This master thesis started the study funded by FCT, which first required the submission of the necessary paperwork regarding ethics and data protection from *Centro Hospitalar Universitário de São João* where the patients and healthy donors were going to be recruited.

Obtaining ethical and data protection approval is crucial when conducting research involving human participants. This approval ensures the protection of their well-being, rights, and dignity, as well as, the protection of data relative to the participants. In order to proceed the research of iNKT cells in Fabry disease patients and healthy controls, the study had to be approved by the *Centro Hospitalar Universitário de São João* Ethical Committee and Data Protection Officer.

Ten documents had to be submitted to the committee, which included the "Protocol of the study/research project, with the respective instruments", "Participant information" and "Data protection impact assessment" (all the information was available in CHUSJ website in the section "*Submissão de projetos de investigação ao CHUSJ*").

Little did I know about writing ethical and data protection documents and the minor details sometimes were the most important ones (it could be a word that was not in accordance with the appropriate language and the project could be rejected). The help from the i3S Data Protection Officer, Gabriela Almeida, was fundamental to fill in the "Data protection impact assessment" document. Besides data protection, Prof. João Paulo Oliveira always puts the interests and safety of his patients first and the meetings with him were crucial to be sure the document involving all the data that was being collected from the patients was always taking into account the patients primarily.

Documents were submitted and the research was accepted at the first attempt by the *Centro Hospitalar Universitário de São João* ethical committee and Data Protection

Officer. The documents with the approval from Ethical Committee and Data Protection Officer are present in **Appendix I** and **Appendix II**, respectively.

2. Design, optimisation and validation of experimental conditions for human iNKT cell phenotype analyses

When working with human patients, especially with a rare disease, all experimental protocol steps, reagents and materials must be well defined and tested before proceeding with the patients' samples. Although this is a known truth for every research field, there is no space for error when the samples are limited. In this part of the results, the design, titrations, experimental set up and optimisations will be described.

2.1 Design of the flow cytometry panel

iNKT cells were immunophenotyped by Flow Cytometry, using a variety of markers, and, for that, samples were acquired in a 4 Laser Cytek® Aurora Flow Cytometer which leverages full spectrum technology. This type of technology, by measuring the full spectrum of light emissions, enables the collection of the entire spectral profile (or signature) of fluorochromes, differentiating combinations of fluorochromes that conventional Flow Cytometry cannot. As a result, it is possible to develop highly complex multicolour panels for analyses by flow cytometry[200–202].

Prior to designing a flow cytometry panel, many considerations need to be taken into account, especially when the panel is going to be composed by many markers (meaning many fluorochromes)[203]:

1) The frequency of the cells positive for each marker and its Median Fluorescence Intensity (MFI), a measure of the fluorescence intensity of the cells that varies in accordance with the tissue the cells are being analysed in;
2) Apply fluorochromes to each marker based on 1): higher MFI needs a dimmer fluorochrome whereas a lower MFI requires a brighter one; Besides this, it needs to be taken into account that when we are dealing with rare populations of cells, like iNKT cells, a brighter fluorochrome is usually needed;

3) After selecting the ones that need to have a brighter or dimmer fluorochrome, other fluorochromes are attributed to other markers, including a viability dye;
4) Although it's easy to create this "imaginary" panel, the next step is to look into the supplier's antibodies/ tetramers and see if the fluorochrome attributed to each marker is available. If not, start by changing the ones that are rarer and attribute those an adequate fluorochrome; Antibodies against CD3 or CD4, for example, are easy to find and all fluorochromes are often available, so they can be the last to be chosen;
5) Finally, check if all markers are attributed the right fluorochrome and purchase the antibodies, tetramers and fixable viability dye.

In order to study the iNKT cells, *ex vivo* and *in vitro* analyses were going to be performed, thence, three flow cytometry panels were designed. The first panel (**Table 6**) was going to be used to study iNKT cells preceding enrichment with anti-iNKT MicroBeads. With this panel it is possible to identify iNKT cells (CD1d PBS-57 Tetramer and Anti-CD3) and study their frequency before enrichment. Besides this, B cells (Anti-CD19) and monocyte (Anti-CD14) frequencies can also be evaluated as well as monocyte activation state (Anti-CD40 and Anti-CD86).

Table 6. Antibodies, Tetramers and Viability Dye list for ex vivo analyses of human iNKT cells prior Anti-iNKT MicroBeads enrichment. Antibodies, Tetramers and Viability Dye that are going to be used in the mix for iNKT cells analyses prior Anti-iNKT MicroBeads enrichment are listed as well as respective clone (for antibodies) and fluorochrome.

Antibody/ Tetramer	Clone	Fluorochrome
Human CD1d PBS-57 Tetramer	-----	BV421
Anti-human CD3	OKT3	PerCP-Cy5.5
Anti-human CD19	HIB19	PE-Cy7
Anti-human CD14	OFC14D	PerCP
Anti-human CD40	5C3	FITC
Anti-human CD86	BU63	APC
Fixable Viability Dye		Zombie Aqua

On the second panel (**Table 7**), after Anti-iNKT MicroBeads enrichment, iNKT cells, were going to be analysed (CD1d PBS-57 Tetramer and anti-CD3) along with MAIT cells (MR1 5-OP-RU Tetramer). Note that we didn't want to obtain 100% iNKT cells with the anti-iNKT MicroBeads enrichment, in order to investigate other T lymphocytes (See **section 2.3) Anti-human iNKT cell Microbeads**). T cells (Anti-CD3) and iNKT cells were going to be studied taking into account the phenotype (Anti-CD4, anti-CD8α and CD8β) and exhaustion state (Anti-TIM-3 and anti-PD-1). Moreover, the circulating population of iNKT cells discovered by Cui et al.[181] was going to be analysed in Fabry disease patients and healthy controls (Anti-CD244 and anti-CXCR6).

Table 7. Antibodies, Tetramers and Viability Dye list for ex vivo analyses of human iNKT cells after Anti-iNKT MicroBeads enrichment. Antibodies, Tetramers and Viability Dye that are going to be used in the mix for iNKT cells analyses after Anti-iNKT MicroBeads enrichment are listed as well as respective clone (for antibodies) and fluorochrome.

Antibody/ Tetramer	Clone	Fluorochrome
Human CD1d PBS-57 Tetramer	-----	BV421
Human MR1 5-OP-RU Tetramer	-----	AF488
Anti-human CD3	OKT3	PerCP-Cy5.5
Anti-human CD4	RPA-T4	PE-Cy7
Anti-human CD8α	HIT8a	APC-Cy7
Anti-human CD8β	SIDI8BEE	PE
Anti-human TIM-3 (CD366)	F38-2E2	BV711
Anti-human PD-1 (CD279)	EH12.2H7	BV785
Anti-human CD244 (2B4)	K041E5	APC
Anti-human CXCR6 (CD186)	C1.7	PE-Cy5
Fixable Viability Dye		Zombie Aqua

Last but not least, after Anti-iNKT MicroBeads enrichment, iNKT cells were going to be stimulated in order to study the cytokine production. The third panel (**Table 8**), besides enabling the study of stimulated T cells (Anti-CD3) and iNKT cells (CD1d PBS-57 Tetramer and Anti-CD3) phenotype, it also inspects the cytokine production (Anti-IFN-γ

and anti-IL-4) by these cells. Cell viability was going to be evaluated in all panels using a fixable viability dye (Zombie Aqua- **Tables 6**, **7** and **8**).

Table 8. Antibodies, Tetramers and Viability Dye list for in vitro analyses of human stimulated iNKT cells after Anti-iNKT MicroBeads enrichment. Antibodies, Tetramers and Viability Dye that are going to be used in the mix for stimulated iNKT cells analyses after Anti-iNKT MicroBeads enrichment are listed as well as respective clone (for antibodies) and fluorochrome.

Antibody/ Tetramer	Clone	Fluorochrome
Human CD1d PBS-57 Tetramer	-----	BV421
Anti-human CD3	OKT3	FITC
Anti-human CD4	RPA-T4	PE-Cy7
Anti-human CD8α	HIT8a	APC-Cy7
Anti-human CD8β	SIDI8BEE	PE
Anti-human IFN-γ	4S.B3	BV711
Anti-human IL-4	8D4-8	APC
Fixable Viability Dye		Zombie Aqua

These three panels were first defined based on the markers that wanted to be studied and, afterwards, the fluorochromes were selected. In order to select the correct fluorochromes, their brightness needed to be taken into account: phycoerythrin (PE), Brilliant Violet 421 (BV421), BV711 and Phycoerythrin-Cy5 (PE-Cy5) are very bright fluorochromes, whereas Peridinin chlorophyll (PerCP) is dim. In-between these, there are bright [BV605, Allophycocyanin (APC), Alexa Fluor 488 (AF488) and PE-Cy7] and moderate fluorochromes [peridinin chlorophyll-Cy5.5 (PerCP-Cy5.5) and fluorescein isothiocyanate (FITC)].

Starting with iNKT cells, they are identified using the CD1d PBS-57 Tetramer, which can be obtained from NIH tetramer core facility. However, there aren't many fluorochrome options available for the tetramer. Taking into account that the percentage of iNKT cells is low in peripheral blood (usually between 0.001% and 0.1%), but the MFI of these cells is considerably high, BV421 was the chosen fluorochrome for the three panels (**Tables 6**, **7** and **8**)[104,144,145]. APC labelled CD1d PBS-57 tetramer was also acquired in case another panel was designed. MAIT cells are identified by using the MR1

5-OP-RU Tetramer which is also available at NIH tetramer core facility and few fluorochromes are provided. Like iNKT cells, the frequency of circulating MAIT cells is low and their MFI is high, so, AF488 was the chosen fluorochrome for the MR1 tetramer[183,187,204]. Additionally, BV421 labelled MR1 5-OP-RU tetramer was selected in case this tetramer was used in other mix without the CD1d PBS-57 tetramer. The rest of antibodies for the first panel (**Table 6**) have already been tested and used in the lab by other researchers, except anti-CD3. The fluorochrome for antibody against CD3 was only selected at the end to fit the first and second panels (**Tables 6** and **7**, respectively).

For the second panel (**Table 7**), as the CD1d PBS-57 tetramer was already defined, BV711 and BV785 were the fluorochromes selected for anti-TIM-3 and anti-PD-1, respectively, as the frequency and MFI of these markers on iNKT cells are low[178–180]. anti-CD8β isn't commonly used and, for that reason, doesn't dispose of many fluorochromes and it also needs a bright one, since it is expected a low percentage of positive cells for CD8β[147]. PE was the chosen fluorochrome for anti-CD8β. Little is known about the expression of CXCR6 and CD244 on iNKT cells, so APC and PE-Cy5 were the fluorochromes selected for the antibodies against these markers, respectively. The fluorochrome APC-Cy7 was selected for the antibody anti-CD8α since the frequency of $CD8\alpha^+$ iNKT cells is low[147,170]. Based on this panel, the fluorochrome PE-Cy7 was chosen for anti-CD4 since it was already available in the lab. Besides this, PerCP-Cy5.5 labelled anti-CD3 was selected for both before and after enrichment with Anti-iNKT MicroBeads panels, without stimulation (**Tables 6** and **7**, respectively), since it was already available in the lab.

Last but foremost, for the third panel (**Table 8**), used to study stimulated iNKT cells after enrichment, almost every fluorochrome was decided, except for the cytokines. BV711 and APC were the chosen fluorochromes for IFN-γ and IL-4, respectively. Furthermore, another fluorochrome was chosen for anti-CD3, FITC, to use in this panel. The fixable viability dye was the last to be chosen in order to be adequate for all panels: Zombie Aqua (excited by the Violet Laser at 405 nm). After designing each panel, the spectra of the fluorochromes were analysed to evaluated if the peaks didn't overlap and it is possible to observe that in fact they don't (**Figure 12**).

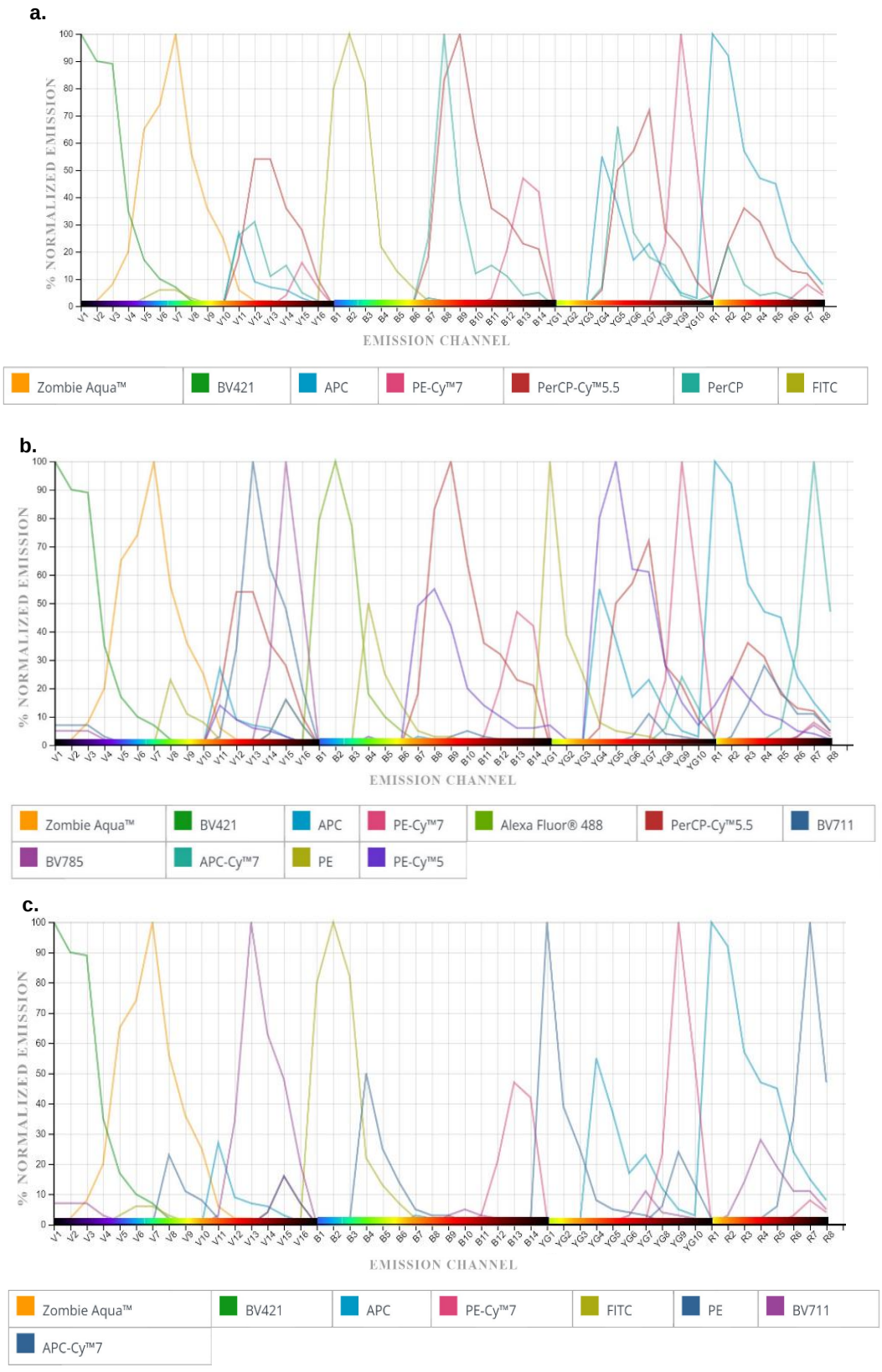

Figure 12. Fluorochromes spectra of flow cytometry panels. a. Fluorochromes spectra of flow cytometry panel for iNKT cell analyses before enrichment with Anti-iNKT MicroBeads. **b.** Fluorochromes spectra of flow cytometry panel for iNKT cell analyses after enrichment with Anti-iNKT MicroBeads. **c.** Fluorochromes spectra of flow cytometry panel for stimulated iNKT cell analyses after enrichment with Anti-iNKT MicroBeads. Spectra were created with Cytek® Full Spectrum Viewer.

The Similarity Indices of each mix were also measured. The Similarity™ Index, varying from 0-1, measures the uniqueness of dye pair: values close to 0 indicate that the full spectrum signatures of the 2 dyes exhibit significant dissimilarity, while values close to 1 indicate a high degree of similarity between the signatures. Two dyes can be used if Similarity™ Index < 0.98 (information provided by Cytek®). Looking at **Table 9** (**a.**, **b.** and **c.**), the fluorochromes chosen for each panel can be used, because they all have a Similarity™ Index < 0.98.

Table 9. Values of Similarity Indices of the fluorochromes from the flow cytometry panel. a. iNKT cell analyses before enrichment with Anti-iNKT MicroBeads. **b.** iNKT cell analyses after enrichment with Anti-iNKT MicroBeads. **c.** stimulated iNKT cell analyses after enrichment with Anti-iNKT MicroBeads. Tables were created with Cytek® Full Spectrum Viewer.

a.

	Zombie Aqua	BV421	APC	PE-Cy7	PerCP-Cy5.5	PerCP	FITC
Zombie Aqua	1	0.16	0.01	0	0	0.01	0.06
BV421	0.16	1	0	0	0	0.01	0.01
APC	0.01	0	1	0.05	0.36	0.33	0
PE-Cy7	0	0	0.05	1	0.23	0.09	0
PerCP-Cy5.5	0	0	0.36	0.23	1	0.8	0
PerCP	0.01	0.01	0.33	0.09	0.8	1	0.01
FITC	0.06	0.01	0	0	0	0.01	1

b.

	Zombie Aqua	BV421	APC	PE-Cy7	Alexa Fluor 488	PerCP-Cy5.5	BV711	BV785	APC-Cy7	PE	PE-Cy5
Zombie Aqua	1	0.16	0.01	0	0.01	0	0.03	0.02	0	0.09	0.01
BV421	0.16	1	0	0	0	0	0.09	0.08	0	0	0
APC	0.01	0	1	0.05	0	0.36	0.22	0.04	0.18	0.04	0.52
PE-Cy7	0	0	0.05	1	0	0.23	0.11	0.17	0.29	0.02	0.14
Alexa Fluor 488	0.01	0	0	0	1	0	0	0	0	0.07	0.01
PerCP-Cy5.5	0	0	0.36	0.23	0	1	0.49	0.19	0.14	0.05	0.72
BV711	0.03	0.09	0.22	0.11	0	0.49	1	0.49	0.19	0.01	0.14
BV785	0.02	0.08	0.04	0.17	0	0.19	0.49	1	0.22	0	0.03
APC-Cy7	0	0	0.18	0.29	0	0.14	0.19	0.22	1	0	0.08
PE	0.09	0	0.04	0.02	0.07	0.05	0.01	0	0	1	0.14
PE-Cy5	0.01	0	0.52	0.14	0.01	0.72	0.14	0.03	0.08	0.14	1

c.

	Zombie Aqua	BV421	APC	PE-Cy7	FITC	PE	BV711	APC-Cy7
Zombie Aqua	1	0.16	0.01	0	0.06	0.09	0.03	0
BV421	0.16	1	0	0	0.01	0	0.09	0
APC	0.01	0	1	0.05	0	0.04	0.22	0.18
PE-Cy7	0	0	0.05	1	0	0.02	0.11	0.29
FITC	0.06	0.01	0	0	1	0.09	0	0
PE	0.09	0	0.04	0.02	0.09	1	0.01	0
BV711	0.03	0.09	0.22	0.11	0	0.01	1	0.19
APC-Cy7	0	0	0.18	0.29	0	0	0.19	1

After all antibodies, tetramers and fixable viability dye being decided for the flow cytometry panels, they were then titrated and the chosen titter was tested in the mix with all reagents from each panel.

2.2 Titration of Antibodies, Viability Dye and Tetramers

Before using an antibody or tetramer for flow cytometric analyses, its optimal concentration needs to be determined. This is obtained by perfoming titrations in which the antibody amount is determined resulting from the highest signal of the positive population along with the lowest signal of the negative population.

Titrations experiments were analysed using the Staining Index plugin from FlowJo software. PBMCs isolated from Buffy Coats or iNKT cells from a cell line were stained with a series of dilutions of the different antibodies and tetramers, ranging from 1:100 to 1:800. When these concentrations weren't sufficient to detect the marker, dilution range was shifted to 1:50 to 1:200 and 1:20 to 1:160, depending on the antibody. The SI values were calculated based on the MFI of the antibodies/ tetramers positive and negative populations. The ideal concentration was chosen taking into account the highest SI values and the greatest positive and negative populations separation.

From the blood samples that were received from Fabry disease patients, PBMCs were isolated and, afterwards, markers were identified in fresh iNKT cells, isolated using Anti-iNKT microbeads. Firstly, these microbeads needed to be tested before being used with patient's samples. However, in order to test the microbeads, the optimal antibodies/ tetramers concentrations had to be already known, since the quantity of iNKT cells obtained is usually not enough to test the four dilutions of the antibodies. And, even if it was, it wouldn't be enough to titrate several antibodies/tetramers at the same time, leading to time and cost expenses. Thus, to solve this problem, PBMCs isolated from Buffy Coats and/or an iNKT cell line were used to titrate the antibodies and tetramers. The type of cells chosen was dependent of the level of expression of the marker in the cells. The cell markers CD3, CD4, CD8α, CD8β, CD244, CD161 are considerably expressed in lymphocytes and, therefore, they were titrated in PBMCs. The viability dye, Zombie Aqua, as the name itself says, is used to distinguish the live from the dead cells so it was titrated using PBMCs as well. TIM-3 and PD-1 were first titrated using the iNKT cell

line, since they are more expressed in non-activated iNKT cells than in conventional T cell lymphocytes[178–180] and the chosen antibody concentration was tested using PBMCs. CD1d PBS57 Tetramers were first titrated using the iNKT Cell line and PBMCs (1:1), then with the iNKT Cell line only (which is not 100% pure, so we were able to distinguish a positive and a negative populations for the tetramer) and finally using PBMCs, in order to confirm if the optimal tetramer concentration in the iNKT Cell line also worked in fresh iNKT cells. MR1 tetramers, which recognise MAIT cells, were titrated in PBMCs. ICOS was titrated in fresh lymphocytes and iNKT cells. The marker CXCR6 was an exceptional case, since its antibody was tested in several conditions because the results that were being obtained weren't the expected[181]: PBMCs, iNKT Cell line (extracellular and intracellular staining), fresh iNKT Cell with or without anti-iNKT cell isolation (see **section 2.2.4) Titration of Anti-CXCR6**). Anti-IL-4 and anti-IFN-γ were titrated in stimulated PBMCs, since these markers are not expressed on resting lymphocytes, but are inducible in response to activation or other stimuli[197,205].

2.2.1 Titration of Anti-CD3, Anti-CD4, Anti-CD8α, Anti-CD8β, Anti-CD244, Anti-CD161 and Zombie Aqua (Viability Dye) in PBMCs

Anti-CD3, anti-CD4, anti-CD8α, anti-CD8β, anti-CD244, anti-CD161 and Zombie Aqua (Viability Dye) were titrated in PBMCs isolated from Buffy Coats. After PBMCs isolation, extracellular staining was performed for each dilution, ranging from 1:100 to 1:800, and stained cells were acquired in Cytek® Aurora Spectral Flow Cytometer.

The flow cytometry gating strategy used for the analyses of lymphocytes from the isolated PBMCs is shown in **Figure 13**. Briefly, lymphocytes were gated according to their size (forward scatter – FSC) and granularity (side scatter – SSC), followed by singlets selection. The positive cells were selected according to the cells stained for each antibody or Viability Dye and also based on the unstained sample. Then, fcs files from the different antibody dilutions and unstained were concatenated in order to have a better perspective of the separation of the positive and negative cells in each dilution (bottom right plot of **Figure 13**).

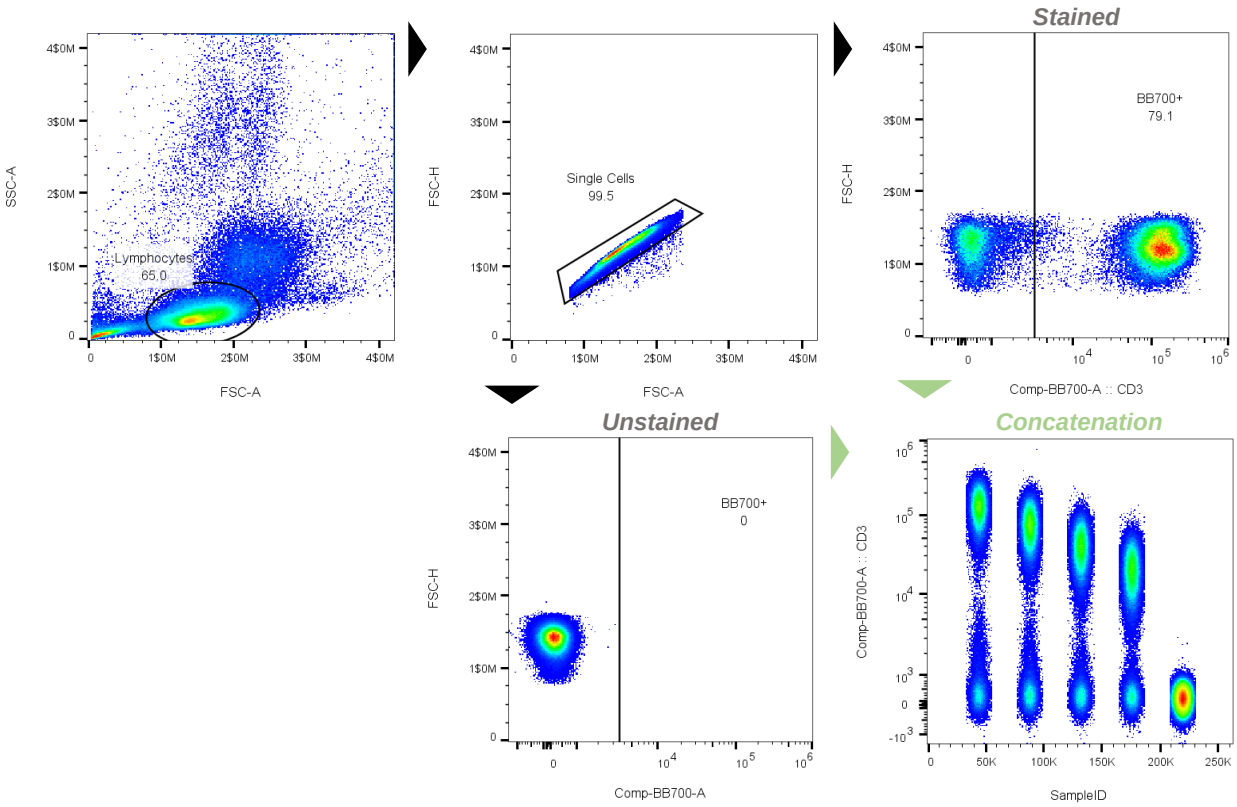

Figure 13. Representative gating strategy used to titrate the antibodies and viability dye in PBMCs isolated from Buffy Coats. Lymphocytes were gated according to their size (forward scatter – FSC) and granularity (side scatter – SSC), followed by singlets selection. Positive cells were selected according to the cells stained for each antibody or Viability Dye. Each dilution along with the unstained sample (left bottom plot) were concatenated (right bottom plot).

SI values for each antibody and viability dye concentration were calculated and the optimal antibody and viability dye volumes were selected based on these values and positive and negative populations separation, looking at the concatenated plots (**Figure 14**).

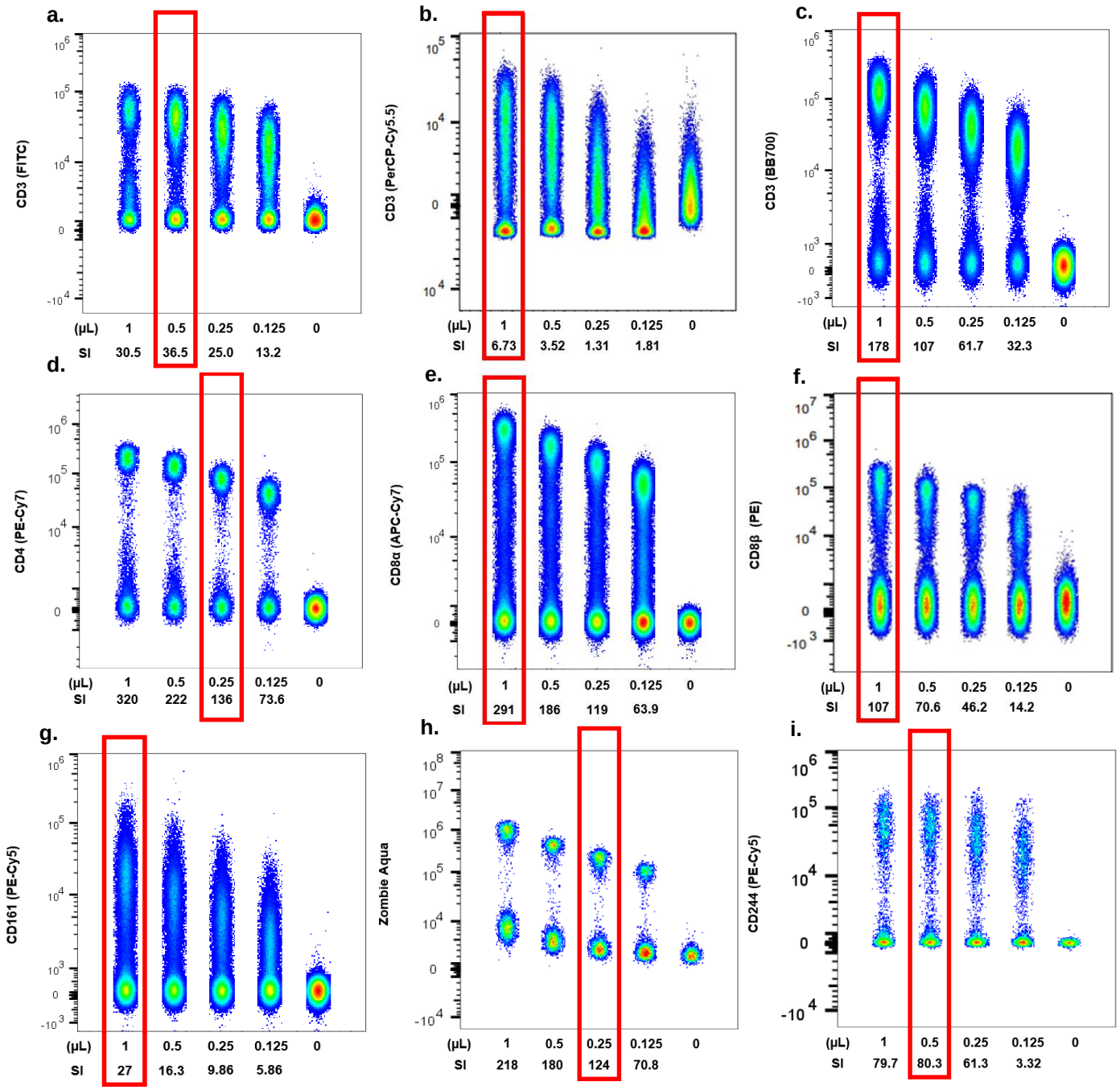

Figure 14. Titrations of antibodies and viability dye used in this project. Titrations were done using isolated PBMCs from Buffy Coats in 6 different experiments (6 healthy donors were used). Dilutions are represented in µL of stock antibody concentration diluted in 100 µL of FACS Buffer. 0 µL represents the unstained cells. The Staining Index (SI) was calculated for each dilution using the formula: SI = [(Median of positive cells) – (Median of negative cells)]/ (2 × Standard Deviation of negative cells). The red box demarcates the selected dilutions. From plots a. till i., titrations of Anti-CD3 FITC (200 µg/mL), Anti-CD3 PerCP-Cy5.5 (50 µg/mL), Anti-CD3 BB700 (100 µg/mL), Anti-CD4 PE-Cy7 (200 µg/mL), Anti-CD8α APC-Cy7 (100 µg/mL), Anti-CD8β PE (25 µg/mL), Anti-CD161 PE-Cy5 (200 µg/mL), Fixable Viability Dye (Zombie Aqua) and Anti-CD244 PE-Cy5 (100 µg/mL) are represented, respectively.

The optimal concentration for anti-CD3 FITC (**Figure 14 a.**) and anti-CD244 PE-Cy5 (**Figure 14 i.**) is 1:200, since the SI value for this dilution is the highest in both cases (36.5 and 80.3, respectively) and it is the one that best separates the positive from the negative cells. 1:100 was the chosen dilution for the anti-CD3 PerCP-Cy5.5 (**Figure 14 b.**), anti-CD3 BB700 (**Figure 14 c.**), anti-CD8α APC-Cy7 (**Figure 14 e.**), anti-CD8β PE (**Figure 14 f.**) and anti-161 PE-Cy5 (**Figure 14 g.**) antibodies, in view of the fact that 1:100 present the highest SI value (6.73, 178, 291, 107 and 27, respectively) and separation of negative and positive cells. Anti-CD4 PE-Cy7 is going to be used with a dilution of 1:400 (0.25 µL in 100 µL), because, even though 1:100 presents the highest SI value (320), 1:400 has less non-specific background around the $CD4^-$ population than the higher concentrations (**Figure 14 d.**). In the case of the Fixable Viability Dye (Zombie Aqua), although 1:100 dilution has the highest SI value and separates better the positive and negative populations, 1:400 was chosen as the optimal concentration (**Figure 14 h.**). This is given to the fact that Zombie Aqua is only used to distinguish live from dead cells and that can be done when using just 1:400.

In spite of the three antibodies anti-CD3 titrated being from the same clone, OKT3, as they possess different fluorochromes, the separation between positive and negative cells for CD3 is different (**Figures 14 a.**, **b.** and **c.**). In panels 1 and 2 (**Tables 6** and **7**, respectively), PerCP-Cy5.5 was the chosen fluorochrome for anti-CD3. However, and as it is observed in **Figure 14 b.**, $CD3^+$ population is not completely clear, and as our identification of iNKT cells also depends on this marker, an anti-CD3 labelled with BB700 was tested (**Figure 14 c.**). BB700 belongs to same channel as PerCP-Cy5.5. BB700 labelled anti-CD3 was the chosen antibody for CD3 because a distinct separation of $CD3^+$ and $CD3^-$ cells is observed.

2.2.2 Titration of Anti-PD-1 and Anti-TIM-3

TIM-3 and PD-1 are more expressed in iNKT cells than in conventional T cells[178–180], as mentioned above, having a better chance of being optimally titrated in iNKT cells rather than in lymphocytes. The iNKT Cell line was used to titrate these antibodies (**Figure 15**) and the optimal concentrations were then tested in PBMCs (**Figure 16**).

In spite of needing cell activation to have more expression at the cell surface, TIM-3 and PD-1 are apoptosis and exhaustion markers and Fabry disease patients' PBMCs were not going to be activated because that is one of the questions that needs to be clarified: are iNKT cells more exhausted or in apoptosis in Fabry disease patients? As so, the titration had to be performed in the same conditions, without stimulation.

According to Nakagawa et al., the optimal concentration of each antibody, using activated cells, is 5 µl of anti-PD-1 in 100 µl of FACS Buffer (1:20) and 0.3 µl of anti-TIM-3 in 100 µl of FACS Buffer (0.3:100)[206]. For anti-TIM-3, although the fluorochrome used by Nakagawa et al. is the same as ours (BV711), the clone is different as well as the supplier. On the other hand, anti-PD-1 possesses the same clone (EH12.2H17) and it's from the same supplier as the one used by Nakagawa et al., but ours is labelled with a different fluorochrome. Despite these differences and looking at the concentrations used by the authors, these antibodies may need more concentration than the rest of the antibodies titrated, whose titrations concentrations ranged from 1:100 to 1:800. Therefore, anti-PD-1 was titrated using the concentrations 1:20, 1:40, 1:80 and 1:160 whereas anti-TIM-3 was titrated with 1:50, 1:100 and 1:200 concentrations. For anti-TIM-3 higher concentrations were used than in the article, because the optimal concentration obtained by the researchers is even lower than the ones chosen for antibodies that don't need activated cells.

The flow cytometry gating strategy used to analyse iNKT cells from the cell line is the equivalent to the one shown in **Figure 13**. However, iNKT cells were gated according to their size (forward scatter – FSC) and granularity (side scatter – SSC), instead of lymphocytes, followed by singlets selection (**Figure 15 a.**). Afterwards, the same strategy for concatenation and SI plugin was also used.

Consistent with the SI values, looking at the plots of anti-TIM-3 (**Figure 15 b.**), 2 µl of anti-TIM-3 in 100 µl of FACS Buffer (1:50) is the ideal concentration for this antibody. Therefore, 1:50 was the chosen dilution to use anti-TIM-3.

According to the SI values, 5 µl of anti-PD-1 in 100 µl of FACS Buffer (1:20) is the optimal anti-PD-1 concentration (10.3). Nonetheless, with the second highest concentration is still possible to observe distinct positive and negative populations and

the SI value is still 8.59. Hence, the selected dilution for this antibody was 1:40 (**Figure 15 c.**).

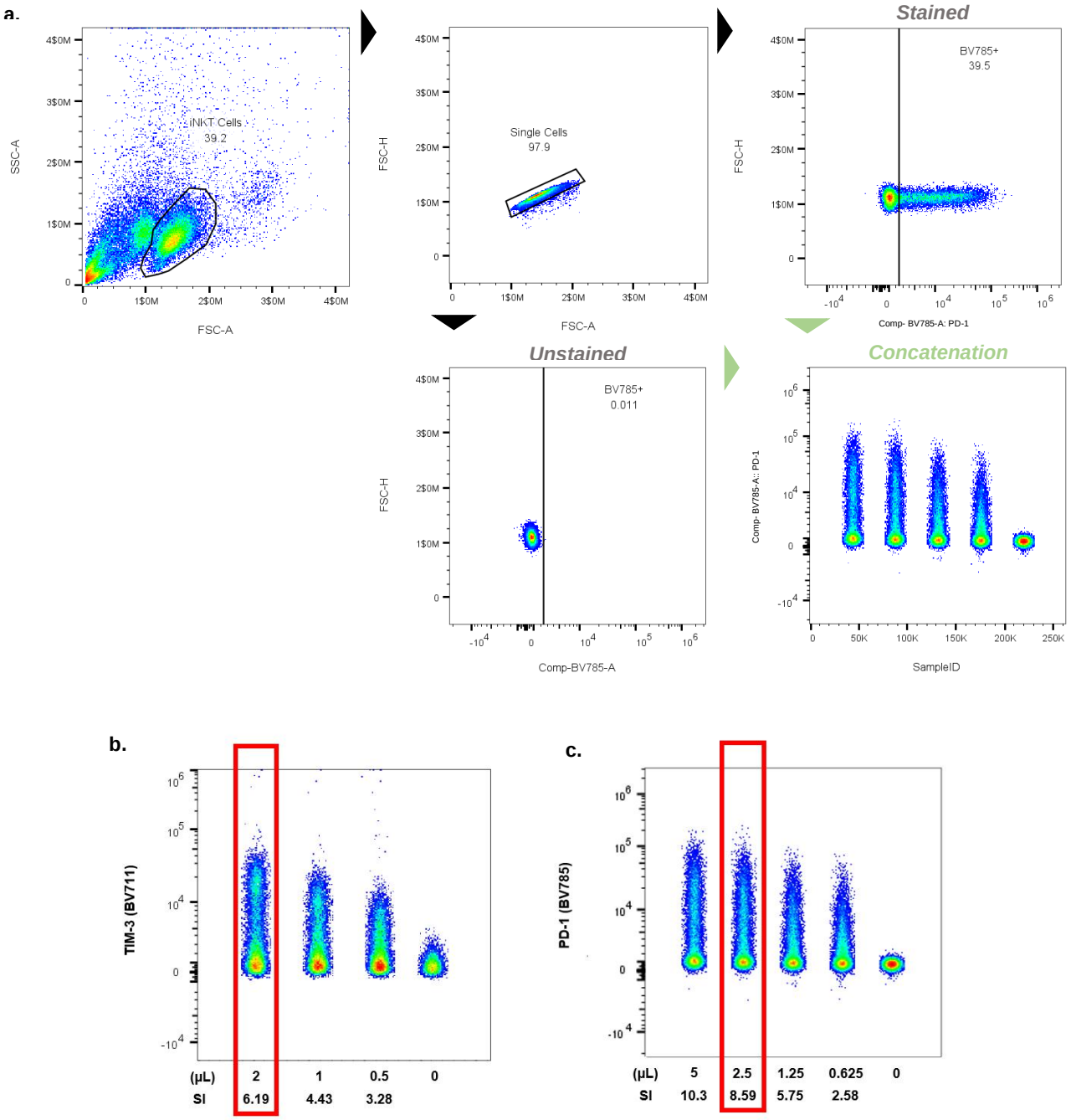

Figure 15. Titrations of antibodies anti-TIM-3 BV711 and Anti-PD-1 BV785. a. Representative gating strategy used to titrate the antibodies anti-TIM-3 and PD-1 in the iNKT Cell line. **b., c.** Titrations of anti-TIM-3 BV711 (100 µg/mL) and anti-PD-1 BV785 (100 µg/mL), respectively. Titrations were done using the iNKT cell line. Dilutions are represented in µl of stock antibody concentration diluted in 100 µl of FACS Buffer. 0 µl represents the unstained cells. The Staining Index (SI) was calculated for each dilution using the formula: SI = [(Median of positive cells) – (Median of negative cells)]/ (2 × Standard Deviation of negative cells). The red box demarcates the selected dilutions.

The next step was to test the optimal concentrations of anti-TIM-3 and anti-PD-1 in fresh iNKT cells obtained from PBMCs isolated from a Buffy Coat. From **Figure 16**, it is possible to observe that anti-PD-1 was working as planned: there was staining with the optimal concentration (1:40) and a spread of cells, which was also possible to observe in the titration (**Figure 15 c.**) and in published articles[178–180,206].

Surprisingly, it was not possible to observe positive cells for TIM-3 (**Figures 16 d.** and **e.**). Since it was possible to prove that the antibody anti-TIM-3 was working (**Figure 15 b.**), the experiment was repeated using donor A (from the left plot of **Figure 16**). Despite the new repetition, anti-TIM-3 showed no staining in fresh iNKT cells, using the optimal concentration (1:50) (**Figure 16 c.**), selected by using the iNKT cell line. In parallel with other experiments, anti-TIM-3 was added to the mix and the results were always the same: no positive cells por TIM-3 (results not shown). This may mean that fresh iNKT cells need to be activated in order to be possible to detect TIM-3.

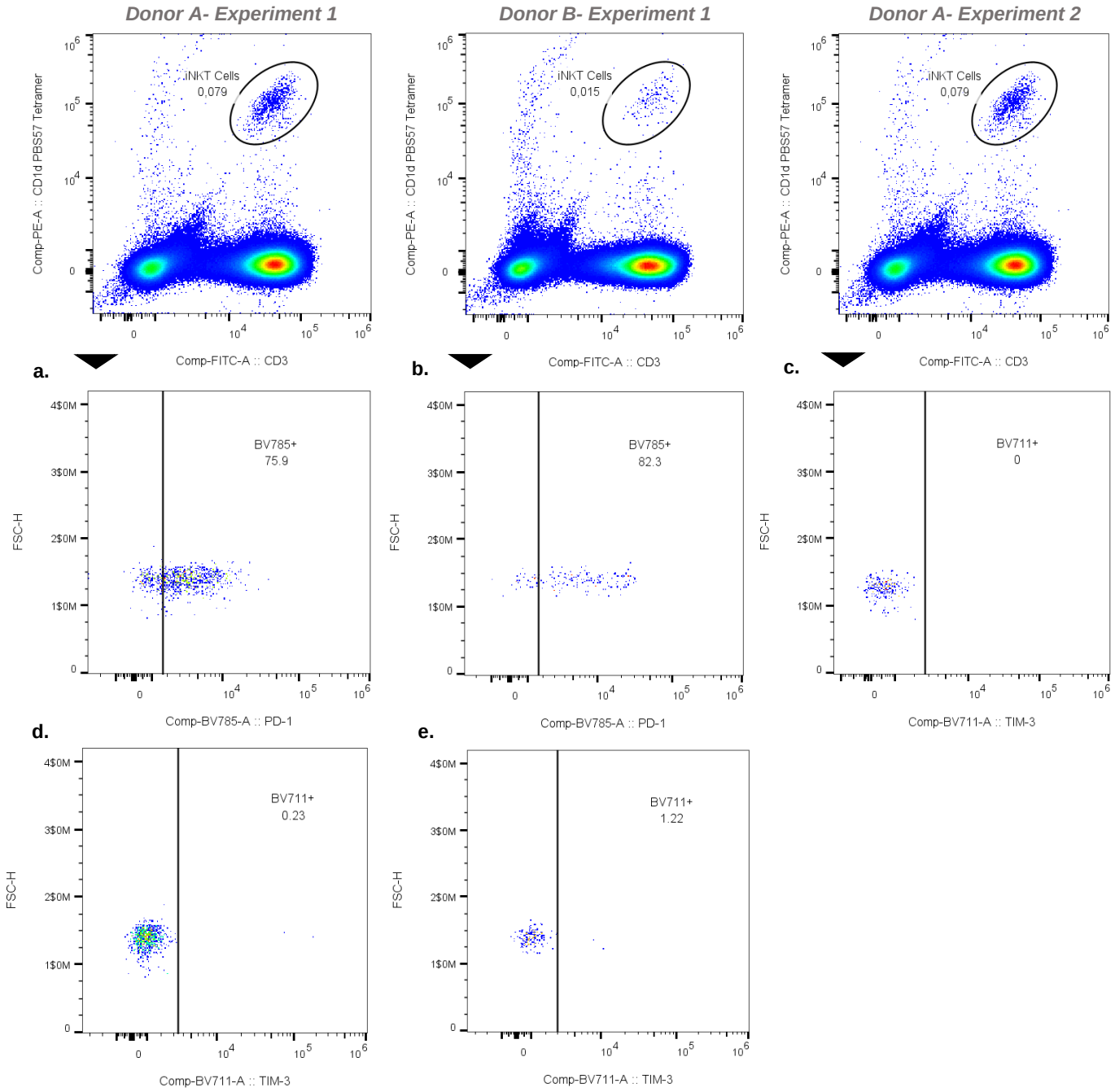

Figure 16. Test the optimal concentrations of anti-TIM-3 and anti-PD-1 in fresh iNKT cells. Fresh iNKT cells isolated from two different healthy donors were used to test anti-PD-1 and Anti-TIM-3. Cells were fluorescently stained with CD1d PBS57 PE (1:100), Anti-CD3-FITC (1:200), Anti-PD-1 BV785 (1:40) and/or Anti-TIM-3 BV711 (1:50). Percentage of positive cells are represented for each antibody. Positive cells were gated based on the unstained and single. **a., b.:** Staining of fresh iNKT cells with anti-PD-1. **c., d., e.:** Staining of fresh iNKT cells with anti-TIM-3.

2.2.3 Titration of CD1d PBS-57 Tetramers

Mouse or human iNKT cells are effectively detected by the CD1d Tetramer loaded with PBS-57, a developed analogue of α-GalCer, that was shown to have indistinguishable activity from α-GalCer[207]. An unloaded CD1d tetramer needed to be used as a control for nonspecific binding.

CD1d PBS-57 Tetramers labelled with BV421 or APC were titrated at the same time as the unloaded tetramers in order to inspect which tetramer concentration would have: 1) a better positive and negative populations separation and 2) less nonspecific background.

Firstly, both APC and BV421 tetramers were titrated in a 1:1 ratio PBMCs to iNKT cells from the cell line. The iNKT cell line is positive for CD1d PBS-57 tetramer (~96% purity), enabling to have a greater percentage of positive cells for the tetramer, and PBMCs allow to have higher percentage of negative cells for the tetramers. PBMCs were isolated from a Buffy Coat the day before the experiment.

The same gating strategy as in **Figure 13** was followed to gate the positive cells for CD1d tetramers unloaded or loaded with PBS-57. The results relative to the titration of APC labelled CD1d Tetramers, loaded and unloaded, are displayed in **Figure 17**. Surprisingly, the unloaded CD1d tetramer (**right plots of Figure 17**) presented a significative percentage of nonspecific binding (between 7.60% and 14.9%), even when the lowest concentration tittered of the tetramer was used (**bottom right plot of Figure 17**). The fact that PBMCs were not freshly isolated and a viability dye wasn't used, may be an explanation. Although there was more percentage of positive cells for CD1d PBS-57 Tetramer with 1:100 concentration (upper left plot **Figure 17**), there was a better separation of the negative and positive populations with 1:400 and 1:800 (two bottom left plots of **Figure 17**). However, this result is not reliable because of the nonspecific binding with the unloaded tetramer.

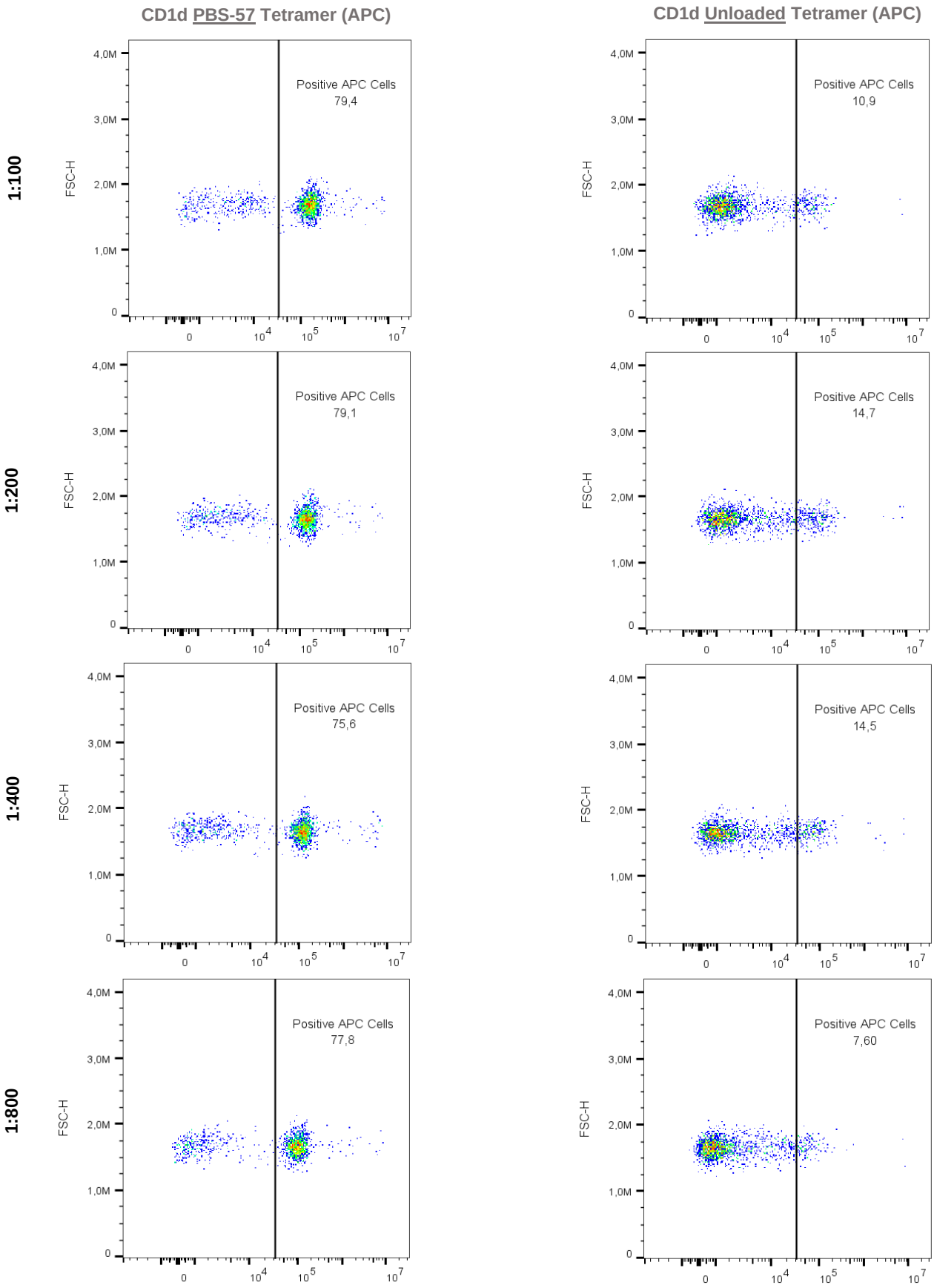

Figure 17. Titration of CD1d APC Tetramers (1.42 mg/mL) in PBMCs and iNKT Cell line (1:1). On the left, plots of CD1d PBS57 Tetramer APC dilutions (1:100, 1:200, 1:400, 1:800) are represented. On the right, the corresponding plots of CD1d Unloaded Tetramer APC dilutions are represented.

The results regarding the titration of CD1d loaded and unloaded tetramer labelled with BV421 are represented in **Figure 18**. The nonspecific binding also occurred with the unloaded tetramer, ranging between 6.14% and 13.3% (right plots of **Figure 18**). The dilution 1:800 presented the highest percentage of positive cells for the BV421 labelled CD1d PBS-57 Tetramer (bottom left plot of **Figure 18**) and it was also the concentration that presented a better positive/ negative populations separation and less nonspecific binding. In any case, there was still a high percentage of nonspecific binding, making it not possible to rely on these results.

On the account of the results from **Figures 17** and **18**, the experiment was repeated using just the iNKT cell line and the most promising dilutions of the tetramers: 1:200 (to have comparison with a higher concentration), 1:400 and 1:800 for APC labelled tetramers and 1:400 (to have comparison with a higher concentration) and 1:800 for BV421 labelled tetramers.

The iNKT Cell line showed much less percentage of nonspecific binding in both APC and BV421 labelled CD1d Tetramers (right plots of **Figures 19** and **20**). On the account of the CD1d PBS-57 Tetramer labelled with APC (**Figure 19**), 1:400 and 1:800 dilutions (two bottom left plots of **Figure 19**) presented the same percentage of positive APC cells for the unloaded tetramer and less than the 1:200 dilution (upper left plot of **Figure 19**). Besides this, the first two dilutions had a higher percentage of positive cells for the loaded tetramer and presented a better separation between the negative and positive cells (two bottom right plots of **Figure 19**) when compared to the higher concentration (upper left plot of **Figure 19**). Consequently, 1:400 and 1:800 were the concentrations of the APC labelled CD1d tetramer tested in fresh iNKT cells.

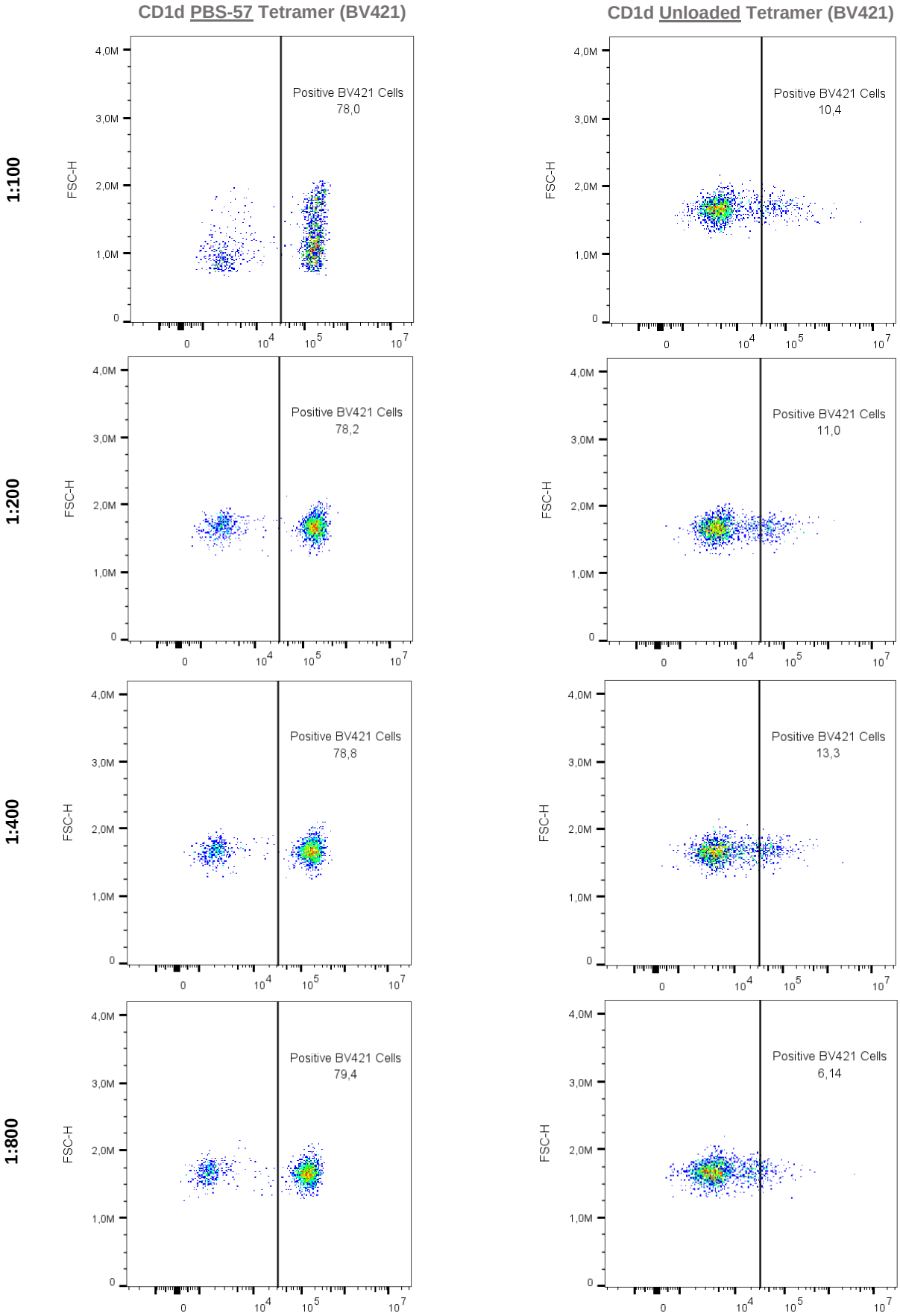

Figure 18. Titration of CD1d BV421 Tetramers (1.17 mg/mL) in PBMCs and iNKT Cell line (1:1). On the left, plots of CD1d PBS57 Tetramer BV421 dilutions (1:100, 1:200, 1:400, 1:800) are represented. On the right, the respective plots of CD1d Unloaded Tetramer BV421 dilutions are represented.

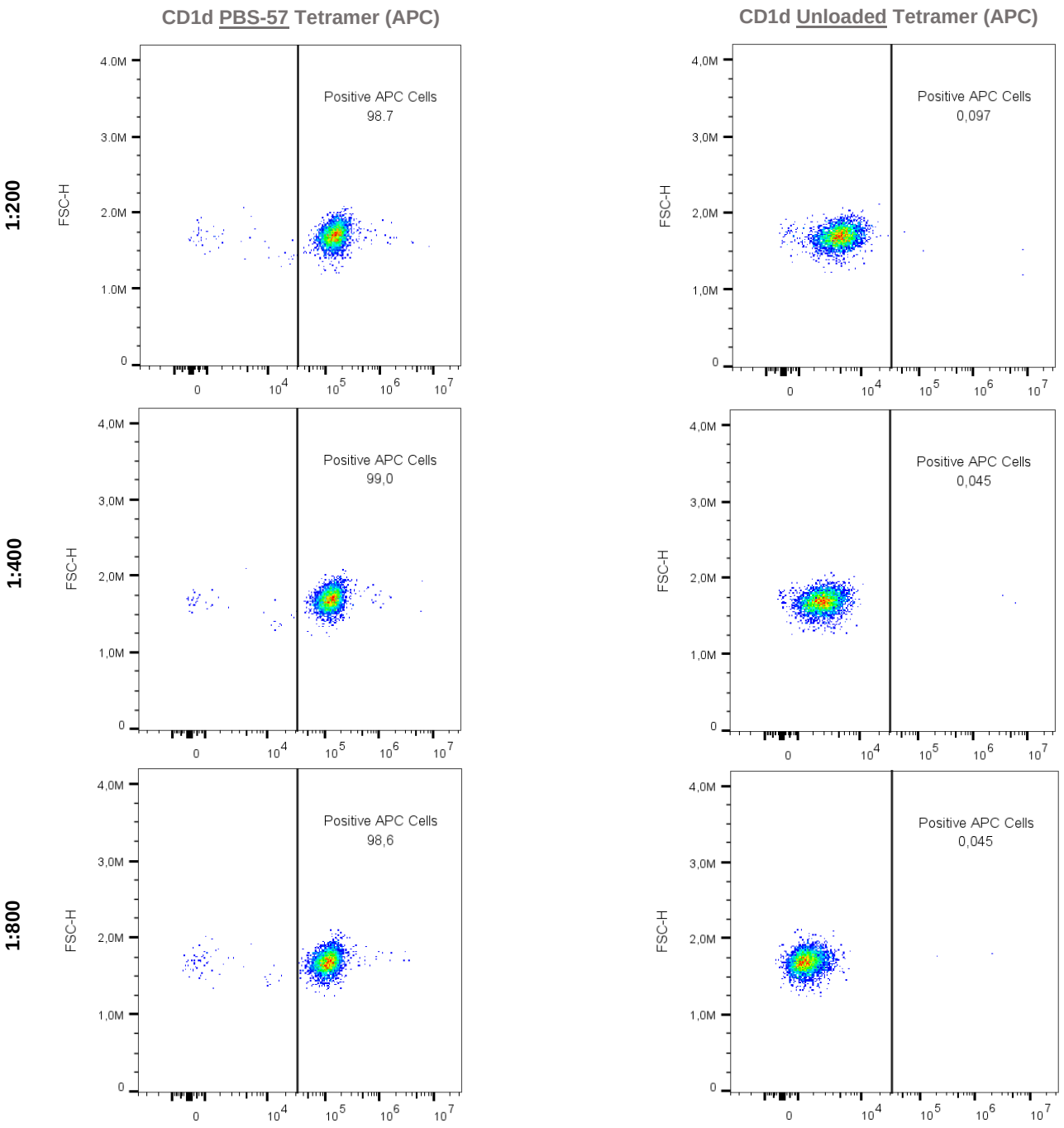

Figure 19. Titration of CD1d APC Tetramers in the iNKT Cell line. On the left, plots of CD1d PBS57 Tetramer APC dilutions (1:200, 1:400, 1:800) are represented. On the right, the corresponding plots of CD1d Unloaded Tetramer APC dilutions are represented.

Regarding the BV421 labelled CD1d PBS-57 Tetramer, the higher dilution (1:800) (upper left plot of **Figure 20**) presented less nonspecific binding than the 1:400 concentration (bottom left plot of **Figure 20**). Additionally, the 1:800 dilution had a better separation between the negative and positive populations (bottom right plot of **Figure 20**). Looking

at the plot, it could be possible that a higher dilution than 1:800 had a better separation of the two populations. Thus, 1:800 and a higher dilution (1:1600) of BV421 CD1d tetramer were tested in fresh iNKT cells.

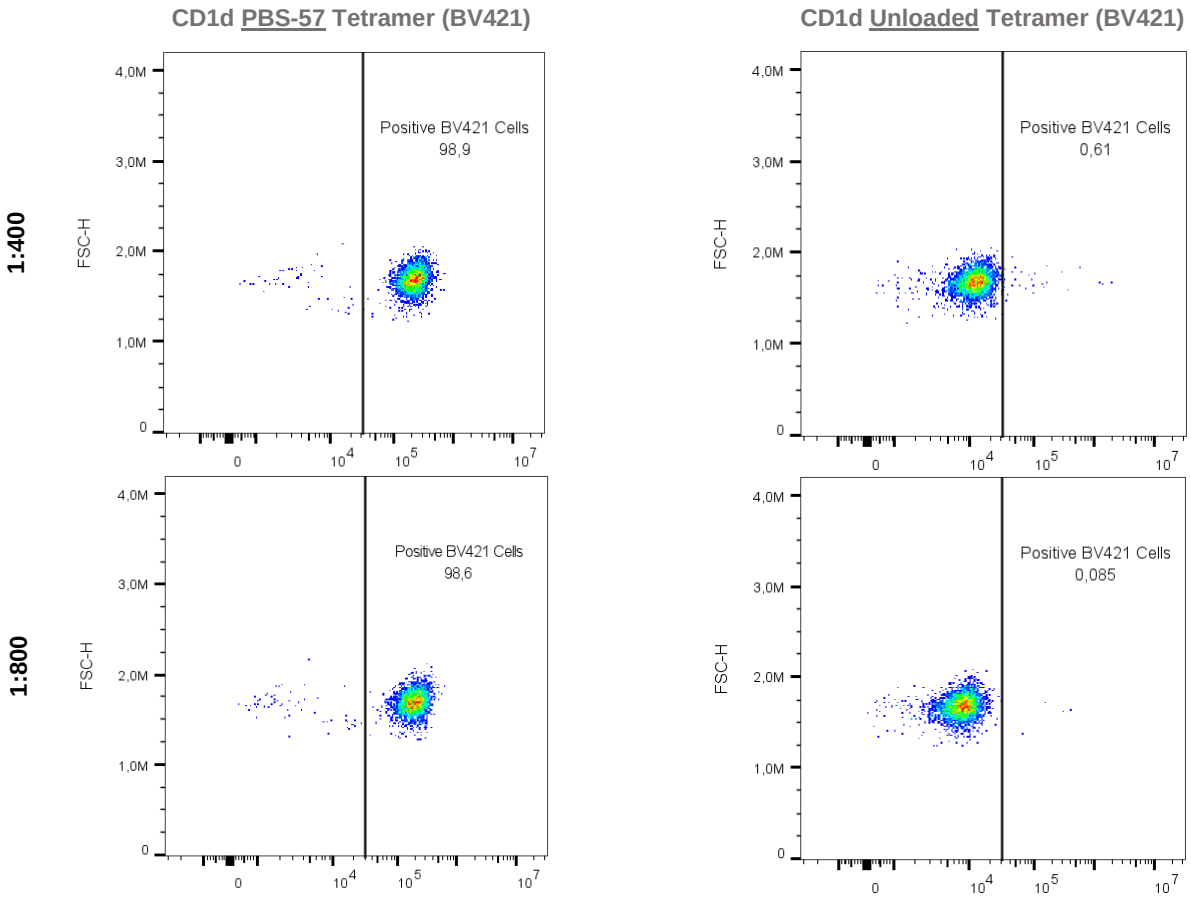

Figure 20. Titration of CD1d BV421 Tetramers in the iNKT Cell line. On the left, plots of CD1d PBS57 Tetramer BV421 dilutions (1:400 and 1:800) are represented. On the right, the corresponding plots of CD1d Unloaded Tetramer BV421 dilutions are represented.

In **Figure 21**, the flow cytometry gating strategy used for the analysis of fresh iNKT cells is represented. T lymphocytes were selected based on the cells stained for anti-CD3 and, in $CD3^+$ cells, iNKT cells positive cells were selected according to the cells stained for CD1d PBS-57 Tetramer labelled with APC or BV421 (**Figure 21**).

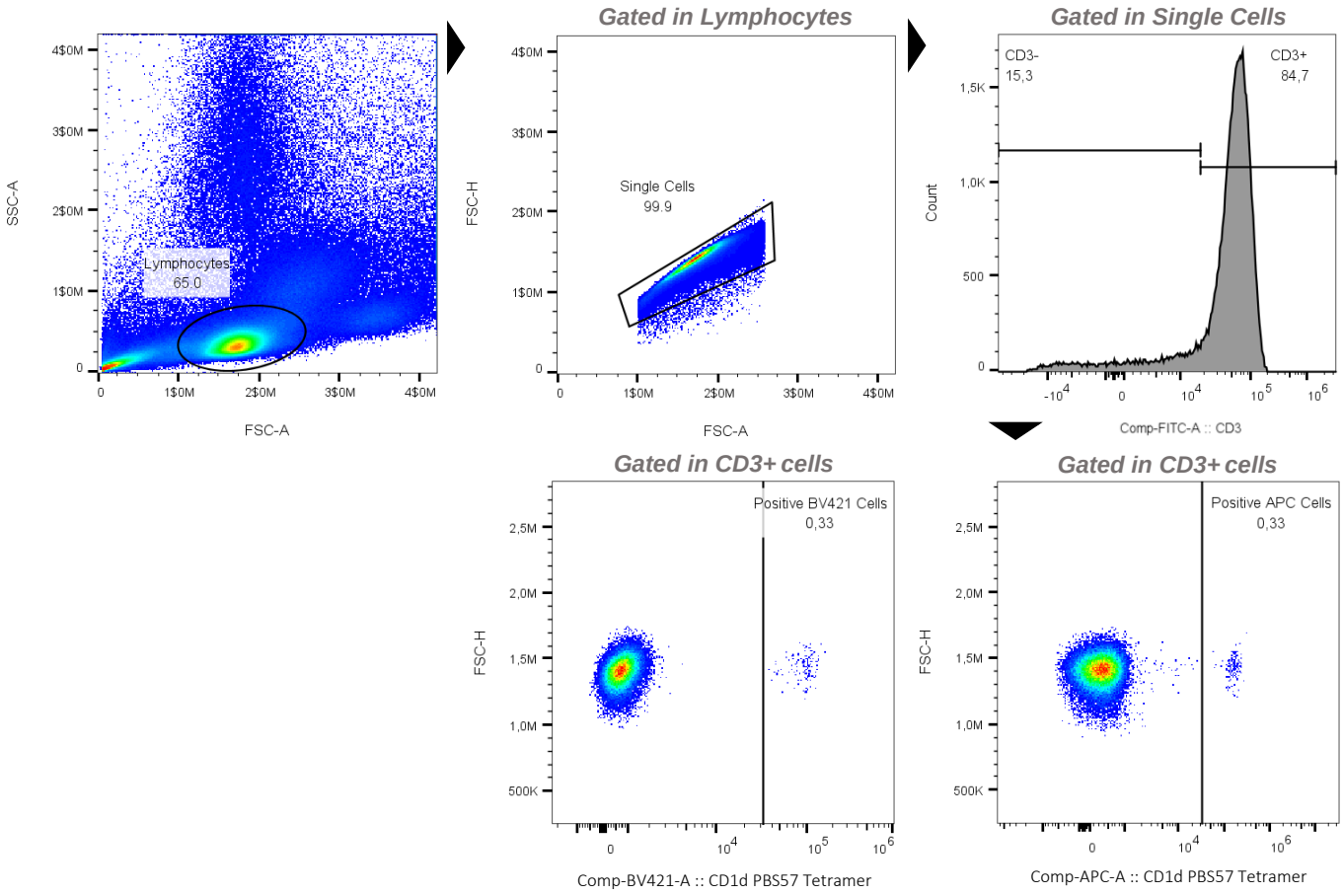

Figure 21. Representative gating strategy used to test the CD1d Tetramers (loaded and unloaded) labelled with APC and BV421 in fresh iNKT cells. Lymphocytes were gated according to their size (forward scatter – FSC) and granularity (side scatter – SSC), followed by singlets selection. T lymphocytes were selected based on the cells stained for Anti-CD3 and, in CD3+ cells, iNKT cells positive cells were selected according to the cells stained for CD1d PBS-57 Tetramer labelled with APC and BV421.

The results of the APC labelled CD1d loaded and unloaded tetramers test in fresh iNKT cells are represented in **Figure 22 a.**. An isolated population of iNKT cells was observed in both dilutions of CD1d PBS-57 Tetramer. 1:800 dilution presented more percentage of iNKT cells (0.35%- bottom left plot of **Figure 22 a.**) and a better separation of the negative and positive populations for the loaded tetramer when compared to 1:400 (0.33%- upper left plot of **Figure 22 a.**). Along with this, the higher dilution of the unloaded tetramer exhibited less nonspecific binding (upper right plot of **Figure 22 a.**). Hence, the optimal concentration for the APC labelled CD1d PBS-57 Tetramer was 1:800.

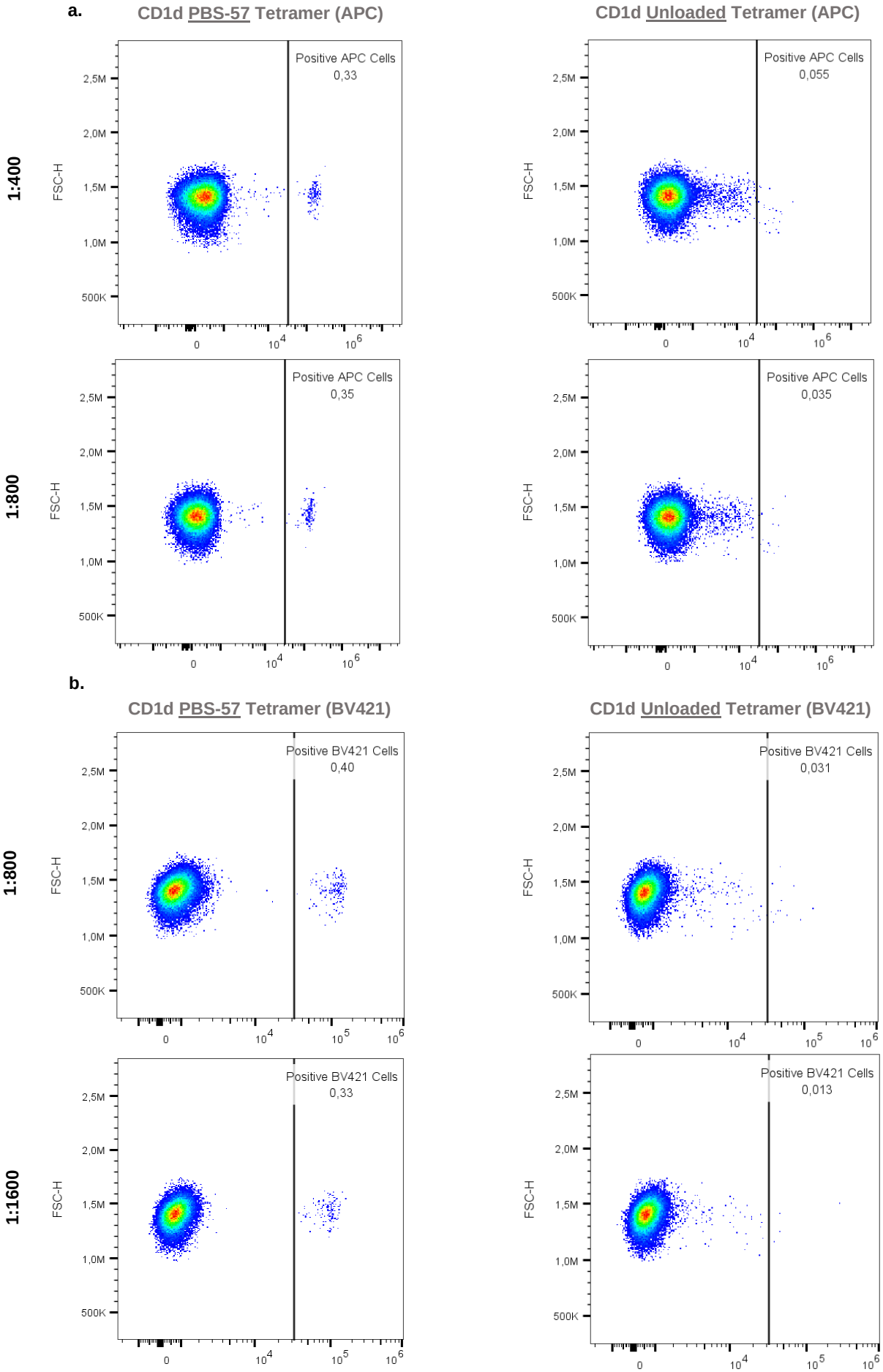

Figure 22. Titration of BV421 and APC labelled CD1d Tetramers in fresh iNKT cells isolated from a healthy donor's PBMCs. a. Titration of APC labelled CD1d Tetramers. On the left, plots of CD1d PBS57 Tetramer APC dilutions (1:400 and 1:800) are represented. On the right, the corresponding plots of CD1d Unloaded Tetramer APC dilutions are represented. **b.** Titration of BV421 labelled CD1d Tetramers. On the left, plots of CD1d PBS57 Tetramer BV421 dilutions (1:800 and 1:1600) are represented. On the right, the corresponding plots of CD1d Unloaded Tetramer BV421 dilutions are represented.

As for the BV421 labelled CD1d loaded and unloaded tetramers test in fresh iNKT cells, it is shown in **Figure 22 b.**. It was also possible to observe an isolated population of iNKT cells using both 1:800 and 1:1600 dilutions (left plots of **Figure 22 b.**). Although 1:800 had 0.018% more nonspecific binding (right plots of **Figure 22 b.**) than 1:1600, it presented more 0.07% iNKT cells than the highest dilution (left plots of **Figure 22 b.**). The separation of the negative and positive populations between the two dilutions was similar. Thereby, 1:800 was the optimal concentration for the BV421 labelled CD1d PBS-57 Tetramer.

Besides all these results, and looking at the left plots of **Figures 22 a.** and **b.**, both tetramers stain approximately the same percentage of iNKT cells (between 0.33% and 0.4%) using the same healthy donor's PBMCs, which means that that are working correctly.

2.2.4 Titration of Anti-CXCR6

In 2022, Cui et al. described for the first time a circulating population of iNKT cells, defined by $CXCR6^{+}CD244^{+}$ expression, presenting high cytotoxic properties[181]. We were interested in studying this population in Fabry disease patients and compare with healthy subjects. According to the authors, inside iNKT cells, there are ~41% $CXCR6^{+}CD244^{-}$ iNKT cells in young human donors and ~58% in aged human donors. In the case of $CXCR6^{+}CD244^{+}$ population, there is ~43% and ~26% in young and aged human donors, respectively[181].

First, anti-CXCR6 was titrated in PBMCs as in **Figures 13** and **14**, showing no significant staining (**Figure 23**), which was unexpected since Cui et al. used this marker in isolated PBMCs without stimulation.

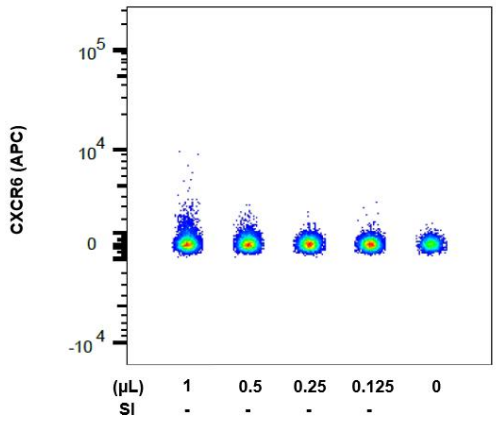

Figure 23. Titration of anti-CXCR6 in PBMCs. Titration was done using isolated PBMCs from Buffy Coats. Dilutions are represented in µl of Anti-CXCR6 APC antibody concentration (100 µg/mL) diluted in 100 µl of FACS Buffer. 0 µl represents the unstained cells.

In order to test if the antibody concentration was the problem and, at the same time if the anti-CXCR6 antibody was working, 1:50, 1:100 and 1:200 dilutions were used to stain iNKT cells from the cell line. In view of the fact that CXCR6 is a chemokine receptor and a transmembrane protein[174,181], extracellular and intracellular staining were done to understand if these protein could have more expression intracellularly.

Gating strategy from **Figure 15 a.** was used to determine CXCR6 expression in iNKT cells from the cell line and titrate anti-CXCR6. It is possible to notice in **Figure 24** that there are positive cells in both extracellular and intracellular staining and that 1:100 is the best antibody concentration in both staining, according to the SI values [3.59 in extracellular staining (**Figure 24 a.**) and 3.86 in intracellular staining (**Figure 24 b.**)]. However, 1:50 concentration (2 µL of anti-CXCR6 diluted in 100 µL FACS Buffer) SI values [3.31 in extracellular staining (**Figure 24 a.**) and 3.81 in intracellular staining (**Figure 24 b.**)] don't differ much from 1:100 concentration SI values and looking at the plot, 1:50 seemed to be a better choice of concentration. Moreover, with the 1:100 dilution it wasn't possible to observe positive cells for CXCR6 in PBMCs previously (**Figure 23**). On that account, 1:50 was the chosen dilution (**Figure 24**).

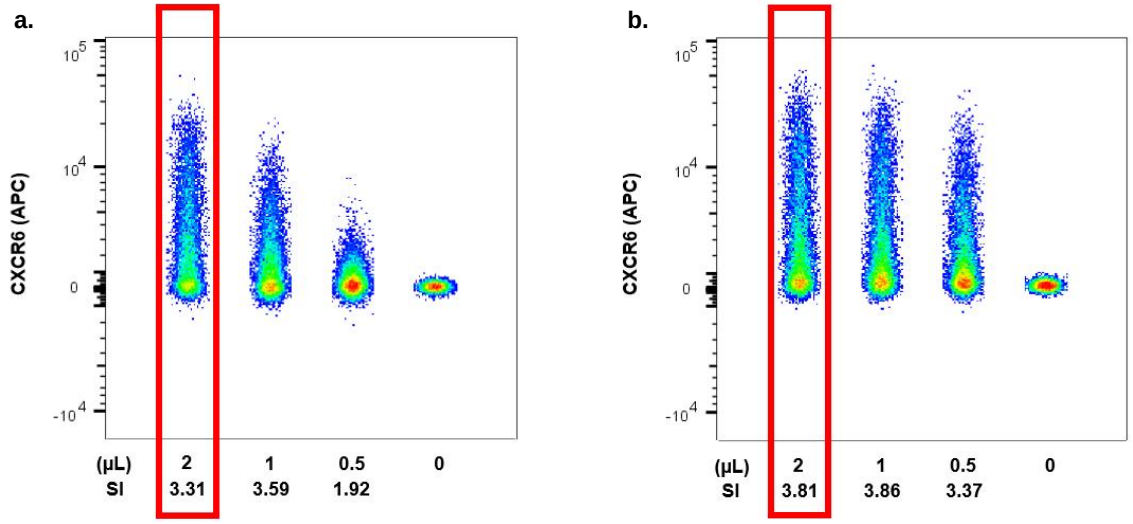

Figure 24. Titration of Anti-CXCR6 in the iNKT Cell line. Titrations were done using iNKT cells from the cell line. Dilutions are represented in µl of Anti-CXCR6 antibody concentration diluted in 100 µl of FACS Buffer. 0 µl represents the unstained cells. The Staining Index (SI) was calculated for each dilution using the formula: SI = [(Median of positive cells) – (Median of negative cells)]/ (2 × Standard Deviation of negative cells). The red box demarcates the selected dilutions. **a.** Extracellular staining of Anti-CXCR6. **b.** Intracellular staining of Anti-CXCR6.

From this last experiment (**Figure 24**), it is also possible to conclude that the anti-CXCR6 antibody was working. That being so, using the optimal anti-CXCR6 concentration, the same gating strategy from Cui et al. was used to determine the circulating iNKT Cell population[181]. Briefly, PBMCs were gated according to their size (forward scatter – FSC) and granularity (side scatter – SSC) for lymphocytes selection, followed by singlets selection (**Figure 25 a.**). In the single cells, iNKT cells were gated (CD1d PBS57 Tetramer$^+$ CD3$^+$) and inside this population, positive and negative populations for CXCR6 and/or CD244 populations were gated in iNKT cells (**Figure 25 a.**).

In **Figure 25 b.**, flow cytometric analyses of fresh iNKT cells from 4 different donors (from two independent experiments) are presented. Curiously, none of the iNKT cell populations positive or negative for CXCR6 and/ or CD244 were similar between the 4 healthy donors, except the presence of CXCR6$^-$CD244$^+$ iNKT cell population in three donors, which was not our population of interest and was not even represented in the article (**Figure 25 b.**)[181].

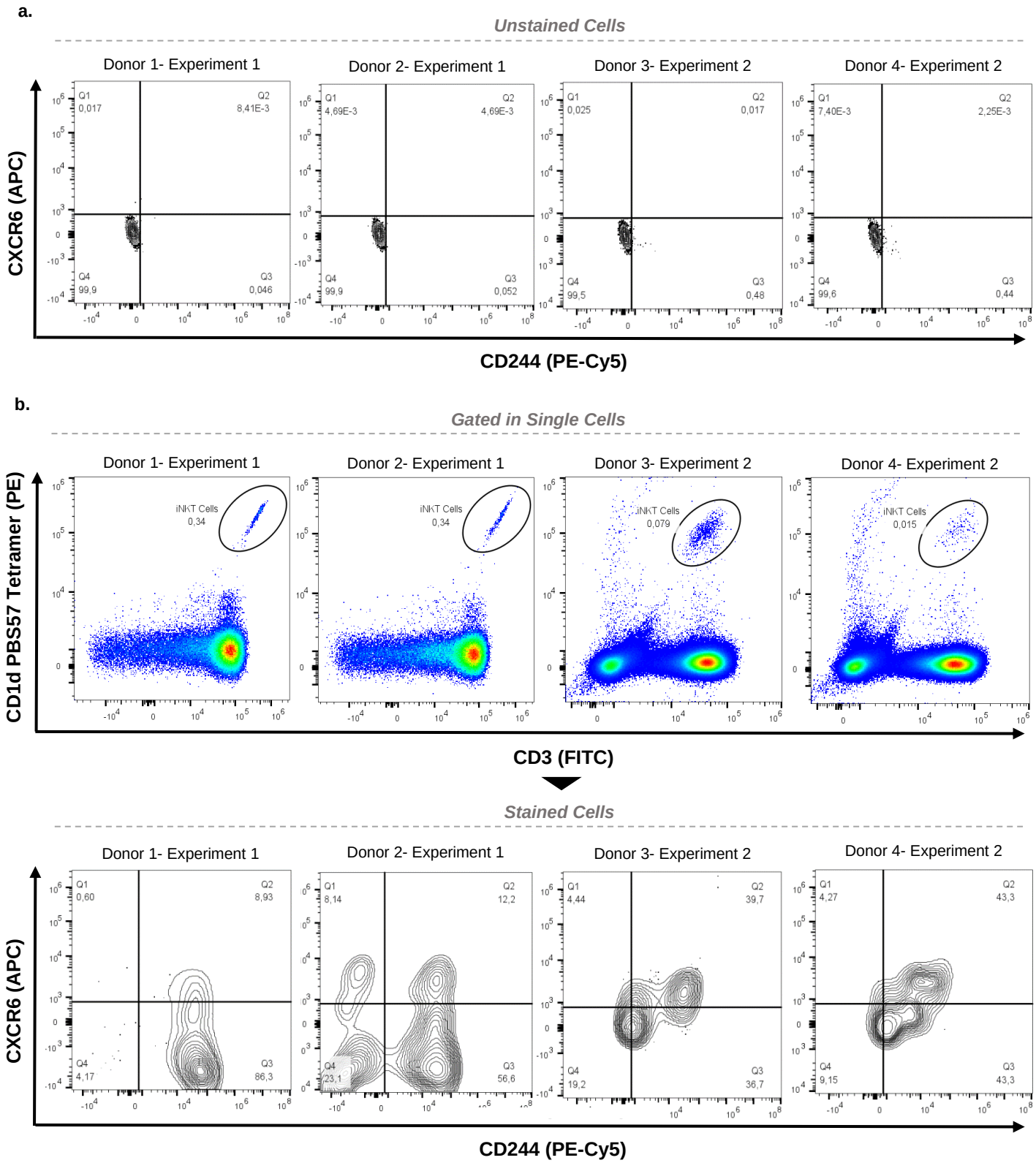

Figure 25. Flow cytometric analyses of human iNKT cells populations from 4 healthy donors PBMCs. Cells were fluorescently stained with CD1d PBS57 PE (1:100), Anti-CD3-FITC (1:200), Anti-CD244 PE-Cy5 (1:200) and Anti-CXCR6 APC (1:50). The two left plots present fixated cells (experiment 1) whereas the two right plots present non-fixated cells (experiment 2): gating may not be equal due to that reason. **a.** Unstained cells for CXCR6 and CD244 gated on lymphocytes single cells. **b.** Expression of CXCR6 and CD244 in fresh iNKT cells from 4 healthy donors (stained cells). iNKT cells were gated on lymphocytes single cells.

The antibodies clones of anti-CD244 and anti-CXCR6 used in this study were the ones used by Cui and colleagues: K041E5 and C1.7, respectively[181]. Therefore, different clones are not in question here, since they are the same and cannot be the reason for the iNKT cell population differences observed. Healthy donors used in these experiments were Portuguese donors (**Figure 25**) whereas Cui et al. studied Japanese donors. This can be a reason why iNKT cell populations positive or negative for CXCR6 and/or CD244 were different from what was expected.

Since these markers did not present the expected expression and little is known about this circulating iNKT cell population, with our results questioning its existence, they were not reliable to be used in patients yet. Therefore, and so that the flow cytometry panel wasn't incomplete, anti-CXCR6 and anti-CD244 fluorochromes, APC and PE-Cy5 respectively, were attributted to other markers: Inducible T-cell Costimulator (ICOS) and CD161. Invariant NKT cells constitutively express ICOS and which plays a crucial role in these cells activation[208]. CD161 is a NK cell marker, that is expressed in iNKT cells, involved in pro-inflamatory responses[209]. Anti-CD161 was titrated the same was as the markers described in **section 2.2.3)** and it is represented in **Figure 14 g.**. Anti-ICOS titration is described in **section 2.2.5) Titration of Anti-ICOS in PBMCs**.

2.2.5 Titration of Anti-ICOS in PBMCs

The antibody anti-ICOS was first titrated in fresh iNKT cells, with concentrations ranging from 1:100 to 1:800 (**Figure 26 c.**). However, from this titration, it wasn´t possible to observe distinct positive and negative populations and, consequently, the SI plugin didn't work accurately. Thus, using the same sample of PBMCs, anti-ICOS was titrated gated in lymphocytes (**Figure 26 b.**). This time, although not completely separated, it was possible to detect two populations. The highest SI value (7.33) was attributed to the lowest antibody concentration but, when looking at the plot, the concentration 1:100 (the most concentrated) was the one that best separated the negative and positive cell populations for anti-ICOS (**Figure 26 b.**).

Besides this, the percentage of iNKT cells positive for anti-ICOS is higher (30.3%) when the antibody was more concentrated (1:100) than when the lowest concentration was used (1.55%) (**Figure 26 c.**).

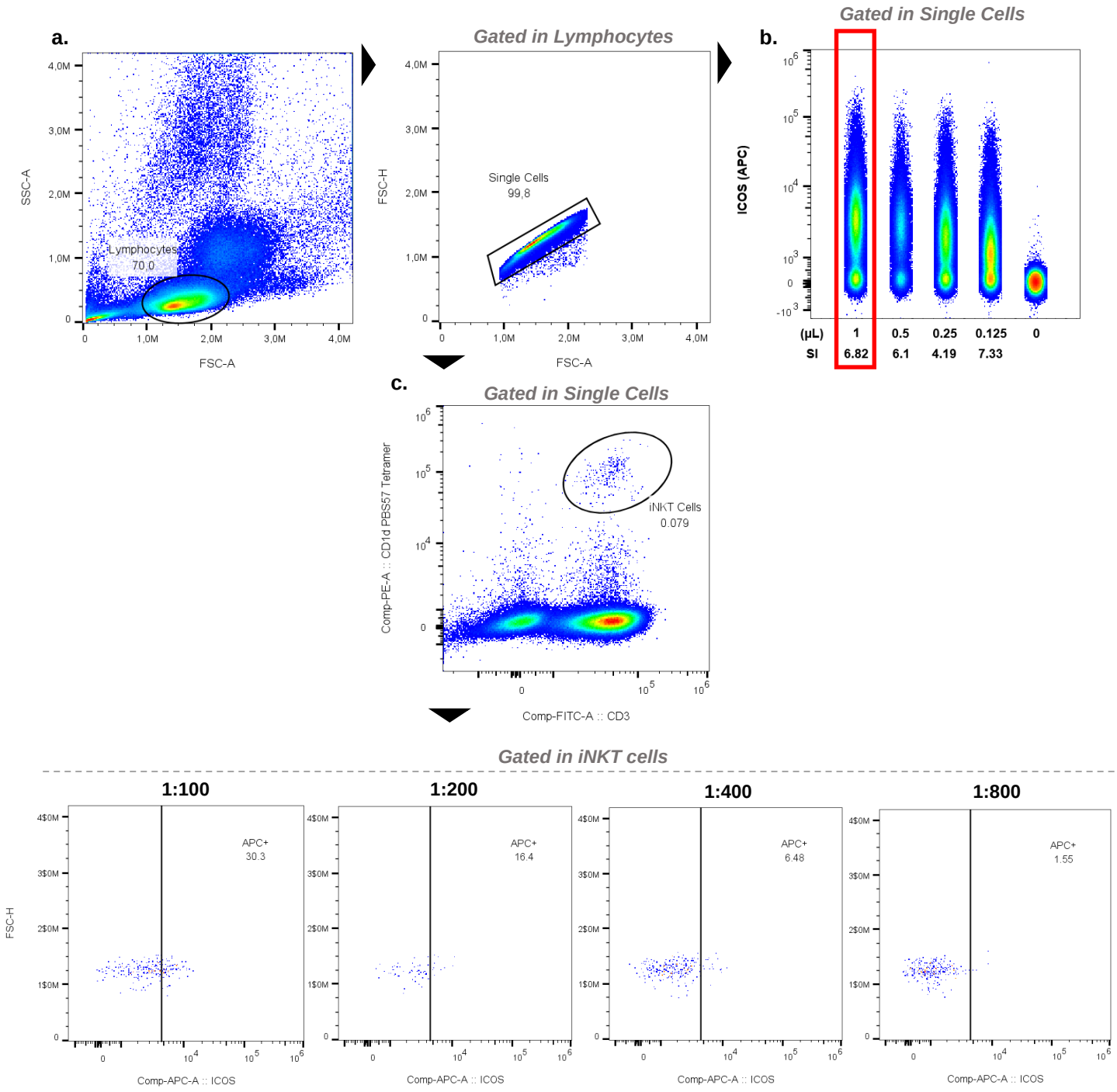

Figure 26. Titration of the antibody Anti-ICOS in PBMCs. Cells were fluorescently stained with CD1d PBS57 PE (1:100), Anti-CD3-FITC (1:200), and Anti-ICOS APC (1:100, 1:200, 1:400 and 1:800). a. Gating strategy used to titrate anti-ICOS. **b.** Titration of Anti-ICOS APC (0.2 mg/mL) was done using isolated PBMCs from Buffy Coats. Dilutions are represented in µl of stock antibody concentration diluted in 100 µl of FACS Buffer. 0 µl represents the unstained cells. The Staining Index (SI) was calculated for each dilution using the formula: SI = [(Median of positive cells) – (Median of negative cells)]/ (2 × Standard Deviation of negative cells). The red box demarcates the selected dilution. **c.** Titration of Anti-ICOS APC (0.2 mg/mL) was performed in fresh iNKT cells from PBMCs. Four plots with four different dilutions are represented, gated in iNKT cells.

Hence, based on these two key factors, 1:100 was the chosen concentration for the antibody anti-ICOS.

2.2.6 Titration of MR1 Tetramers

MAIT cells are identified by using the MR1-5-(2-oxopropylideneamino)-6-D-ribitylaminouracil (5-OP-RU) Tetramer, which is an agonist of MAIT cells[204]. A non-agonist of MAIT cells, MR1-6-formyl pterin (6-FP)[210], was used as a control for nonspecific binding.

MR1 5-OP-RU Tetramers labelled with AF488 or BV421 were titrated at the same time as the 6-FP tetramers in order to investigate which tetramer concentration would have: 1) a better positive and negative populations separation and 2) less nonspecific background.

The same rules for choosing the optimal concentration for CD1d tetramers (**section 2.2.3) Titration of CD1d PBS-57 Tetramers**) were applied for MR1 tetramers.

Initially, both AF488 and BV421 MR1 tetramers were titrated in PBMCs using for dilutions: 1:100, 1:200, 1:400 and 1:800. The results of these titrations are represented in **Figures 27** and **28**. Both AF488 and BV421 5-OP-RU tetramers stained an isolated population of MAIT cells (left plots of **Figures 27** and **28**, respectively). Along with that, the 6-FP tetramers presented no significative nonspecific binding (right plots of **Figures 27** and **28**, respectively).

In the case of AF488 labelled MR1 5-OP-RU Tetramer, 1:100 and 1:200 dilutions (upper left plots of **Figure 27**) separated better the negative and positive populations for 5-OP-RU tetramer when compared to the higher dilutions (bottom left plots of **Figure 27**). Consequently, 1:100 and 1:200 dilutions were tested again in PBMCs (**Figure 29**).

In terms of the MR1 5-OP-RU Tetramer labelled with BV421, 1:200 was the dilution that presented the highest percentage of MAIT cells (second left plot of **Figure 28**) and the 6-FP tetramer presented no nonspecific binding (second right plot of **Figure 28**). As a result, 1:200 was the optimal concentration for the BV421 labelled MR1 5-OP-RU Tetramer.

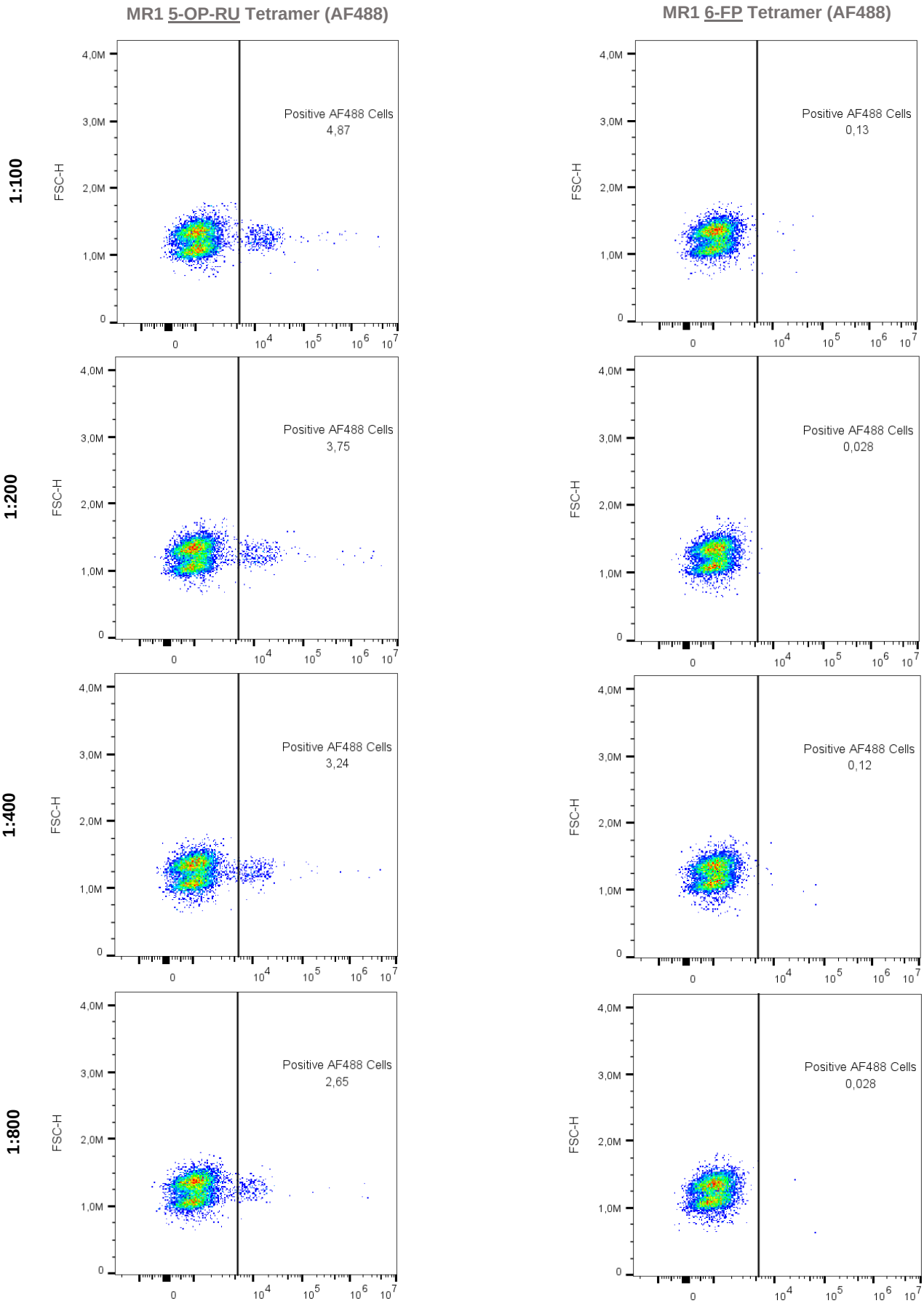

Figure 27. Titration of MR1 AF488 Tetramers (1.61 mg/mL) in PBMCs. On the left, plots of MR1 5-OP-RU Tetramer AF488 dilutions (1:100, 1:200, 1:400, 1:800) are represented. On the right, the corresponding plots of MR1 6-FP Tetramer AF488 dilutions are represented.

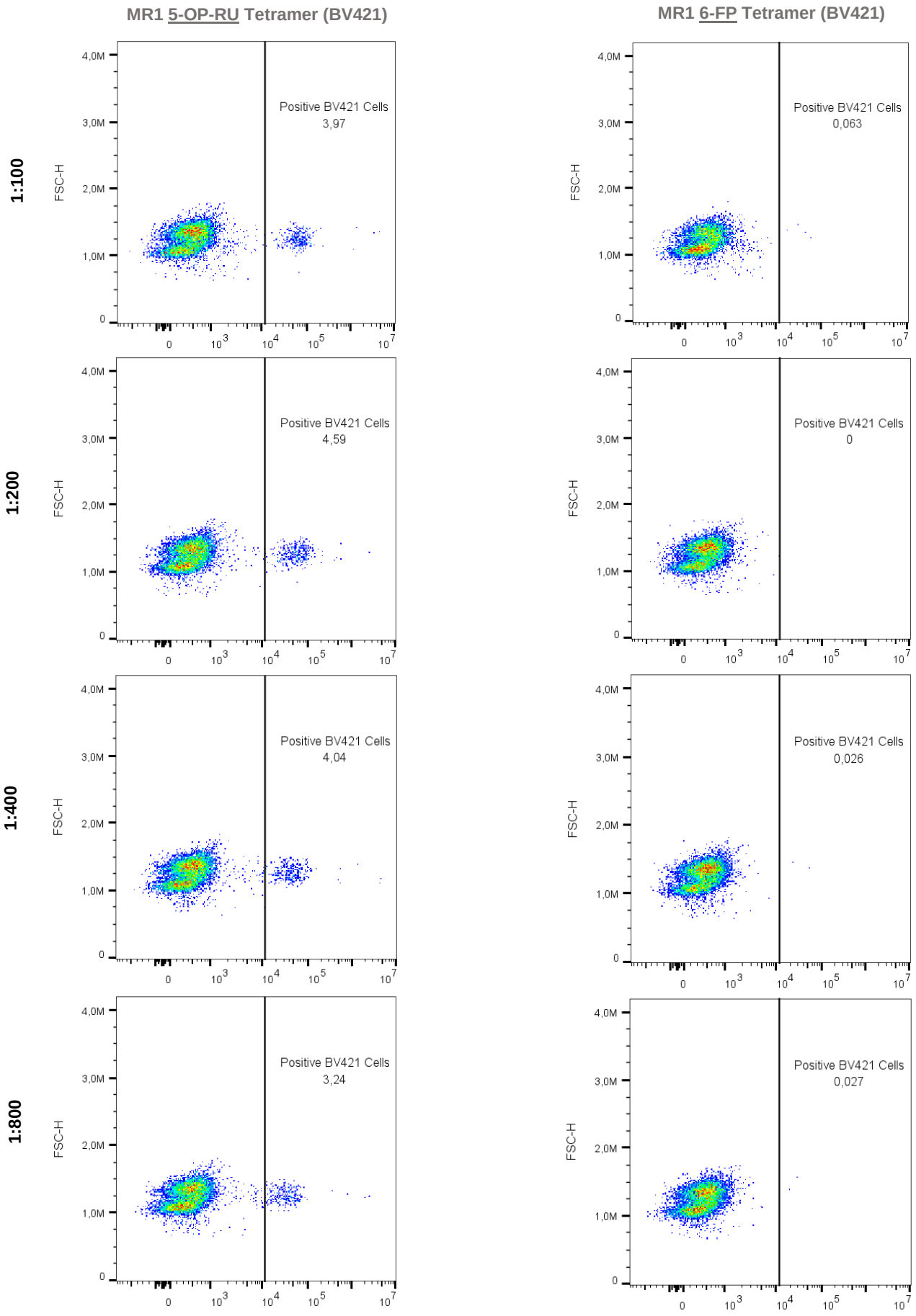

Figure 28. Titration of MR1 BV421 Tetramers (1.2 mg/mL) in PBMCs. On the left, plots of MR1 5-OP-RU Tetramer BV421 dilutions (1:100, 1:200, 1:400, 1:800) are represented. On the right, the respective plots of MR1 6-FP Tetramer BV421 dilutions are represented.

The new titration of AF488 labelled MR1 tetramers, using 1:100 and 1:200, was performed more than a month later after the first titration, and the results were inconclusive, since it was not possible to observe an isolated population of MAIT cells (left plots of **Figure 29**). This could have happened due to a low frequency of MAIT cells from the healthy donor.

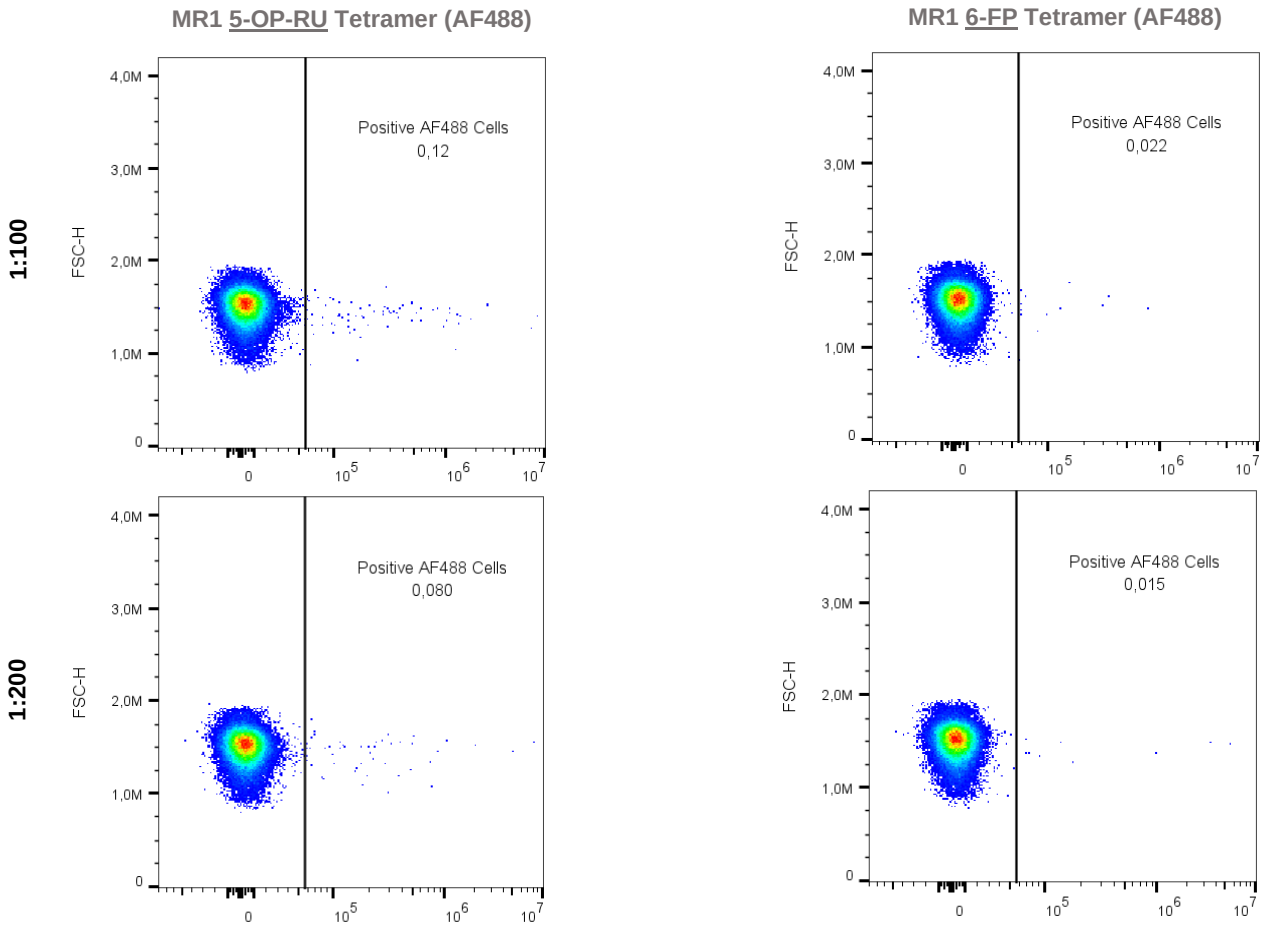

Figure 29. Titration of MR1 AF488 Tetramers in PBMCs. On the left, plots of MR1 5-OP-RU Tetramer AF488 dilutions (1:100 and 1:200) are represented. On the right, the corresponding plots of MR1 6-FP Tetramer AF488 dilutions are represented.

Hence, the experiment was repeated using two donors and the BV421 labelled MR1 tetramers (5-OP-RU and 6-FP) was also used, to make sure it wasn't a problem with the AF488 tetramer. Only the 1:200 concentration was used for both AF488 and BV421 tetramers. These results are shown in **Figure 30**.

Looking at the left bottom plots of BV421 labelled MR1 5-OP-RU Tetramer (**Figure 30**), there was an isolated population of MAIT cells in both donors 1 (1.26%) and 2 (1.99%), which means that these donors had MAIT cells and in a percentage that was easily observed. However, this population was not detected when the AF488 MR1 5-OP-RU Tetramer was used (upper left plots of **Figure 30**), leading us to believe that, if only this tetramer was used, the donors had no MAIT cells.

Considering the experiments from **Figures 27**, **29** and **30**, it can be inferred that the MR1 5-OP-RU Tetramer labelled with AF488 stopped working and this was reported to National Institute of Health tetramer core facility.

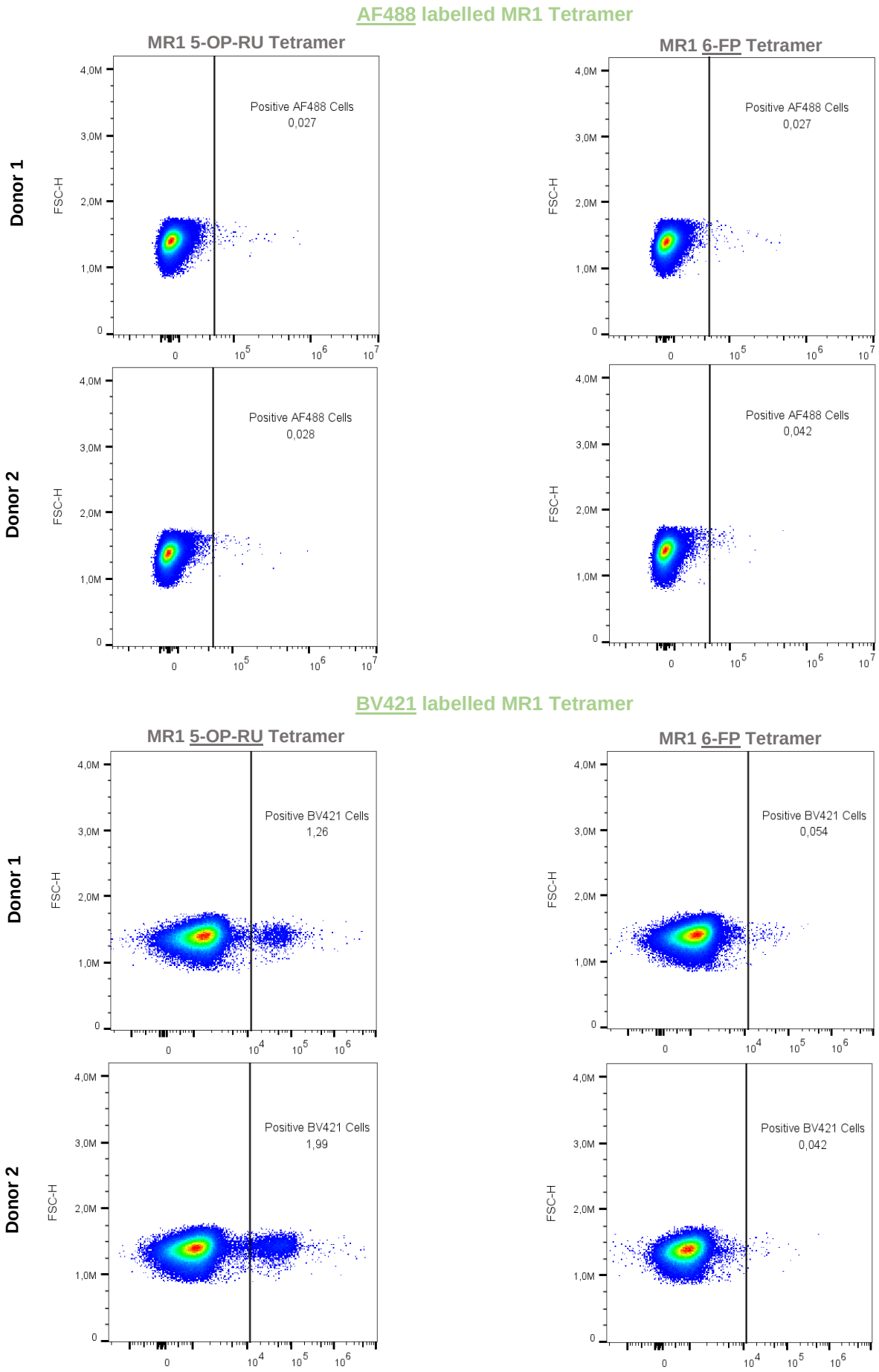

Figure 30. Test of MR1 5-OP-RU Tetramer AF488 in 2 donors PBMCs. BV421 labelled MR1 Tetramers were used as controls (bottom plots). 1:200 was the dilution used for both AF488 and BV421 tetramers. On the left, plots of MR1 5-OP-RU Tetramers are represented. On the right, the corresponding plots of MR1 6-FP Tetramer are represented.

2.2.7 Titration of Anti-IFN-γ and Anti-IL-4 in stimulated PBMCs

Cytokine expression was going to be analysed in stimulated iNKT cells from Fabry disease patients and healthy donors. Hence, and considering these cytokines are also produced by conventional T cells, anti-IFN-γ and anti-IL-4 antibodies were titrated, with a series of dilutions ranging from 1:100 to 1:800, in stimulated PBMCs isolated from a Buffy Coat. PBMCs were stimulated for 5 h with PMA and ionomycin, and BFA was added to inhibit the secretion of cytokines (they accumulate inside the cell).

The gating strategy from **Figure 13** was used to titrate these antibodies and an unstained and non-stimulated cells were used as controls (non-stimulated cells were stained with the highest concentration of each antibody).

In **Figure 31**, the results of anti-IFN-γ BV711 titration are represented. The unstimulated control stained with 1:100 of anti-IFN-γ is also represented (**Figure 31 a.**) and no positive cells for IFN-γ were observed, which was expected. According to the SI values and the plots of the different dilutions of the antibody tested in stimulated PBMCs, 1:100 was the optimal concentration for anti-IFN-γ BV711 (**Figure 31 b.**).

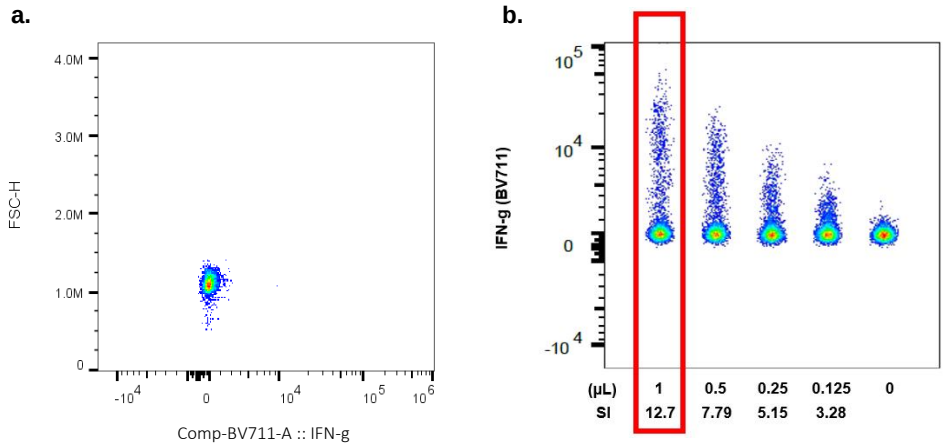

Figure 31. Titration of Anti-IFN-γ BV711 in stimulated PBMCs. a. Non-stimulated cells stained with Anti-IFN-γ BV711 (50 µg/mL). **b.** Titration of Anti-IFN-γ BV711 (50 µg/mL). Dilutions are represented in µl of Anti-IFN-γ antibody concentration diluted in 100 µl of FACS Buffer. 0 µl represents the unstained cells. The Staining Index (SI) was calculated for each dilution using the formula: SI = [(Median of positive cells) – (Median of negative cells)]/ (2 × Standard Deviation of negative cells). The red box demarcates the selected dilutions.

The results of anti-IL-4 APC are shown in **Figure 32**. No staining for anti-IL-4 was detected in both stimulated and non-stimulated cells (**Figures 32 b.** and **a.**, respectively)

and thereupon the SI values couldn't be calculated. The fact that the antibody anti-IL-4 APC expired 10 years ago may have led to a disaggregation of the fluorochrome APC from the antibody.

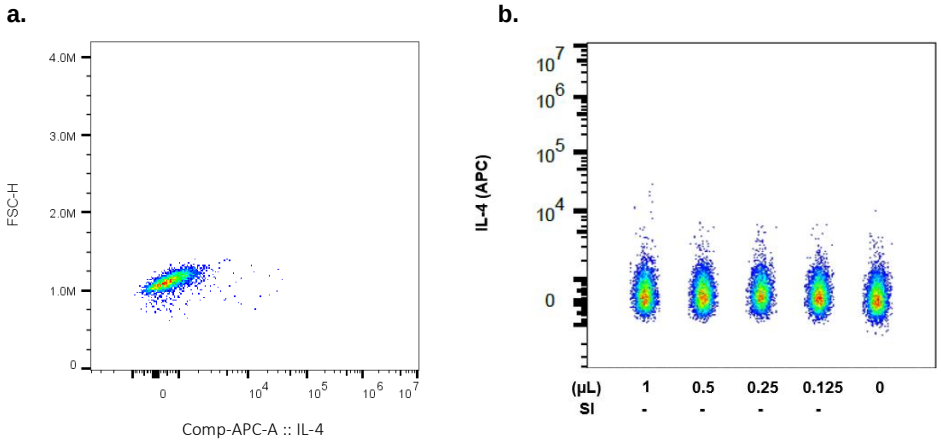

Figure 32. Titration of Anti-IL-4 APC in stimulated PBMCs. a. Non-stimulated cells stained with Anti-IL-4 APC (12 µg/mL). **b.** Titration of Anti-IL-4 APC (12 µg/mL). Dilutions are represented in µl of Anti-IL-4 antibody concentration diluted in 100 µl of FACS Buffer. 0 µl represents the unstained cells. The Staining Index (SI) was calculated for each dilution using the formula: SI = [(Median of positive cells) – (Median of negative cells)]/ (2 × Standard Deviation of negative cells). The red box demarcates the selected dilutions.

A new experiment for anti-IL-4 APC was performed using: 1) the expired anti-IL-4 APC antibody with the dilutions 1:50, 1:100 and 1:200, to check if a higher concentration was needed; 2) a new antibody anti-IL-4 APC with the dilutions 1:50, 1:100 and 1:200, to check if the problem was the expired antibody; 3) anti-IFN-γ BV711 (1:100) already titrated as a control of the stimulation technique. For all antibodies, a non-stimulated control was done.

In **Figure 33**, the flow cytometric results of this new test for anti-IL-4 are represented and the gating strategy from **Figure 13** was followed. The plots from **Figures 33 a.**, **e.** and **i.** illustrate the non-stimulated PBMCs stained with the new anti-IL-4 APC, expired anti-IL-4 APC and anti-IFN-γ, respectively. Only in the non-stimulated PBMCs stained with the old anti-IL-4 APC is observed some staining for IL-4, even more than in stimulated PBMCs (**Figures 33 f.**, **g.** and **h.**).

PBMCs were stimulated according to plan since it was possible to observe the expression of IFN-γ (**Figure 33 j.**). Nevertheless, it is not possible to say that there was, without any doubt, IL-4 expression using neither of the new or expired anti-IL-4 APC antibodies

(**Figures 33 b.**, **c.**, **d.**, **f.**, **g.** and **h.**). Once again, no conclusions can be taken about the anti-IL-4 APC titration.

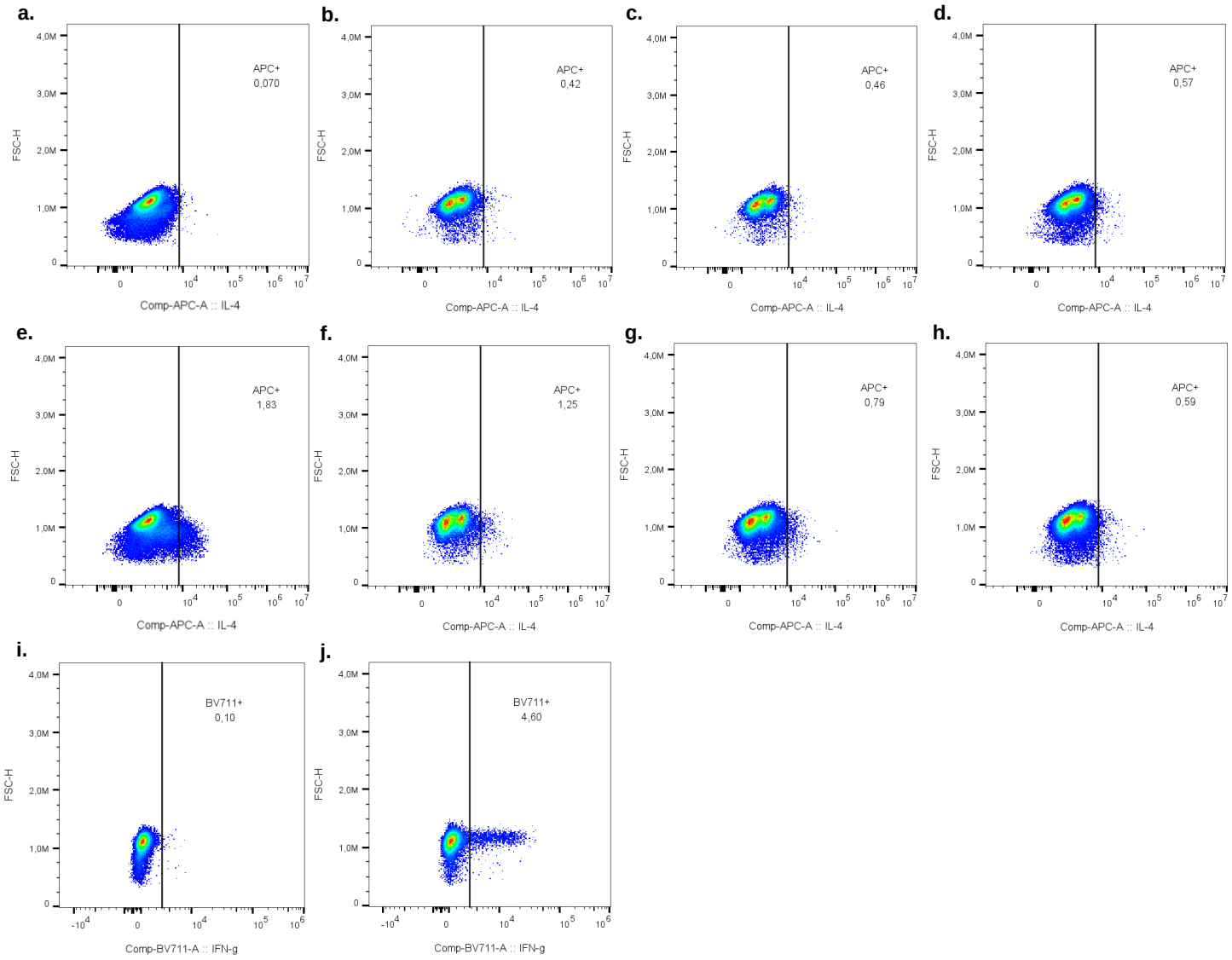

Figure 33. New test of Anti-IL-4 using a new antibody. Titration of IL-4 APC in stimulated PBMCs. **a.** Non-stimulated cells stained with the new Anti-IL-4 APC (12 µg/mL) using a dilution of 1:50. **b., c. and d.** Stimulated PBMCs stained with the new Anti-IL-4 APC with the concentrations 1:50, 1:100 and 1:200, respectively. **e.** Non-stimulated cells stained with the expired Anti-IL-4 APC (12 µg/mL) using a dilution of 1:50. **f., g. and h.** Stimulated PBMCs stained with the expired Anti-IL-4 APC with the concentrations 1:50, 1:100 and 1:200, respectively. **i.** Non-stimulated cells stained with the optimal Anti-IFN-γ BV711 concentration (1:100). **j.** Stimulated PBMCs stained with the optimal Anti-IFN-γ BV711 concentration (1:100).

For the anti-IL-4 APC single-stained sample, an antibody against some other higher expressed antigen should have been used in order to discard compensation errors, since IL-4$^+$ cells are rare. The time of incubation of PBMCs with PMA and ionomycin could have been increased to 6 hours to check if any difference was observed in the IL-4 expression.

As a result, the cytokines were not analysed in Fabry disease patients in this present study.

2.3 Anti-human iNKT cell Microbeads

iNKT cells, a rare population in PBMCs with a frequency of 0.001% to 0.1%[104,144,145], are insufficient in number for studying their properties. Using Anti-human iNKT MicroBeads, an enriched fraction of iNKT cells can be obtained from limited PBMCs (only a maximum of ~54x10^6 PBMCs will be obtained from 18 mL of blood[211]), facilitating the research of these cells in Fabry disease patients.

Half of the recommended amount of Anti-human iNKT cell MicroBeads by the manufacturer was used because: 1) 100% purity of iNKT cells after isolation was not wanted since conventional T cells phenotype was also going to be studied; 2) 0% of iNKT cells in the negative fraction was the aim for this microbeads isolation.

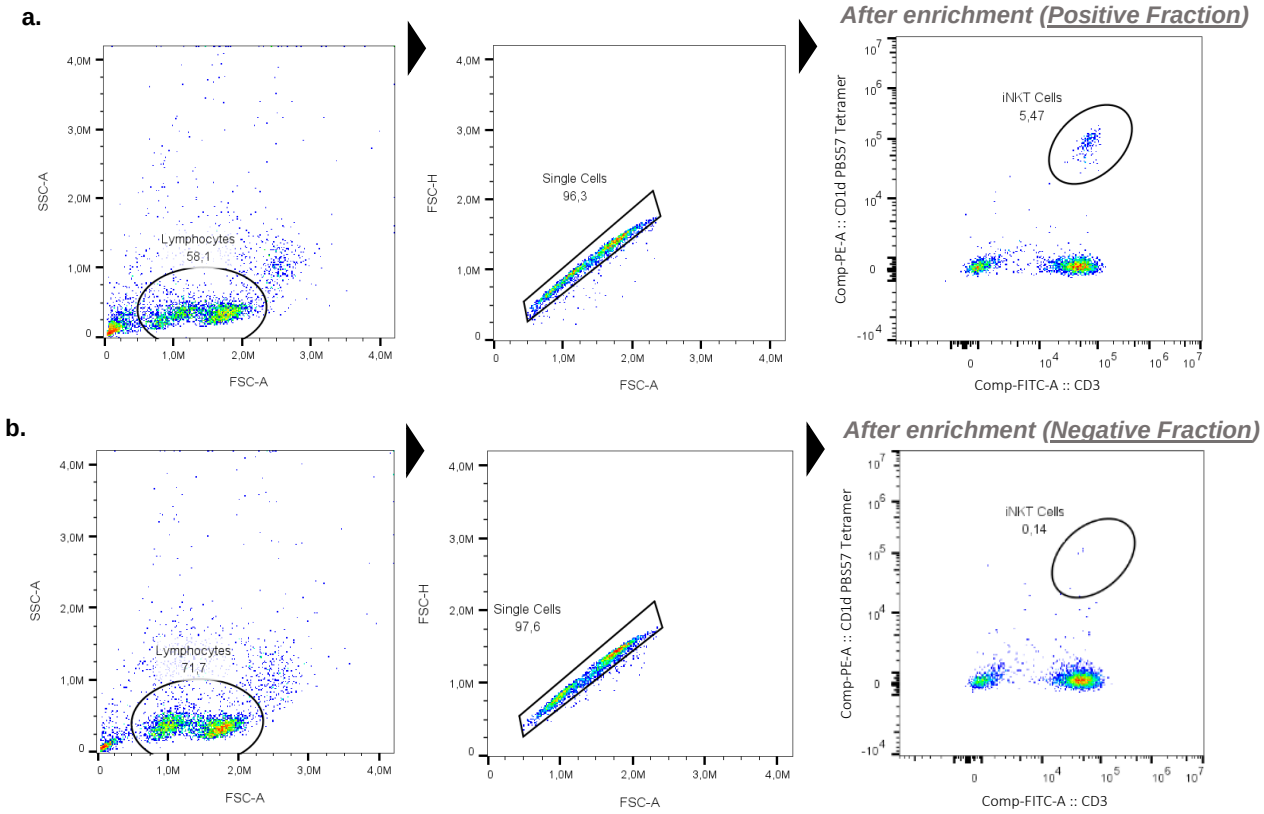

Figure 34. iNKT Cell isolation using Anti-human iNKT cell MicroBeads. The iNKT cells were isolated from human PBMCs using Anti-iNKT MicroBeads, a LS Column, and a MiniMACS™ Separator. Half of the recommended amount of microbeads was used (50 µL per 100x10^6 cells instead of 100 µL). Cells were fluorescently stained with CD1d PBS57 PE (1:100) and Anti-CD3 FITC (1:100). Lymphocytes were gated according to their size (forward scatter – FSC) and granularity (side scatter – SSC), followed by singlets selection. iNKT cells were selected based on the positivity for Anti-CD3 FITC and CD1d PBS-57 Tetramer PE. **a.** Positive fraction of isolated cells with iNKT microbeads. **b.** Negative fraction of isolated cells with iNKT microbeads.

Using half of the recommended amount of Anti-human iNKT cell MicroBeads was enough to have 0% of iNKT cells in the negative fraction (**Figure 34 b.**): Only 5 cells represented the 0.14% observed, which do not constitute a defined iNKT cell population.

There was 5.47% of iNKT cells present after microbeads isolation (**Figure 34 a.**), but the enrichment was not possible to calculate since cells prior microbeads isolation weren't staining for CD3 and CD1d PBS-57 tetramer. Nevertheless, using just 50 µL per $100x10^6$ cells, instead of the recommended 100 µL, is enough to obtain the ~0% of iNKT cells in the negative fraction and less than 100% purity of iNKT cells.

This experiment was repeated, this time staining cells with anti-CD3 and CD1d PBS-57 tetramer prior enrichment, in order to calculate the enrichment obtained using half of the recommended volume of anti-iNKT MicroBeads. In **Figure 35**, the percentage of iNKT cells before and after enrichment are represented, as well as the percentage in the negative fraction (**Figures 35 a.**, **b.**, **c.**, respectively).

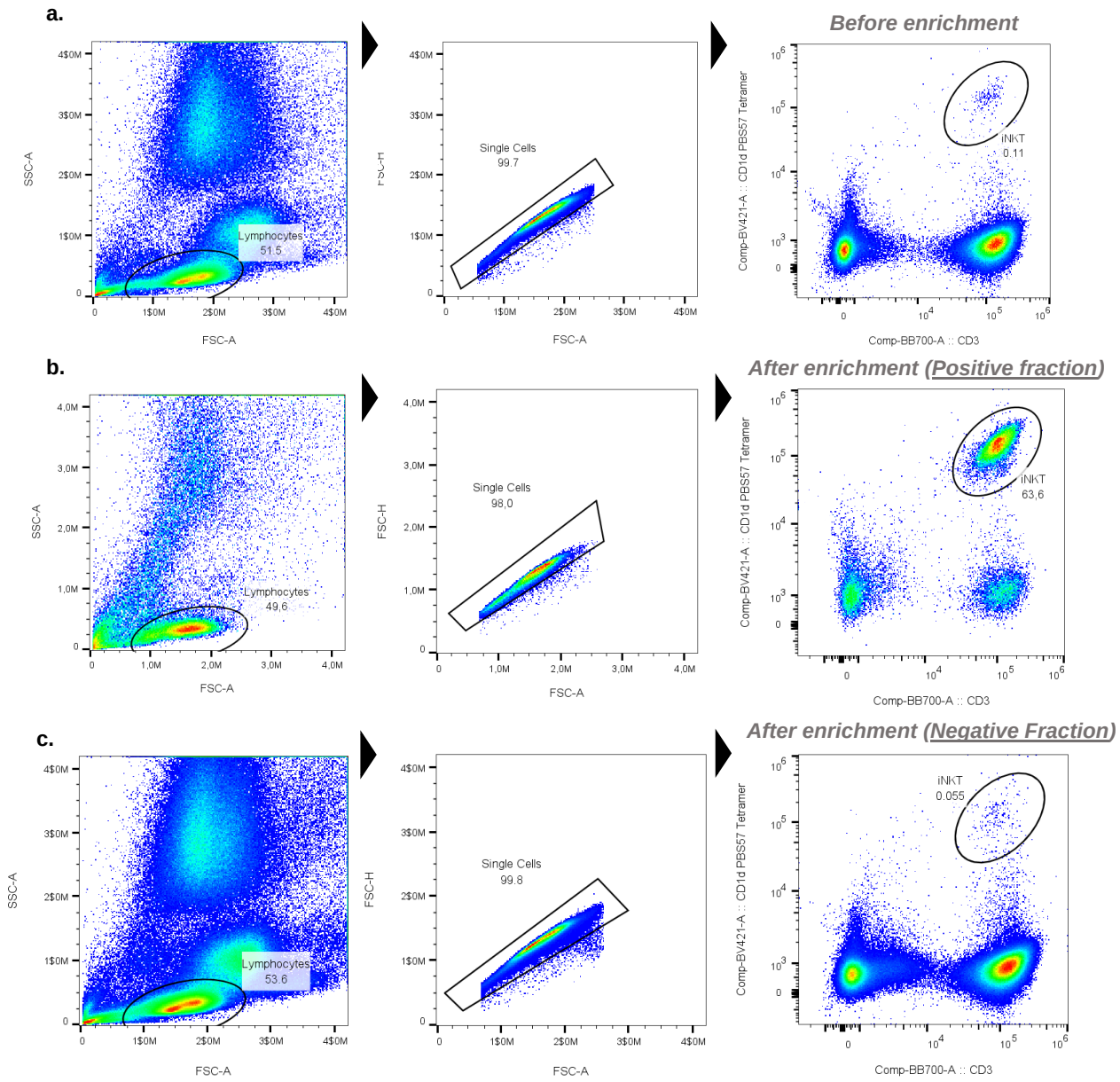

Figure 35. iNKT Cell isolation using Anti-human iNKT cell MicroBeads. The iNKT cells were isolated from human PBMCs using Anti-iNKT MicroBeads, a LS Column, and a MiniMACS™ Separator. Half of the recommended amount of microbeads was used (50 µL per 100x10⁶ cells instead of 100 µL). Cells were fluorescently stained with CD1d PBS57 BV421 (1:800) and Anti-CD3 BB700 (1:100). Lymphocytes were gated according to their size (forward scatter – FSC) and granularity (side scatter – SSC), followed by singlets selection. iNKT cells were selected based on the positivity for Anti-CD3 BB700 and CD1d PBS-57 Tetramer BV421. **a.** iNKT cells before enrichment. **b.** Positive fraction of isolated cells with iNKT microbeads. **c.** Negative fraction of isolated cells with iNKT microbeads.

This donor had 0.11% of iNKT cells in PBMCs (**Figure 35 a.**), which was augmented to 63.6% after anti-iNKT MicroBeads enrichment (**Figure 35 b.**). There was an enrichment of 578 x (%iNKT cells after enrichment (positive fraction) / %iNKT cells before enrichment) using half of the recommended amount of MicroBeads. Although there was still 0.055% of iNKT cells present in the negative fraction, this percentage is not

significant compared to the enrichment obtained (**Figure 35 c.**). Considering the results from the first experiment using the Anti-iNKT MicroBeads (**Figure 34**) and the last one, where the PBMCs before enrichment were also analysed (**Figure 35**), 50 µL per $100x10^6$ PBMCs (half of the recommended amount) was the defined amount of Anti-iNKT MicroBeads to use with Fabry disease patients and healthy controls.

Anti-human iNKT MicroBeads were used in eight experiments. The percentage of iNKT cells present in PBMCs (prior enrichment), in the positive and negative fractions (after enrichment) was always analysed. The negative fraction was used as a control over the enrichment and to see if iNKT cells weren't being lost to the negative fraction. In **Figure 36**, the results from the analyses of the percentage of iNKT cells among different fractions of Anti-iNKT MicroBeads enrichment are represented. Looking at the percentage of iNKT in PBMCs and in the positive fraction, it is possible to see that there was enrichment of iNKT cells as expected ($p < 0.001$) (**Figure 36**). Regarding the percentage of these cells in PBMCs compared to the negative fraction, although it was seen that there was a reduction in the percentage of iNKT cells in the negative fraction, when compared with the percentage before enrichment, it does not reach statistical significance ($p=0.0581$) (**Figure 36**). In five out of eight experiments, the percentage of iNKT cells in the negative fraction decreased compared to the percentage before enrichment (experiments 1, 3, 4, 6, 7, **Table 10**- rows highlighted with dark green). In the other three experiments, this decrease was not observed (experiments 2, 5 and 8, **Table10- rows that are not highlighted**).

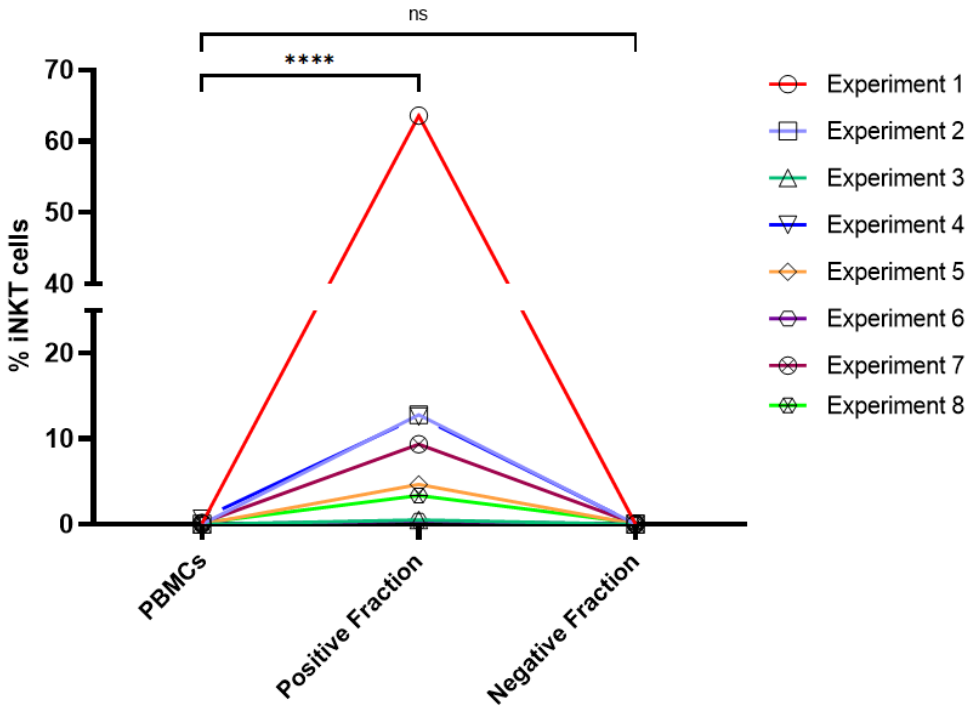

Figure 36. iNKT cell percentage among different fractions of anti-iNKT MicroBeads enrichment. Percentage of iNKT cells before enrichment ("PBMCs"), after enrichment ("Positive Fraction") and negative fraction of the enrichment ("Negative Fraction") of 8 different experiments (each corresponds to a different Buffy Coat donor or Fabry disease patients' blood samples) are represented. Experiments 1-5 correspond to Buffy Coat donors (healthy donors) and experiments 6-8 correspond to blood samples from Fabry disease patients. Different line colours and symbols are associated with different experiments. iNKT cells were identified as CD3+ cells and as positive for CD1d-PBS57 tetramer. Statistical analysis was performed by paired T-Test with Welch's correction. p **** <0.0001; ns (not significant): $p \geq 0.05$.

The enrichment was very variable inter experiments albeit it was possible to conclude that it was not dependent on the iNKT percentage in PBMCs. Looking at **Table 10**, where the enrichment of each experiment is represented, even though it seemed that when a donor/ patient has a higher iNKT cell percentage in PBMCs, a higher iNKT cells percentage was obtained in the positive fraction, this did not translate into a higher enrichment. For instance, the donor from experiment 4 had 0.65% of iNKT cells before enrichment and this percentage augmented to 12.6% after enrichment (**Table 10**). In spite of being a high percentage of iNKT cells, the enrichment was only 19.4 x. On the other hand, the donor from experiment 2 only had 0.036% of iNKT cells prior enrichment and 12.8% after enrichment. Nevertheless, there was an enrichment of 355.6 x, much more than in experiment 4 (**Table 10**).

Table 10. iNKT cell percentage among different fractions of Anti-human iNKT MicroBeads enrichment and respective enrichment. Percentage of iNKT cells before enrichment ("PBMCs"), after enrichment ("Positive Fraction") and negative fraction of the enrichment ("Negative Fraction") of 8 different experiments (each corresponds to a different Buffy Coat donor or Fabry disease patients' blood samples) are represented. Experiments 1-5 correspond to Buffy Coat donors (healthy donors) and experiments 6-8 correspond to blood samples from Fabry disease patients. The enrichment was calculated by using the formula: % iNKT cells after enrichment (positive fraction) / % iNKT cells before enrichment (PBMCs). The rows highlighted with dark green represent the experiments where decrease of % iNKT in the negative fraction, compared to %iNKT cells before enrichment, was observed.

Experiment	*PBMCs*	*Positive Fraction*	*Negative Fraction*	*Enrichment*
1	0.11	63.6	0.055	578.18
2	0.036	12.8	0.038	355.56
3	0.0069	0.54	0.0024	78.26
4	0.65	12.6	0.048	19.38
5	0.037	4.69	0.045	120.26
6	0.0067	0.44	0.0034	65.67
7	0.2	9.36	0.083	46.8
8	0.2	3.38	0.2	16.9

Notwithstanding the variability of the Anti-human iNKT MicroBeads enrichment between experiments, there was always enrichment of iNKT cells. Despite the enrichment, in some experiments it was not enough to study all the markers wanted in iNKT cells: **Figures 46** (**b.** and **c.**), **47** and **48** (**a.** and **c.**).

2.4 Optimisation and validation of instrument and reagents settings

The optimal amount of all reagents (antibodies, tetramers, fixable viability dye and Anti-iNKT MicroBeads) that were going to be used to analyse iNKT cells of Fabry disease patients and healthy subjects had been determined. The combination of all these reagents had to be tested to evaluate if some changes in the volumes/ concentrations were needed.

The number of iNKT cells obtained from blood tubes is low (if only 9-54x10^6 PBMCs can be obtained from two blood tubes with 9 mL each- 0.5-3x10^6 PBMCs per mL of blood[211], then from these PBMCs we would only get 0.001-0.54 x10^6 iNKT cells), so the number of analyses is limited. In line with this, compensation beads were used to do the antibodies single-stained controls for flow cytometry. CD1d PBS-57 tetramer single-stained control was done using the iNKT cell line and the Fixable Viability Dye single-

stained control was done with live and dead PBMCs. Besides this, FMO controls for the antibodies anti-PD-1 and anti-ICOS were done (i.e., samples stained with all the fluorochromes in the panel, minus anti-PD-1 or anti-ICOS, respectively), since there is no distinction between the positive and negative cells for the markers. Although with anti-TIM-3 was not possible to observe a separation between the positive and negative populations as well, no staining was obtained using non-stimulated PBMCs (stained cells with anti-TIM-3 = unstained cells; **Figure 16**), meaning that with the healthy subjects we wouldn't obtain it neither. Thus, they were going to be used as controls for the gating of the positive cells for TIM-3 if they were detected in Fabry disease patients.

B cells and monocytes frequencies were evaluated as well as the monocyte activation state, using antibodies against the co-stimulatory molecules CD40 and CD86, in the donor's PBMCs prior enrichment with Anti-iNKT MicroBeads. Within the lymphocyte population of PBMCs, this donor, analysed to validate the settings, had the $CD19^{+}$ B cells within the normal range[212] (Q3 from right bottom plot of **Figure 37**).

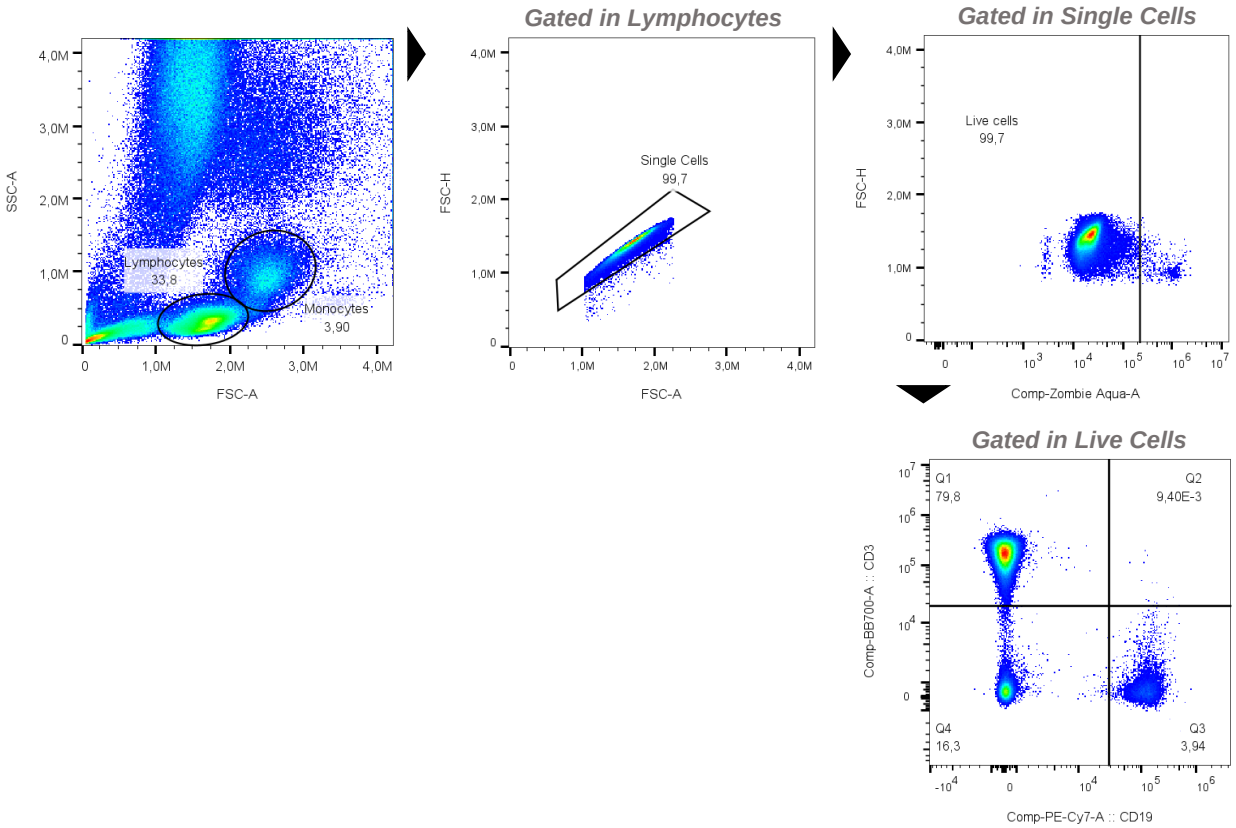

Figure 37. Flow cytometric analyses of human B cells of health donor's PBMCs (before anti-iNKT MicroBeads enrichment). Cells were fluorescently stained with Anti-CD3 BB700 (1:100), Anti-CD19 PE-Cy7 (1.5:100) and Fixable viability dye Zombie Aqua (1:400). Lymphocytes were gated according to their size (forward scatter – FSC) and granularity (side scatter – SSC), followed by singlets selection. Cells non-fluorescent with Zombie Aqua were considered live/ viable cells. Inside live cells, B cells were selected based on the positivity for Anti-CD19 PE-Cy7 and negativity for Anti-CD3 BB700.

This healthy donor presented a normal percentage of monocytes in PBMCs (left plot of **Figure 38**) as well as $CD14^+$ monocytes frequency within the normal range (middle right plot of **Figure 38**) [213,214]. $CD14^+$ monocytes from this donor were not stimulated, since there was no expression of CD40 nor CD86. This was expected because the monocytes hadn't been stimulated, being in resting state in healthy individuals[215,216].

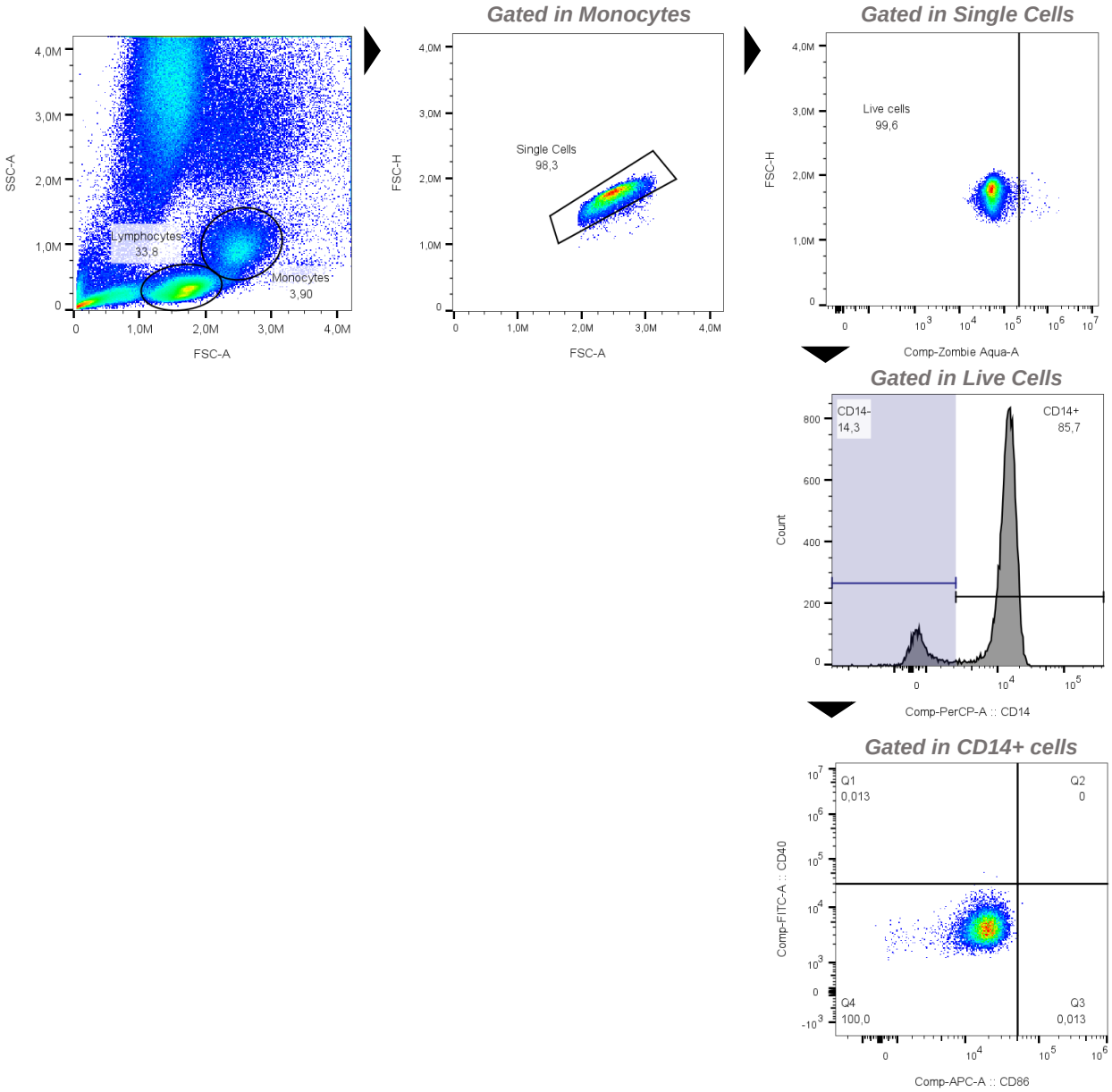

Figure 38. Flow cytometric analyses of human monocytes of health donor's PBMCs (before anti-iNKT MicroBeads enrichment). Cells were fluorescently stained with Anti-CD14 PerCP (1:100), Anti-CD40 FITC (3:100), Anti-CD86 APC (1:50) and Fixable viability dye Zombie Aqua (1:400). Monocytes were gated according to their size (forward scatter – FSC) and granularity (side scatter – SSC), followed by singlets selection. Cells non-fluorescent with Zombie Aqua were considered live/ viable cells. Inside live cells, CD14+ cells were selected based on the positivity for Anti-CD14 PerCP. CD14+ cells were analysed for activation markers, by gating Anti-CD40 FITC vs Anti-CD86 APC.

Lastly, iNKT cells phenotype was studied after enrichment with Anti-iNKT MicroBeads (**Figures 39** and **40**). $CD3^+$ T cells were always analysed in parallel with iNKT cells. CD4 and CD8 expression was analysed in both types of cells (**Figure 39**). The analyses of these subsets in iNKT cells showed a high predominance of $CD4^+$ iNKT cells as well (upper right plot of **Figure 39**). DN and $CD8^+$ iNKT cell subsets were also observed, although there were few iNKT cells (upper right plot of **Figure 39**). Regarding $CD3^+$ T cells, $CD4^+$ subset presented the highest percentage (56%) (left bottom plot of **Figure 39**). DN and DP $CD3^+$ T cell subsets were also observed in this donor, although they are the least common (usually between 1 and 3%, range that may vary)[217–219]. Regarding the expression of CD8 dimers, it was not possible to study CD8 dimers in iNKT cells in this healthy donor since few cells positive for CD8α were acquired, making it not reliable to evaluate. Nevertheless, the analyses were possible in $CD3^+$ T cells: 82% of the $CD8^+$ $CD3^+$ T cells expressed CD8αβ heterodimers, and the rest expressed CD8αα (right bottom plot of **Figure 39**). CD8ββ homodimers don't occur naturally[220].

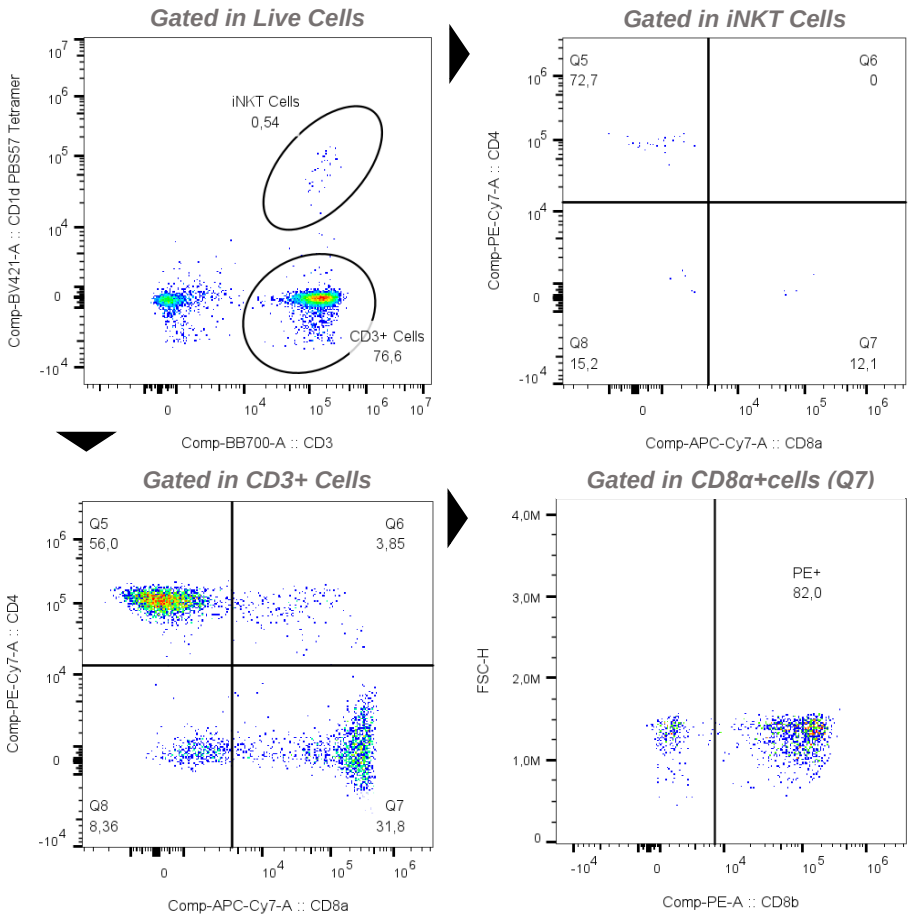

Figure 39. Flow cytometric analyses of CD4, CD8 and CD8 dimers expression on CD3+ T cells and iNKT cells of a health donor's PBMCs after anti-iNKT MicroBeads enrichment. Cells were fluorescently stained with Anti-CD3 BB700 (1:100), CD1d PBS-57 tetramer BV421 (1:800), Anti-CD4 PE-Cy7 (1:100), Anti-CD8α PE-Cy5 (1:100), Anti-CD8β (1:100) and Fixable viability dye Zombie Aqua (1:400). After iNKT cell selection based on the positivity for CD1d PBS-57 tetramer and CD3 and T cell selection (CD3+ and CD1d PBS-57 tetramer-), the frequency of CD4 and CD8α was analysed. The frequency of CD8αβ was analysed inside CD8α.

Afterwards, TIM-3, PD-1, ICOS and CD161 expression was analysed in both T and iNKT cells (**Figure 40**). As expected, there was no expression of TIM-3 on $CD3^+$ T cells and on iNKT cells (upper and bottom left plots of **Figure 40**, respectively). Both types of cells expressed little PD-1 and ICOS (second and third bottom plots counting from the left of **Figure 40**, respectively). Taking into account that it is not possible to reliably gate the positive population for ICOS, this marker expression was evaluated in Fabry disease patients and healthy subjects using its MFI value. Two distinct populations can be observed when cells were stained with anti-CD161.

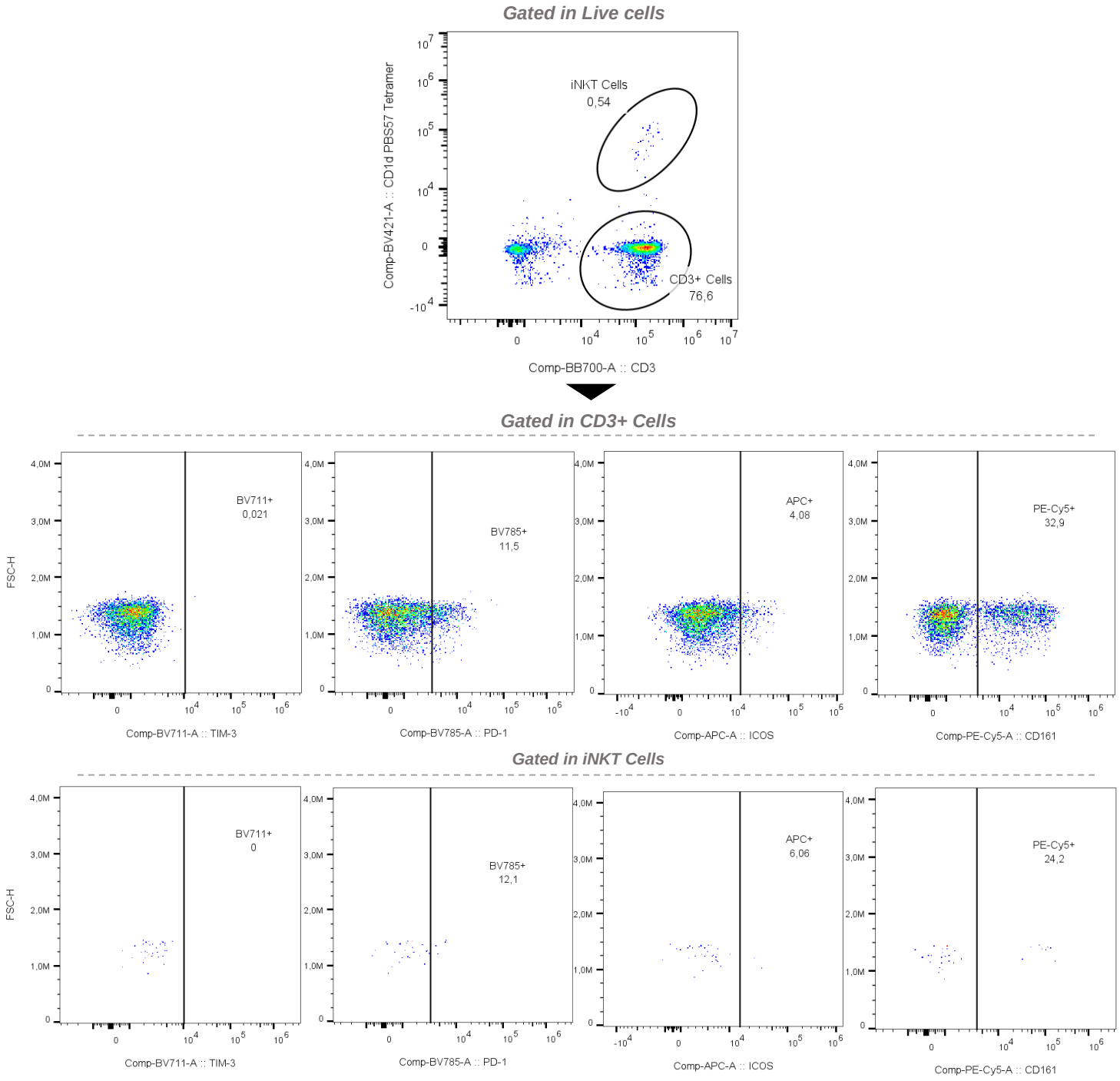

Figure 40. Flow cytometric analyses of TIM-3, PD-1, ICOS and CD161 expression on CD3+ T cells and iNKT cells of a health donor's PBMCs after anti-iNKT MicroBeads enrichment. Cells were fluorescently stained with Anti-CD3 BB700 (1:100), CD1d PBS-57 tetramer BV421 (1:800), Anti-TIM-3 BV711 (1:50), Anti-PD-1 BV785 (1:40), Anti-ICOS (1:100), Anti-CD161 (1:100) and Fixable viability dye Zombie Aqua (1:400). After iNKT cell selection based on the positivity for CD1d PBS-57 tetramer and CD3 and T cell selection (CD3+ and CD1d PBS-57 tetramer-), the frequency of each marker was analysed in iNKT cells and T cells (CD3+).

The results presented in **Figures 36-40** demonstrate that the optimal concentrations and amounts of the reagents defined are correct and can be used with Fabry disease patients and healthy subjects.

2.5 Final remarks on the optimisations

One of our interests was to determine if the circulating iNKT cell subpopulation with a cytotoxic phenotype, discovered by Cui et al.[181], existed. After titrating the exactly the same antibodies (and clones) used by the authors to find this population, the same results were not obtained, questioning the existence of this circulating population in human iNKT cells and the results from the article. Albeit the cohort of healthy PBMCs donors was not the same as Cui and colleagues used (Cui et al. acquired PBMCs from Japanese healthy donors[181] whereas our healthy donors were Portuguese), it is not sufficient to have such a difference in this iNKT cell population. The authors have been questioned by us about the methods they have used to isolate PBMCs and their flow cytometry protocol and no differences were detected comparing to our protocol. Therefore, we question the identification of this circulating iNKT cell subpopulation with a cytotoxic phenotype by Cui and colleagues. More studies need to be done regarding this population and evaluate if it there is variation among different donors. Anti-CXCR6 and anti-CD244 antibodies were replaced with anti-ICOS APC and anti-CD161 PE-Cy5, respectively.

AF488 labelled MR1 5-OP-RU tetramer stopped working and it is not going to be used until further notice from NIH, since the panel was designed based on the fluorochromes available for this tetramer and it was not possible to include other available fluorochrome in the panel (**Table 7**).

Although CD14 was present in the first panel (**Table 6**), it would only be used to detect monocytes which is easily done just by looking at the plot SSC-A vs FSC-A, since it is a defined population of cells. Hence, this antibody was not used to analyse the monocytes in Fabry disease patients and healthy subjects.

In **Table 11**, the optimal concentrations of the antibodies, tetramers and viability dye, as well as the amount of Anti-iNKT MicroBeads, that were titrated and used to study the iNKT cells of Fabry disease patients and healthy donors are represented.

Table 11. Optimal concentrations of the antibodies, tetramers, viability dye and amount of Anti-human iNKT MicroBeads that were titrated in this project. Clones, fluorochrome and supplier of each reagent are also represented.

Reagents	Clone	Fluorochrome	Supplier	Optimal Concentration
Anti-human CD3	OKT3	FITC	Biolegend	1:200
Anti-human CD3	OKT3	BB700	BD Biosciences	1:100
Anti-human CD3	OKT3	PerCP-Cy5.5		1:100
Anti-human CD4	RPA-T4	PE-Cy7	Biolegend	1:400
Anti-human C8α	HIT8a	APC-Cy7	Biolegend	1:100
Anti-human CD8β	SIDI8BEE	PE	Thermo Fisher	1:100
Anti-human CD161	HP-3G10	PE-Cy5	Biolegend	1:100
Anti-human ICOS	C398.4A	APC	Biolegend	1:100
Anti-human PD-1	EH12.2H7	BV785	Biolegend	1:40
Anti-human TIM-3	F38-2E2	BV711	Biolegend	1:50
Anti-human CD244	K041E5	APC	Biolegend	1:200
Anti-human CXCR6	C1.7	PE-Cy5	Biolegend	1:50
Human CD1d PBS-57 Tetramer	----	APC	NIH	1:800
Human CD1d PBS-57 Tetramer	----	BV421	NIH	1:800
Human MR1 5-OP-RU Tetramer	----	BV421	NIH	1:200
Anti-human IFN-γ	4S.B3	BV711	Biolegend	1:100
Fixable Viability Dye	----	Zombie Aqua	Biolegend	1:400
Anti-human iNKT MicroBeads	----	----	Miltenyi	50 µL per $100x10^6$ cells

Abbreviations: APC – Allophycocyanin; BV – Brilliant Violet; Cy – Cyanine; FITC – Fluorescein; PE – Phycoerythrin; PerCP - Peridinin chlorophyll protein; PBS-57 – α-GalCer analog; AF- Alexa Fluor: BB- Brilliant Blue; 5-OP-RU: 5-(2-oxopropylideneamino)-6-D-ribitylaminouracil.

3. Analyses of iNKT cell phenotype in Fabry disease patients and healthy subjects

Three Fabry disease patients and four control subjects were included in this study. The control group of this study was composed by two males and two females. In the Fabry disease patients' group, two were female siblings, both presenting the classical variant of the disease, and the other patient, a male, presented the cardiac variant. One of the Fabry disease siblings suffered from ulcerative colitis and the other patient was diagnosed with myeloma. A study showed that Fabry disease was associated with myeloma (there are reported cases demonstrating a potential pathogenic relationship between Fabry disease and myeloma[221]). The male patient was already under ERT at the beginning of the study whereas the siblings were not under any treatment.

From healthy subjects, PBMCs were isolated from Buffy Coats. In the case of the Fabry disease patients, PBMCs were obtained from two 9 mL blood tubes (whole blood).

3.1 Percentage of monocytes, B cells and T cells in Fabry disease patients

PBMCs from Fabry disease and control subjects were stained with an anti-human CD19 antibody (B cells), anti-human CD3 (T cells) and they were analysed by flow cytometry. After defining the lymphocyte gate in the side scatter and forward scatter plot, lymphocytes were selected and the percentages of T cells ($CD3^+$) and B cells ($CD19^+$) were determined (right plot of **Figure 41**). The percentage of monocytes was evaluated based on their size (FSC) and granularity (SSC) (upper left plot of **Figure 41**). The expression of the co-stimulatory molecules CD40 and CD86 was then evaluated (bottom left plot of **Figure 41**).

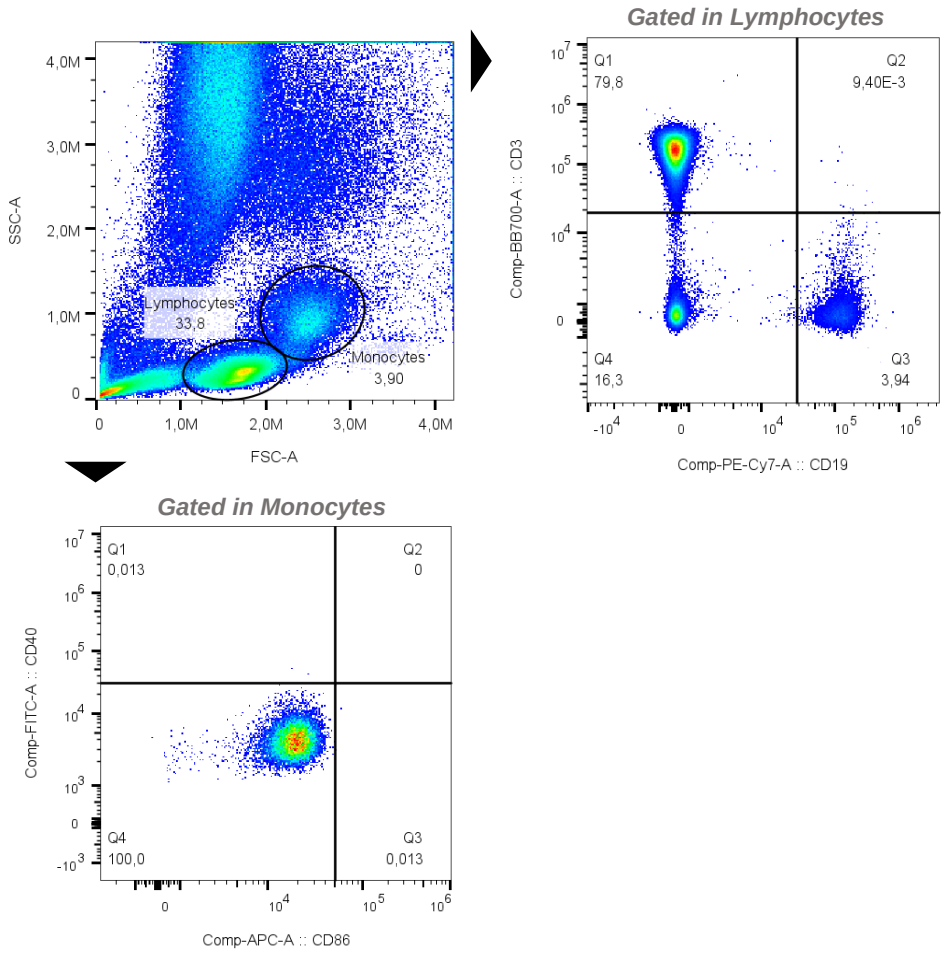

Figure 41. Representative gating strategy used to quantify the percentage of monocytes (and their activation state), B cells and T cells using flow cytometry in Fabry disease patients and healthy subjects. Lymphocytes and monocytes were gated according to their size (forward scatter – FSC) and granularity (side scatter – SSC), followed by singlets selection (not shown). A Fixable Viability Dye was always used to determine the cell viability (not shown). B cells were selected based on their positivity against anti-CD19, whereas T cells were selected based on CD3+ cells. Monocyte activation state was analysed based on the markers CD40 and CD86.

The results regarding the monocytes, B cells and T cells in Fabry disease patients and control subjects are presented in **Figure 42**. A reduction in the percentage of monocytes in Fabry disease patients was observed, but it was not statistically significant when compared with healthy controls (**Figure 42 a.**). As for the activation state of monocytes, neither of subjects (controls and patients) presented expression of CD40 and CD86, being all the plots analysed similar to the one presented in the representative example (bottom left plot of **Figure 41**). $CD19^+$ and $CD3^+$ cells percentage didn't vary between healthy subjects and Fabry disease patients (**Figures 42 a.** and **b.**, respectively).

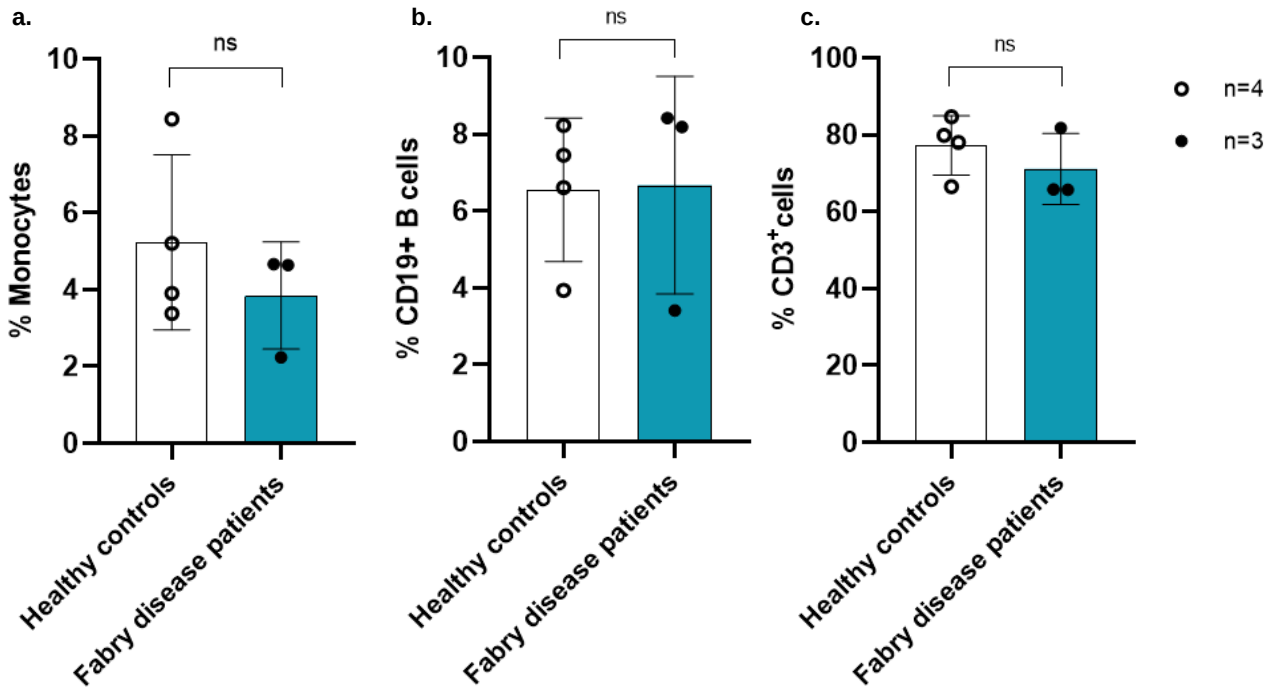

Figure 42. Monocytes, B cells and T cells percentage in Fabry disease patients and healthy controls. a. Comparison between monocytes percentage in Fabry disease patients and control subjects. Monocytes were identified based on their size (forward scatter – FSC) and granularity (side scatter – SSC). **b.** Comparison between B cells percentage in Fabry disease patients and control subjects. B cells were identified based on their positivity for CD19. **c.** Comparison between T cells percentage in Fabry disease patients and control subjects. T cells were identified based on their positivity for CD3. Vertical lines represent means with standard deviation (SD). White dots represent four healthy controls. Black dots represent three Fabry disease patients. White bar represents healthy controls. Blue bar represents Fabry disease patients. Statistical analysis was performed by unpaired T-Test with Welch's correction. ns (not significant): $p \geq 0.05$.

Within the lymphocyte population of PBMCs, $CD19^+$ B cells usually contribute with 5-15% of the total lymphocyte population, although it is important to take into account that the frequencies of human cell types differ among individuals[212]. Monocytes represent 3-8% of the circulating blood cells[222]. The percentage of leukocytes was shown to be altered

in Fabry disease patients[29,71,72]. Rozenfeld et al. demonstrated that patients possessed higher percentage of total lymphocytes and $CD19^+$ cells, in contrast with a decreased proportion of monocytes, when compared to healthy controls[223]. These authors also reported that these alterations were less pronounced in treated Fabry disease patients[223]. The percentage of monocytes in Fabry disease patients analysed in this studied presented a tendency to decrease (**Figure 42 a.**), which is in accordance with the literature. However, the patient under ERT is the patient who presented the lowest percentage of monocytes (2.24%) in comparison with the other two patients who are not under any treatment (**Figure 42 a.**). This does not corroborate the findings from Rozenfeld et al, who reported a less pronounced decrease in monocytes in patients under treatment[223]. In terms of B cells and T cells, no differences were detected (**Figure 42 b.** and **c.**, respectively), contrary to articles published[29,71,72,223]. Nonetheless, the patient under ERT presented less B cells (3.41%) than the patients not treated (**Figure 42 b.**). In the case of T cells, the contrary happened, being the patient under ERT the one who presented the highest percentage of T cells (81.8%), compared to the non-treated patients.

Overall, no statistically significant differences were found between the control and Fabry disease patients' groups in the percentage of monocytes, B cells and T cells. Apart from monocytes, these findings differ from the literature, where differences in leukocyte populations between these two groups were observed, as mentioned above (Fabry disease patients have been reported to present lower percentage of monocytes and higher percentage of T cells and B cells compared to healthy subjects)[29,71,72,223].

3.2 Percentage of iNKT cells in Fabry disease patients

In order to study the percentage of iNKT cells in both control and patients' groups, PBMCs were stained with an anti-human CD3 antibody and the human CD1d tetramer loaded with PBS57 (an α-GalCer analogue) and they were analysed by flow cytometry. After defining the lymphocyte gate in the side scatter and forward scatter plot, iNKT cells were selected based on the positivity for both CD3 and CD1d PBS-57 tetramer (**Figure 43**).

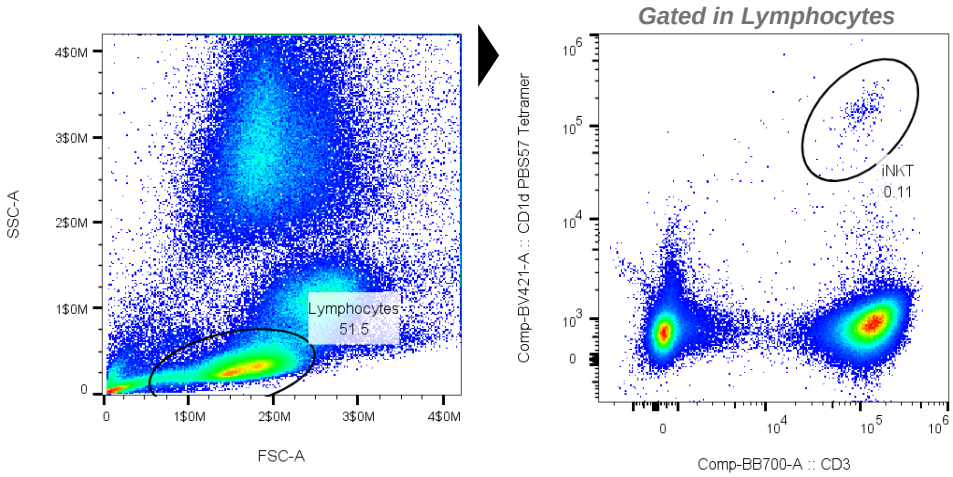

Figure 43. Representative gating strategy used to quantify the percentage of iNKT cells in Fabry disease patients and healthy subjects. Lymphocytes were gated according to their size (forward scatter – FSC) and granularity (side scatter – SSC), followed by singlets selection (not shown). A Fixable Viability Dye was always used to determine the cell viability (not shown). iNKT cells were selected based on their positivity for CD3 and CD1d PBS-57 tetramer.

In **Figure 44**, the results with regard to the iNKT cell percentage in Fabry disease patients and control subjects are represented. Surprisingly, two Fabry disease patients presented higher levels of iNKT cells than control subjects and, interestingly, these two patients are the siblings. Nevertheless, the difference between the patients and control groups is not statistically significant, which corroborates the literature[116].

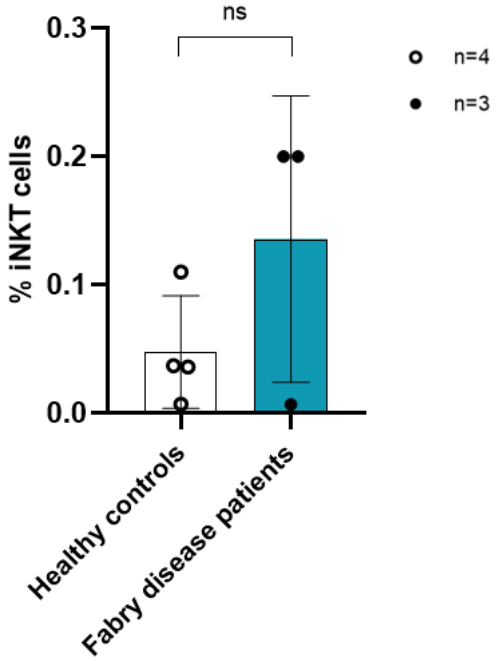

Figure 44. iNKT cell percentage in Fabry disease patients and healthy controls. iNKT cells were identified based on their positivity for CD3 and CD1d PBS-57 tetramer. Comparison between iNKT cell percentage in Fabry disease patients and control subjects. Vertical lines represent means with standard deviation (SD). White dots represent four healthy controls. Black dots represent three Fabry disease patients. White bar represents healthy controls. Blue bar represents Fabry disease patients. Statistical analysis was performed by unpaired T-Test with Welch's correction. ns (not significant): $p \geq 0.05$.

Altogether, no statistically significant differences were found between the control and Fabry disease patients' group in the percentage of iNKT cells. The percentage of iNKT cells was shown to be decreased in Fabry disease mice[190–194], which is not observed in Fabry disease patients[116,197]. As previously described, the iNKT cell percentage in human peripheral blood is highly variable[131,145], which explains the variability of iNKT cells percentage obtained in both patients and healthy controls groups. The variability in patients may also be due to the fact that they present different variants of the disease (and the two siblings who present the same variant have the same percentage of iNKT cells- 0.2%).

3.3 Percentage of iNKT cell subsets in Fabry disease patients

In humans, iNKT cells can be divided into four different subsets according to their CD4 and CD8 expression: $CD4^+$, $CD8^+$ or DN and a very small double positive (DP) subset has also been observed[146,147]. This study focused on the three major subsets of iNKT cells ($CD4^+$, $CD8^+$ and DN). Besides this, two dimers of CD8, CD8αβ and CD8αα, were quantified. These two dimers are distinct in their expression and function[220]. The same analyses were performed in T cells ($CD3^+$) (**Figure 45**). After defining the lymphocyte gate in the side scatter and forward scatter plot, iNKT cells were selected based on the positivity for both CD3 and CD1d PBS-57 tetramer. T cells were selected based on their positivity for CD3 and negativity for CD1d PBS-57 tetramer.

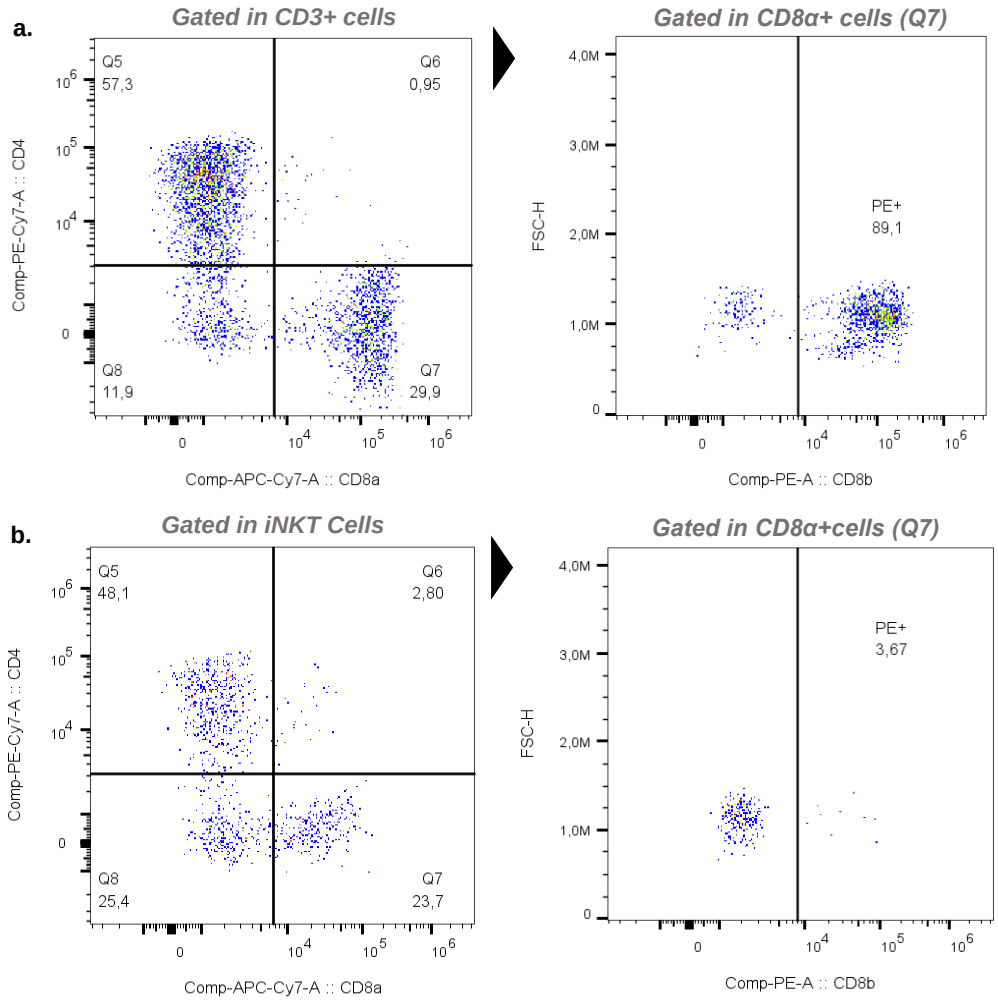

Figure 45. Representative gating strategy used to quantify the percentage of T and iNKT cell subsets in Fabry disease patients and healthy subjects. a. T cell (CD3+) subsets analysed by flow cytometry. **b.** iNKT cell (CD1d PBS-57 tetramer+ and CD3+) subsets analysed by flow cytometry.

The frequencies of iNKT cell and T cell subsets, according to CD4 and CD8 expression, in Fabry disease patients and control subjects are represented in **Figure 46**. Regarding the percentage of $CD4^+$ iNKT cells, no differences were observed between patients and control groups. (**Figure 46 a.**). However, it was expected that patients had a decreased percentage of $CD4^+$ iNKT cell subset[197]. In terms of $CD8^+$ iNKT cells frequency, there was a decrease, albeit not statistically significant, in Fabry disease patients compared to healthy subjects (**Figure 46 b.**), as it has been shown in another study from Pereira et al.[190,197]. Concerning the DN subset, it was observed an increased DN iNKT cells percentage in Fabry disease patients when compared to controls, as it has been demonstrated previously[197], but this difference had no statistical significance (**Figure 46**

c.). No significant differences were observed between the treated patient and not treated patients regarding these subsets (**Figure 46**).

No statistically significant differences were observed in $CD3^+$ T cell subsets when comparing patients and controls. However, interestingly, $CD3^+$ cells presented a much higher expression of CD8 (**Figure 46 b.**) and decreased expression of DN (**Figure 46 c.**), when compared to iNKT cells from Fabry disease patients.

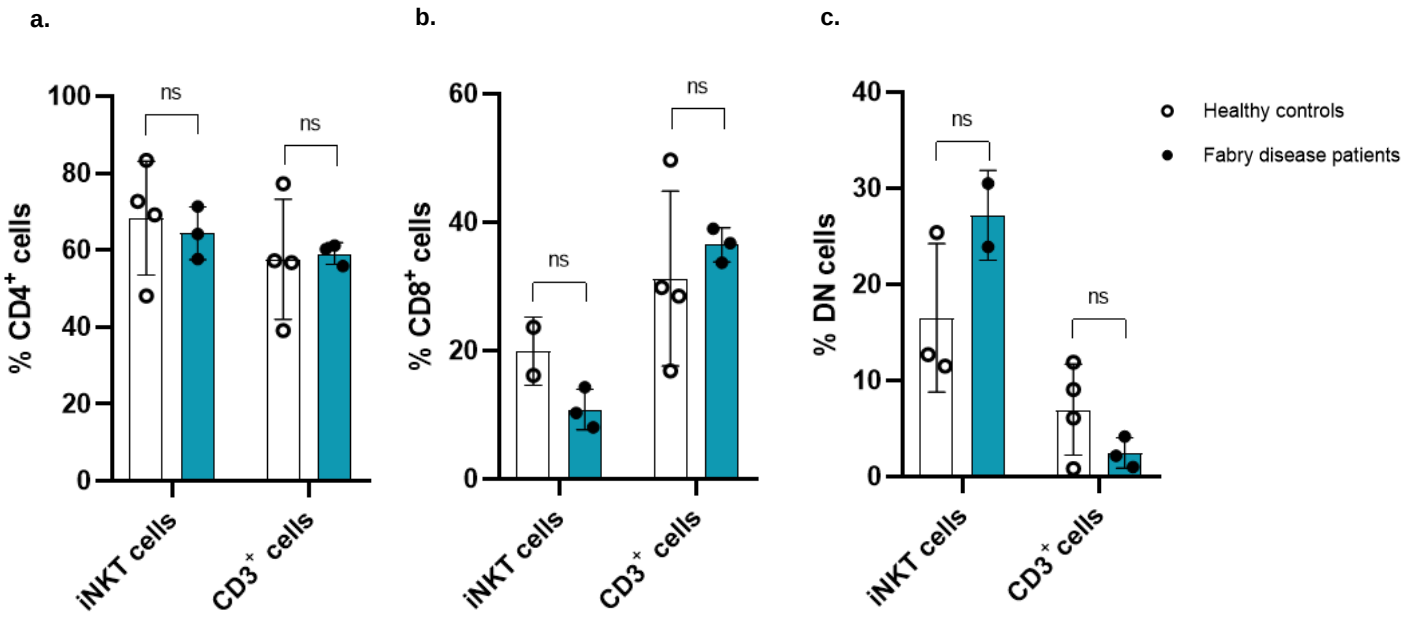

Figure 46. iNKT and T cells (CD3+) subsets percentage in Fabry disease patients and healthy controls. Samples from three patients and four controls were acquired. **a.** iNKT CD4+ cell and T CD3+ CD4+ cell percentage. **b.** iNKT CD8+ cell and T CD3+ CD8+ cell percentage. Only two healthy donors' iNKT cells were analysed due to the low number of CD8+ cells acquired from the other two subjects. **c.** iNKT DN cell and T DN CD4+ cell percentage. Only three healthy donors' iNKT cells and two patients' iNKT cells were analysed due to the low number of DN cells acquired from the other subject. Vertical lines represent means with standard deviation (SD). White dots represent healthy controls. Black dots represent Fabry disease patients. White bar represents healthy controls. Blue bar represents Fabry disease patients. Statistical analysis was performed by unpaired T-Test with Welch's correction. ns (not significant): $p \geq 0.05$.

CD8 dimers (CD8αα and CD8αβ) expression was quantified in both iNKT cells and T cells ($CD3^+$) of healthy subjects and Fabry disease patients. The results are represented in **Figure 47**. Looking at the graphic, an outstanding difference jumps out: in general, iNKT cells express more CD8αα whilst $CD3^+$ cells have more percentage of the isoform CD8αβ (**Figure 47**). Looking in detail at the patients and controls, the frequencies of $CD8\alpha\alpha^+$ iNKT cells, $CD8\alpha\alpha^+$ $CD3^+$ cells, $CD8\alpha\beta^+$ iNKT cells and $CD8\alpha\beta^+$ $CD3^+$ cells didn't differ between controls and Fabry disease patients (**Figure 47**). On the other hand,

differences were observed between healthy subjects' CD8αβ$^+$ iNKT cells and CD8αβ$^+$ CD3$^+$ cells, with CD3$^+$ cells expressing more CD8αβ than iNKT cells (**Figure 47**). This difference was also observed in Fabry disease patients (**Figure 47**). On the contrary, both controls and patients expressed more CD8αα$^+$ iNKT cells than CD8αα$^+$ CD3$^+$ cells (**Figure 47**). Comparing the proportion of CD8αβ and CD8αα in CD3$^+$ cells and iNKT cells, both groups have more CD8αβ T cells (CD3$^+$) than CD8αα T cells (p-value < 0.0001) (**Figure 47**). On the contrary, the majority of iNKT cells in both groups expressed CD8αα, compared to CD8αβ (p-value < 0.0001) (**Figure 47**).

Patients and control groups' iNKT cells tend to express more CD8αα whereas CD3$^+$ cells express more CD8αβ, with low variability among different patients (**Figure 47**). This means that, although healthy donors and Fabry disease patients presented no variation regarding iNKT cells CD8 dimers, in both groups, most of iNKT cells express CD8αα (more than 90%) whereas CD3$^+$ cells express more CD8αβ (more than 82%) than CD8αα (**Figure 47**).

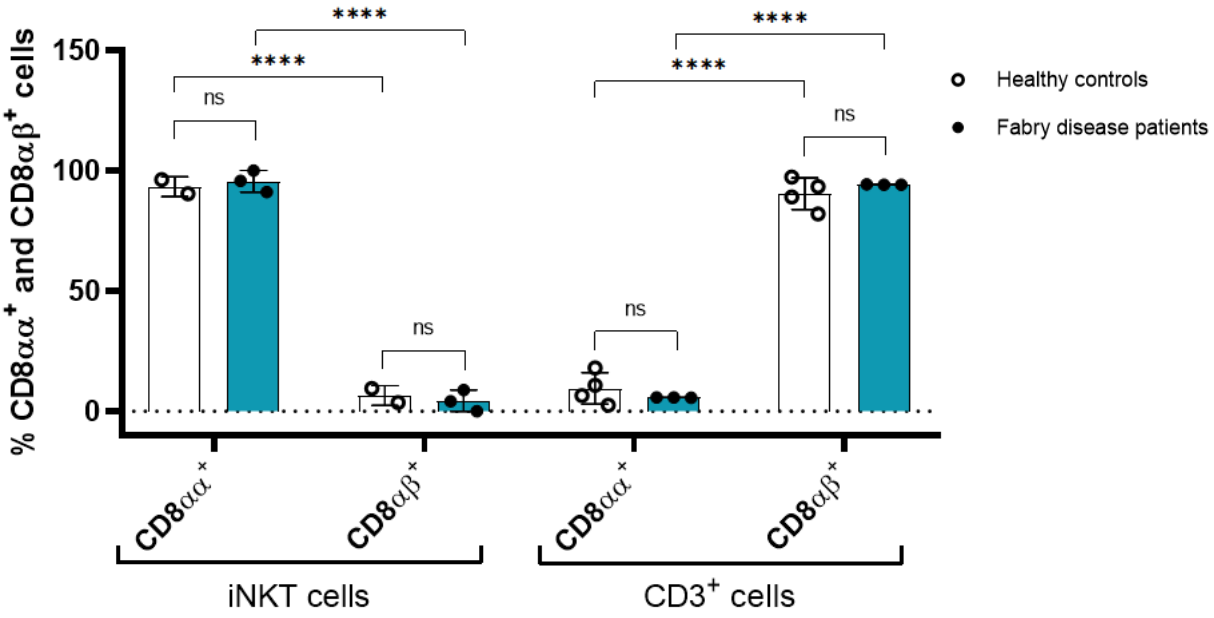

Figure 47. CD8αα and CD8αβ expression in iNKT and T cells (CD3+) subsets percentage in Fabry disease patients and healthy controls. Samples from three patients and four controls were acquired. Due to the low number of iNKT cells that was obtained in two healthy controls, the events acquired were not enough to analyse CD8αα+ and CD8αβ+ iNKT cells from those subjects. Vertical lines represent means with standard deviation (SD). White dots represent healthy controls. Black dots represent Fabry disease patients. White bar represents healthy controls. Blue bar represents Fabry disease patients. Statistical analysis was performed by unpaired T-Test with Welch's correction. p**** <0.0001; ns (not significant): p ≥ 0.05.

In this study, a diminished population of iNKT cells expressing CD8αβ heterodimers was also observed compared to iNKT cells expressing CD8αα homodimers (**Figure 47**). Little is known about the expression of the CD8 dimers in human iNKT cells, and so far, there is no information regarding their expression in Fabry disease. Gumperz et al. showed that iNKT cells from four healthy donors expressed CD8αα homodimers, but almost none expressed CD8αβ heterodimers[147], which corroborates the results obtained in this study concerning the healthy controls. Furthermore, it is known that CD8αα and CD8αβ present functional differences in T cells: CD8αβ acts as a coreceptor for the TCR, boosting functional strength and being consistently expressed on T cells restricted to MHC class I, whereas CD8αα aids in recognition of T cells that deviate from the from the conventional $CD4^+$ or $CD8\alpha\beta^+$ T cells that are chosen in the thymus and restricted by MHC[220]. For instance, intraepithelial lymphocytes subsets possess the unique capacity of expressing CD8αα, which suppresses TCR signals. Some intraepithelial lymphocytes subsets express CD8αβ, which promotes TCR activation. CD8αβ is usually expressed in conventional T cells[224]. The expression of CD8αα by the majority of iNKT cells analysed in this study (**Figure 47**), may indicate that they do not act as conventional T cells and their TCR may have alterations.

3.4 iNKT cells phenotype in Fabry disease patients

iNKT cells are known to express several markers, which characterise their phenotype[145]. In this project, the expression of the markers TIM-3, PD-1, ICOS and CD161 in iNKT cells of Fabry disease patients was evaluated, in parallel with their expression in T cells ($CD3^+$ cells).

iNKT cells and T cells of healthy controls and Fabry disease patients didn't express TIM-3. However, it was possible to observe that PD-1 is expressed and in a wide manner: in general, iNKT cells express more PD-1 than $CD3^+$ cells, which was according to what was expected[178,179] (**Figure 48 a.**). Fabry disease patients' iNKT cells expressed more PD-1 than healthy subjects, even though it wasn't statistically significant (**Figure 48 a.**). The expression of PD-1 on Fabry disease patients $CD3^+$ cells was more variable than on healthy controls, but there wasn't a significative difference between these two groups (**Figure 48 a.**). Regarding the expression of ICOS, evaluated by its MFI, Fabry disease

patients presented higher ICOS MFIs, in both iNKT cells and $CD3^+$ cells, but this increase was not statistically significative (**Figure 48 b.**). $CD3^+$ cells, in both groups, also possessed a higher ICOS MFI than iNKT cells, but once again it was not statistically significative (**Figure 48 b.**). When it comes to the expression of CD161 on iNKT cells and $CD3^+$ cells, there was no statistically significative difference between healthy subjects and Fabry disease patients (**Figure 48 c.**). Nevertheless, iNKT cells expressed more CD161 than $CD3^+$ cells, as expected since this is a marker of NK cells. This difference is more prominent in Fabry disease patients (**Figure 48 c.**).

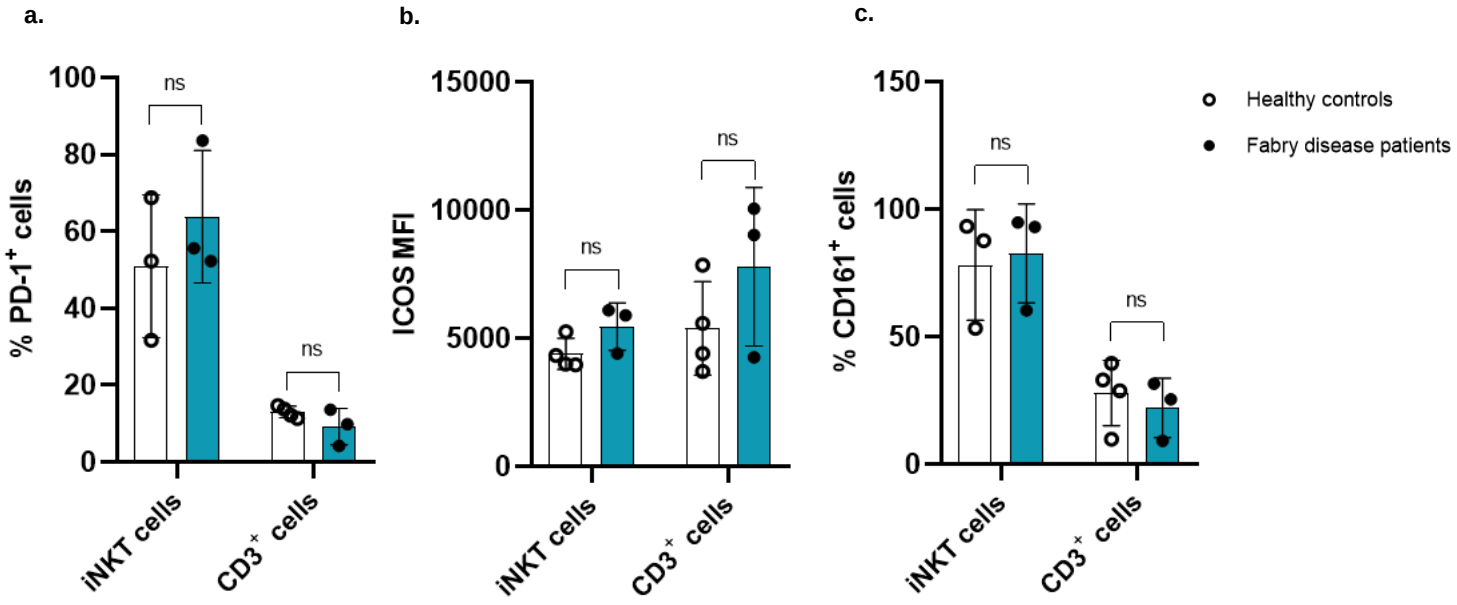

Figure 48. Phenotype analyses of iNKT cells and T cells (CD3+) in Fabry disease patients and healthy controls. a. iNKT PD-1+ cell and T CD3+ PD-1+ cell percentage. **b.** ICOS MFI in iNKT cells and T CD3+ cells. **c.** iNKT CD161+ cell and T CD161+ CD4+ cell percentage. Samples from three patients and four controls were acquired. Due to the low number of iNKT cells that was obtained in a healthy control, the events acquired were not enough to analyse PD-1+ and CD161+ iNKT cells from that subject. Vertical lines represent means with standard deviation (SD). White dots represent healthy controls. Black dots represent Fabry disease patients. White bar represents healthy controls. Blue bar represents Fabry disease patients. Statistical analysis was performed by unpaired T-Test with Welch's correction. ns (not significant): $p \geq 0.05$.

The patient with late onset cardiac variant presented fewer $CD161^+$ iNKT cells (60.3%) when compared to the classical phenotype patients (~94%) (**Figure 48 c.**). Nonetheless, some variance was also observed within the control group.

These markers have not been analysed in iNKT cells from Fabry disease patients, thus no comparison with published data is possible. Thus, more patients need to be analysed in

order to conclude about these markers expression in iNKT cells and what they might influence in this disease.

Overall, no significant differences were observed among the Fabry disease patients presenting different disease phenotypes or between treated and not treated patients.

Due to the low number of patients and healthy controls, it is still early to conclude about differences in leukocyte percentage, including iNKT cells, and iNKT cell phenotype in Fabry disease patients.

Conclusions and Future perscectives

This master's project was the base of a one and a half -year study financed by FCT. With this project, the necessary conditions to study iNKT cells in Fabry disease patients were defined. The approval from ethical and data protection committees from *Centro Hospitalar Universitário de São João*, Porto, Portugal, was obtained to study Fabry disease patients.

A diverse flow cytometry panel was designed and optimised in order to study iNKT cells in these patients. Antibodies, tetramers and fixable viability dye were titrated and tested before being used in patients and healthy subjects.

In 2022, Cui and colleagues described a cytotoxic iNKT cell subpopulation (defined by the markers CXCR6 and CD244)[181], which piqued our interest. Surprisingly, this population was not observed in our healthy donors' fresh iNKT cells (**Figure 25**), questioning the existence of this circulating iNKT cell subpopulation and the results from the article. Hence, this subpopulation was not analysed in Fabry disease patients. More studies need to be done regarding this population and evaluate if it there is variation among different donors. Anti-CXCR6 and anti-CD244 antibodies were replaced with anti-ICOS APC and anti-CD161 PE-Cy5, respectively.

MAIT cells were going to be used as a control in our research, since they constitute a substantial portion, up to 10%, of the T cells present in PBMCs, and present several similarities with iNKT cells (including an invariant TCR α chain), as they are also considered "unconventional" T cells[186–188]. However, the AF488 labelled MR1 5-OP tetramer (which identifies MAIT cells) present in our flow cytometry panel stopped working (**Figures 27**, **29** and **30**), thus, it was not used in patients and healthy subjects' samples. Cytokine production was not evaluated in Fabry disease patients, since the antibody against IL-4 was not staining (**Figures 32** and **33**). One of the next steps should be to increase the incubation time of PBMCs with PMA and ionomycin from 5 hours to 6 hours. Furthermore, the single-stained sample should be done by using an antibody against a higher expressed antigen using the same fluorochrome as anti-IL-4 (APC), in order to discard compensation errors.

iNKT cells had to be enriched from PBMCs in order to analyse the selected markers. Notwithstanding the variability of the anti-iNKT MicroBeads enrichment between experiments, there was always enrichment of iNKT cells. Despite this enrichment, in some experiments it was not enough to study all the markers wanted in iNKT cells (**Table 10**).

This study aimed to characterise iNKT cell frequency and phenotype in Fabry disease patients. Along with this, monocyte, B cell and T cell frequencies were also analysed. From the four healthy subjects and three Fabry disease patients analysed, patients presented a tendency to have a higher percentage of monocytes compared to healthy subjects, albeit it wasn't statistically significative (**Figure 42 a.**). This alteration is in accordance with the literature[29,71,72]. No variations were observed between patients and controls regarding B cell and T cell percentages (**Figure 42 b.** and **c.**), which was surprising since previous studies have reported variation in B cell and T cell frequency when comparing Fabry disease patients and healthy subjects[29,71,72,223]. However, the patient under ERT presented a lower percentage of monocytes (2.24%) and B cells (3.41%) comparing to the other two patients who were not under any treatment (**Figure 42 a.** and **b.**). On the other hand, the patient under ERT possessed a higher percentage of T cells (81.8%), compared to the non-treated (**Figure 42 c.**).

As expected[116], iNKT cell frequency showed no statistical significative variation between the two groups (**Figure 44**).

iNKT cell CD4/ CD8 subsets were analysed in Fabry disease patients and healthy subjects. Contrary to what is described in the literature, no difference was observed between patients and controls in the $CD4^+$ iNKT subset (**Figure 46 a.**). Nonetheless, a reduction was observed in the Fabry disease patients' $CD8^+$ iNKT subset compared to controls (not statistically significative) (**Figure 46 b.**). $CD3^+$ T cells expressed more CD8 than iNKT cells (**Figure 46 b.**), presenting a more cytotoxic phenotype[225]. Regarding the DN iNKT cell subset, Fabry disease patients showed a bias towards an increase of this subset, compared to healthy subjects (not statistically significative) (**Figure 46 c.**). DN iNKT cells are Th1-like, producing cytokines like IFN-γ and TNF-α[168]. It would be interesting to analyse the iNKT cell cytokine production in these Fabry disease patients, due to the different cytokine production profile of the human iNKT cell subsets. The expression of CD8 dimers (CD8αα and CD8αβ) in both iNKT cells and T cells ($CD3^+$)

of healthy subjects and Fabry disease patients was also assessed (**Figure 47**). It was demonstrated that, although healthy donors and Fabry disease patients presented no variation regarding iNKT cells CD8 dimers, in both groups, more than 90% of iNKT cells expressed CD8αα whereas more than 82% of $CD3^+$ cells expressed CD8αβ. Little is known about the expression of the CD8 dimers in human iNKT cells, and so far, there is no information regarding their expression in Fabry disease. Gumperz et al. showed that iNKT cells from four healthy donors expressed CD8αα homodimers, with almost no expression of CD8αβ heterodimers[147], corroborating the results obtained in this study concerning the healthy controls. Furthermore, it is known that CD8αα and CD8αβ present functional differences in T cells. The expression of CD8αα by the majority of iNKT cells analysed in this study, may indicate that they do not act as conventional T cells and that their TCR has alterations.

Regarding iNKT cell phenotype, Fabry disease patients' iNKT cells presented a tendency to express more PD-1 (63.8 ± 17.2), an exhaustion marker, compared to controls (41.2 ± 24.6), but it was not statistically significative (**Figure 48 a.**). This tendency was also observed in ICOS expression, in spite of not being statistically significative (**Figure 48 b.**). CD161 and TIM-3 expression in iNKT cells presented no differences between controls and Fabry disease patients (**Figure 48 c.**). Overall, no significant differences were observed among the Fabry disease patients presenting different disease phenotypes.

Although some of the results in this study are not in accordance with the literature, it needs to be taken into account that Fabry disease is a highly heterogenous disorder, which may alter the frequency and phenotype of immune cells. Due to the low number of patients and healthy controls, it is still early to conclude about differences in leukocyte percentage, including iNKT cells, and iNKT cell phenotype in Fabry disease patients.

Following this study, it would be important to characterise the capacity of early onset Fabry disease patients' monocytes to present endogenous lipid antigens to iNKT cells. Besides this, the cytokine production of these and more Fabry disease patients' iNKT cells should be assessed in order to study the function of iNKT cells in these patients.

iNKT cells have been starting to get the deserved attention in disorders where the immune system is altered. With the study of iNKT cells in Fabry disease patients, we hope to discover novel biomarkers for the disease as well as improve knowledge for iNKT-based

immunotherapies. These immunotherapies may also be helpful for other diseases (e.g., cancer, in which immunotherapies have been in vogue but the existent ones are not sufficient to culminate the disease). In addition, these types of studies may also disclose novel mechanisms participating in Fabry disease pathophysiology.

References

1. de Duve, C., Pressman, B. C., Gianetto, R., Wattiaux, R. & Appelmans, F. Tissue fractionation studies. 6. Intracellular distribution patterns of enzymes in rat-liver tissue. *Biochem. J.* **60**, 604–617 (1955).
2. Parkinson-Lawrence, E. J. *et al.* Lysosomal Storage Disease: Revealing Lysosomal Function and Physiology. *Physiology* **25**, 102–115 (2010).
3. Xu, H. & Ren, D. Lysosomal Physiology. *Annu. Rev. Physiol.* **77**, 57–80 (2015).
4. Vellodi, A. Lysosomal storage disorders. *Br. J. Haematol.* **128**, 413–431 (2005).
5. Parenti, G., Andria, G. & Ballabio, A. Lysosomal Storage Diseases: From Pathophysiology to Therapy. *Annu. Rev. Med.* **66**, 471–486 (2015).
6. Conner, S. D. & Schmid, S. L. Regulated portals of entry into the cell. *Nature* **422**, 37–44 (2003).
7. Settembre, C. & Ballabio, A. Lysosomal Adaptation: How the Lysosome Responds to External Cues. *Cold Spring Harb. Perspect. Biol.* **6**, a016907 (2014).
8. He, C. & Klionsky, D. J. Regulation Mechanisms and Signaling Pathways of Autophagy. *Annu. Rev. Genet.* **43**, 67–93 (2009).
9. Chieregatti, E. & Meldolesi, J. Regulated exocytosis: new organelles for non-secretory purposes. *Nat. Rev. Mol. Cell Biol.* **6**, 181–187 (2005).
10. Zoncu, R. *et al.* mTORC1 senses lysosomal amino acids through an inside-out mechanism that requires the vacuolar H(+)-ATPase. *Science* **334**, 678–683 (2011).
11. Appelqvist, H., Wäster, P., Kågedal, K. & Öllinger, K. The lysosome: from waste bag to potential therapeutic target. *J. Mol. Cell Biol.* **5**, 214–226 (2013).
12. Alroy, J., Garganta, C. & Wiederschain, G. Secondary biochemical and morphological consequences in lysosomal storage diseases. *Biochem. Biokhimiia* **79**, 619–636 (2014).
13. Segatori, L. Impairment of homeostasis in lysosomal storage disorders. *IUBMB Life* **66**, 472–477 (2014).
14. Fuller, M., Meikle, P. J. & Hopwood, J. J. Epidemiology of lysosomal storage diseases: an overview. in *Fabry Disease: Perspectives from 5 Years of FOS* (eds. Mehta, A., Beck, M. & Sunder-Plassmann, G.) (Oxford PharmaGenesis, 2006).
15. Platt, F. M., d'Azzo, A., Davidson, B. L., Neufeld, E. F. & Tifft, C. J. Lysosomal storage diseases. *Nat. Rev. Dis. Primer* **4**, 27 (2018).
16. Pinto, R. *et al.* Prevalence of lysosomal storage diseases in Portugal. *Eur. J. Hum. Genet. EJHG* **12**, 87–92 (2004).
17. Sheth, J. & Nair, A. Treatment for Lysosomal Storage Disorders. *Curr. Pharm. Des.* **26**, 5110–5118 (2020).
18. Fernández-Pereira, C. *et al.* Therapeutic Approaches in Lysosomal Storage Diseases. *Biomolecules* **11**, 1775 (2021).
19. Kolter, T. & Sandhoff, K. Lysosomal degradation of membrane lipids. *FEBS Lett.* **584**, 1700–1712 (2010).

20. Albeituni, S. & Stiban, J. Roles of Ceramides and Other Sphingolipids in Immune Cell Function and Inflammation. *Adv. Exp. Med. Biol.* **1161**, 169–191 (2019).
21. Platt, F. M. Sphingolipid lysosomal storage disorders. *Nature* **510**, 68–75 (2014).
22. Ballabio, A. & Gieselmann, V. Lysosomal disorders: from storage to cellular damage. *Biochim. Biophys. Acta* **1793**, 684–696 (2009).
23. Hirabayashi, Y. A world of sphingolipids and glycolipids in the brain--novel functions of simple lipids modified with glucose. *Proc. Jpn. Acad. Ser. B Phys. Biol. Sci.* **88**, 129–143 (2012).
24. Reza, S., Ugorski, M. & Suchański, J. Glucosylceramide and galactosylceramide, small glycosphingolipids with significant impact on health and disease. *Glycobiology* **31**, 1416–1434 (2021).
25. Abed Rabbo, M., Khodour, Y., Kaguni, L. S. & Stiban, J. Sphingolipid lysosomal storage diseases: from bench to bedside. *Lipids Health Dis.* **20**, 44 (2021).
26. ANDERSON, W., F. R. C. S. A CASE OF "ANGEIO-KERATOMA."*. *Br. J. Dermatol.* **10**, 113–117 (1898).
27. Fabry, J. losa haemorrhagica Hebrae. *Arch. Für Dermatol. Syph.* **43**, 187 (1898).
28. Śnit, M., Przyłudzka, M. & Grzeszczak, W. Fabry disease - a genetically conditioned extremely rare disease with a very unusual course. *Intractable Rare Dis. Res.* **11**, 34–36 (2022).
29. Rigante, D., Cipolla, C., Basile, U., Gulli, F. & Savastano, M. C. Overview of immune abnormalities in lysosomal storage disorders. *Immunol. Lett.* **188**, 79–85 (2017).
30. Desnick, R. J., Ioannou, Y. A. & Eng, C. M. α-Galactosidase A Deficiency: Fabry Disease. in *The Online Metabolic and Molecular Bases of Inherited Disease* (eds. Valle, D. L., Antonarakis, S., Ballabio, A., Beaudet, A. L. & Mitchell, G. A.) (McGraw-Hill Education, 2019).
31. Aerts, J. M. *et al.* Elevated globotriaosylsphingosine is a hallmark of Fabry disease. *Proc. Natl. Acad. Sci. U. S. A.* **105**, 2812–2817 (2008).
32. Germain, D. P. Fabry disease. *Orphanet J. Rare Dis.* **5**, 30 (2010).
33. Wang, R. Y., Lelis, A., Mirocha, J. & Wilcox, W. R. Heterozygous Fabry women are not just carriers, but have a significant burden of disease and impaired quality of life. *Genet. Med. Off. J. Am. Coll. Med. Genet.* **9**, 34–45 (2007).
34. Wang, R. Y., Bodamer, O. A., Watson, M. S., Wilcox, W. R., & ACMG Work Group on Diagnostic Confirmation of Lysosomal Storage Diseases. Lysosomal storage diseases: diagnostic confirmation and management of presymptomatic individuals. *Genet. Med. Off. J. Am. Coll. Med. Genet.* **13**, 457–484 (2011).
35. Bouwman, M. G. *et al.* Prevalence of symptoms in female Fabry disease patients: a case-control survey. *J. Inherit. Metab. Dis.* **35**, 891–898 (2012).
36. Holmes, A. & Laney, D. A Retrospective Survey Studying the Impact of Fabry Disease on Pregnancy. *JIMD Rep.* **21**, 57–63 (2015).
37. Lenders, M. & Brand, E. Fabry Disease: The Current Treatment Landscape. *Drugs* **81**, 635–645 (2021).

38. Eng, C. M. *et al.* Fabry disease: baseline medical characteristics of a cohort of 1765 males and females in the Fabry Registry. *J. Inherit. Metab. Dis.* **30**, 184–192 (2007).
39. Echevarria, L. *et al.* X-chromosome inactivation in female patients with Fabry disease. *Clin. Genet.* **89**, 44–54 (2016).
40. Bokhari, S. R. A., Zulfiqar, H. & Hariz, A. Fabry Disease. in *StatPearls* (StatPearls Publishing, 2023).
41. Vardarli, I., Rischpler, C., Herrmann, K. & Weidemann, F. Diagnosis and Screening of Patients with Fabry Disease. *Ther. Clin. Risk Manag.* **16**, 551–558 (2020).
42. Schiffmann, R., Fuller, M., Clarke, L. A. & Aerts, J. M. F. G. Is it Fabry disease? *Genet. Med.* **18**, 1181–1185 (2016).
43. Amodio, F. *et al.* An Overview of Molecular Mechanisms in Fabry Disease. *Biomolecules* **12**, 1460 (2022).
44. Sezer, O. & Ceylaner, S. Genetic Management Algorithm in High-Risk Fabry Disease Cases; Especially in Female Indexes with Mutations. *Endocr. Metab. Immune Disord. Drug Targets* **21**, 324–337 (2021).
45. GARMAN, S. C. Structure–function relationships in α-galactosidase A. *Acta Paediatr. Oslo Nor. 1992* **96**, 6–16 (2007).
46. van der Veen, S. J., Hollak, C. E. M., van Kuilenburg, A. B. P. & Langeveld, M. Developments in the treatment of Fabry disease. *J. Inherit. Metab. Dis.* **43**, 908–921 (2020).
47. Azevedo, O., Gago, M. F., Miltenberger-Miltenyi, G., Sousa, N. & Cunha, D. Fabry Disease Therapy: State-of-the-Art and Current Challenges. *Int. J. Mol. Sci.* **22**, 206 (2020).
48. Ortiz, A. *et al.* Fabry disease revisited: Management and treatment recommendations for adult patients. *Mol. Genet. Metab.* **123**, 416–427 (2018).
49. van Breemen, M. J. *et al.* Reduction of elevated plasma globotriaosylsphingosine in patients with classic Fabry disease following enzyme replacement therapy. *Biochim. Biophys. Acta* **1812**, 70–76 (2011).
50. Rozenfeld, P. A. Fabry disease: treatment and diagnosis. *IUBMB Life* **61**, 1043–1050 (2009).
51. McCafferty, E. H. & Scott, L. J. Migalastat: A Review in Fabry Disease. *Drugs* **79**, 543–554 (2019).
52. Lenders, M. *et al.* Multicenter Female Fabry Study (MFFS) - clinical survey on current treatment of females with Fabry disease. *Orphanet J. Rare Dis.* **11**, 88 (2016).
53. Rozenfeld, P. & Feriozzi, S. Contribution of inflammatory pathways to Fabry disease pathogenesis. *Mol. Genet. Metab.* **122**, 19–27 (2017).
54. Del Pinto, R. & Ferri, C. The role of Immunity in Fabry Disease and Hypertension: A Review of a Novel Common Pathway. *High Blood Press. Cardiovasc. Prev.* **27**, 539–546 (2020).
55. Castaneda, J. A., Lim, M. J., Cooper, J. D. & Pearce, D. A. Immune system irregularities in lysosomal storage disorders. *Acta Neuropathol. (Berl.)* **115**, 159–174 (2008).

56. Land, W. G. The Role of Damage-Associated Molecular Patterns (DAMPs) in Human Diseases. *Sultan Qaboos Univ. Med. J.* **15**, e157–e170 (2015).
57. Mauhin, W. *et al.* Innate and Adaptive Immune Response in Fabry Disease. in *JIMD Reports, Volume 22* (eds. Zschocke, J. et al.) 1–10 (Springer, 2015). doi:10.1007/8904_2014_371.
58. Biancini, G. B. *et al.* Globotriaosylceramide is correlated with oxidative stress and inflammation in Fabry patients treated with enzyme replacement therapy. *Biochim. Biophys. Acta BBA - Mol. Basis Dis.* **1822**, 226–232 (2012).
59. Pandey, M. K. Exploring Pro-Inflammatory Immunological Mediators: Unraveling the Mechanisms of Neuroinflammation in Lysosomal Storage Diseases. *Biomedicines* **11**, 1067 (2023).
60. De Francesco, P. N., Mucci, J. M., Ceci, R., Fossati, C. A. & Rozenfeld, P. A. Fabry disease peripheral blood immune cells release inflammatory cytokines: role of globotriaosylceramide. *Mol. Genet. Metab.* **109**, 93–99 (2013).
61. Wynn, T. Cellular and molecular mechanisms of fibrosis. *J. Pathol.* **214**, 199–210 (2008).
62. Aratani, S. *et al.* A case of female Fabry disease revealed by renal biopsy. *CEN Case Rep.* **9**, 24–29 (2019).
63. Fogo, A. B. *et al.* Scoring system for renal pathology in Fabry disease: report of the International Study Group of Fabry Nephropathy (ISGFN). *Nephrol. Dial. Transplant.* **25**, 2168–2177 (2010).
64. Zoja, C., Benigni, A. & Remuzzi, G. Cellular responses to protein overload: Key event in renal disease progression. *Curr. Opin. Nephrol. Hypertens.* **13**, 31–37 (2004).
65. Chimenti, C. *et al.* Increased oxidative stress contributes to cardiomyocyte dysfunction and death in patients with Fabry disease cardiomyopathy. *Hum. Pathol.* **46**, 1760–1768 (2015).
66. Kopan, R. Notch Signaling. *Cold Spring Harb. Perspect. Biol.* **4**, a011213 (2012).
67. Sanchez-Niño, M. D. *et al.* Lyso-Gb3 activates Notch1 in human podocytes. *Hum. Mol. Genet.* **24**, 5720–5732 (2015).
68. Anders, H.-J., Banas, B. & Schlöndorff, D. Signaling danger: toll-like receptors and their potential roles in kidney disease. *J. Am. Soc. Nephrol. JASN* **15**, 854–867 (2004).
69. Nitta, T. *et al.* Globo-series glycosphingolipids enhance Toll-like receptor 4-mediated inflammation and play a pathophysiological role in diabetic nephropathy. *Glycobiology* **29**, 260–268 (2019).
70. Sugimoto, J., Satoyoshi, H., Takahata, K. & Muraoka, S. Fabry disease-associated globotriaosylceramide induces mechanical allodynia via activation of signaling through proNGF–p75NTR but not mature NGF–TrkA. *Eur. J. Pharmacol.* **895**, 173882 (2021).
71. Shen, J.-S. *et al.* Globotriaosylceramide induces oxidative stress and up-regulates cell adhesion molecule expression in Fabry disease endothelial cells. *Mol. Genet. Metab.* **95**, 163–168 (2008).

72. DeGraba, T. *et al.* Profile of endothelial and leukocyte activation in Fabry patients. *Ann. Neurol.* **47**, 229–233 (2000).
73. Martinez, P., Aggio, M. & Rozenfeld, P. High incidence of autoantibodies in Fabry disease patients. *J. Inherit. Metab. Dis.* **30**, 365–369 (2007).
74. Tojo, K., Oota, M., Honda, H., Shibasaki, T. & Sakai, O. Possible Thyroidal Involvement in a Case of Fabry Disease. *Intern. Med.* **33**, 172–176 (1994).
75. Faggiano, A. *et al.* Endocrine Dysfunction in Patients with Fabry Disease. *J. Clin. Endocrinol. Metab.* **91**, 4319–4325 (2006).
76. Katsumata, N., Ishiguro, A. & Watanabe, H. Fabry Disease Superimposed on Overt Autoimmune Hypothyroidism. *Clin. Pediatr. Endocrinol.* **20**, 95–98 (2011).
77. Lenders, M. & Brand, E. Mechanisms of Neutralizing Anti-drug Antibody Formation and Clinical Relevance on Therapeutic Efficacy of Enzyme Replacement Therapies in Fabry Disease. *Drugs* **81**, 1969–1981 (2021).
78. Dowds, C. M., Kornell, S.-C., Blumberg, R. S. & Zeissig, S. Lipid antigens in immunity. *Biol. Chem.* **395**, 61–81 (2014).
79. Rock, K. L., Reits, E. & Neefjes, J. Present Yourself! By MHC Class I and MHC Class II Molecules. *Trends Immunol.* **37**, 724–737 (2016).
80. Porcelli, S. *et al.* Recognition of cluster of differentiation 1 antigens by human CD4−CD8>− cytolytic T lymphocyte. *Nature* **341**, 447–450 (1989).
81. Beckman, E. M. *et al.* Recognition of a lipid antigen by CD1-restricted αβ+ T cells. *Nature* **372**, 691–694 (1994).
82. Teyton, L. Role of lipid transfer proteins in loading CD1 antigen-presenting molecules. *J. Lipid Res.* **59**, 1367–1373 (2018).
83. Van Kaer, L., Wu, L. & Joyce, S. Mechanisms and Consequences of Antigen Presentation by CD1. *Trends Immunol.* **37**, 738–754 (2016).
84. Calabi, F. & Milstein, C. A novel family of human major histocompatibility complex-related genes not mapping to chromosome 6. *Nature* **323**, 540–543 (1986).
85. Yu, C. Y. & Milstein, C. A physical map linking the five CD1 human thymocyte differentiation antigen genes. *EMBO J.* **8**, 3727–3732 (1989).
86. Dougan, S. K., Kaser, A. & Blumberg, R. S. CD1 expression on antigen-presenting cells. *Curr. Top. Microbiol. Immunol.* **314**, 113–141 (2007).
87. De Libero, G. & Mori, L. How the immune system detects lipid antigens. *Prog. Lipid Res.* **49**, 120–127 (2010).
88. Strominger, J. L. An Alternative Path for Antigen Presentation: Group 1 CD1 Proteins. *J. Immunol.* **184**, 3303–3305 (2010).
89. Delia, D. *et al.* CD1c but neither CD1a nor CD1b molecules are expressed on normal, activated, and malignant human B cells: identification of a new B-cell subset. *Blood* **72**, 241–247 (1988).
90. Bricard, G. & Porcelli, S. A. Antigen presentation by CD1 molecules and the generation of lipid-specific T cell immunity. *Cell. Mol. Life Sci. CMLS* **64**, 1824–1840 (2007).

91. Salamone, M. C., Rabinovich, G. A., Mendiguren, A. K., Salamone, G. V. & Fainboim, L. Activation-induced expression of CD1d antigen on mature T cells. *J. Leukoc. Biol.* **69**, 207–214 (2001).
92. Huh, J. Y., Park, Y. J. & Kim, J. B. Adipocyte CD1d determines adipose inflammation and insulin resistance in obesity. *Adipocyte* **7**, 129–136 (2018).
93. Rakhshandehroo, M. *et al.* CD1d-mediated presentation of endogenous lipid antigens by adipocytes requires microsomal triglyceride transfer protein. *J. Biol. Chem.* **289**, 22128–22139 (2014).
94. Huh, J. Y. *et al.* A novel function of adipocytes in lipid antigen presentation to iNKT cells. *Mol. Cell. Biol.* **33**, 328–339 (2013).
95. Facciotti, F. *et al.* Fine tuning by human CD1e of lipid-specific immune responses. *Proc. Natl. Acad. Sci.* **108**, 14228–14233 (2011).
96. de la Salle, H. *et al.* Assistance of Microbial Glycolipid Antigen Processing by CD1e. *Science* **310**, 1321–1324 (2005).
97. Zajonc, D. M. The CD1 family: serving lipid antigens to T cells since the Mesozoic era. *Immunogenetics* **68**, 561–576 (2016).
98. Kang, S.-J. & Cresswell, P. Calnexin, calreticulin, and ERp57 cooperate in disulfide bond formation in human CD1d heavy chain. *J. Biol. Chem.* **277**, 44838–44844 (2002).
99. Zeng, Z. *et al.* Crystal structure of mouse CD1: An MHC-like fold with a large hydrophobic binding groove. *Science* **277**, 339–345 (1997).
100. Jayawardena-Wolf, J., Benlagha, K., Chiu, Y. H., Mehr, R. & Bendelac, A. CD1d endosomal trafficking is independently regulated by an intrinsic CD1d-encoded tyrosine motif and by the invariant chain. *Immunity* **15**, 897–908 (2001).
101. Gelin, C., Sloma, I., Charron, D. & Mooney, N. Regulation of MHC II and CD1 antigen presentation: from ubiquity to security. *J. Leukoc. Biol.* **85**, 215–224 (2009).
102. Ly, D. & Moody, D. B. The CD1 size problem: lipid antigens, ligands, and scaffolds. *Cell. Mol. Life Sci. CMLS* **71**, 3069–3079 (2014).
103. Adams, E. J. Lipid presentation by human CD1 molecules and the diverse T cell populations that respond to them. *Curr. Opin. Immunol.* **26**, 1–6 (2014).
104. Pereira, C. S. & Macedo, M. F. CD1-Restricted T Cells at the Crossroad of Innate and Adaptive Immunity. *J. Immunol. Res.* **2016**, e2876275 (2016).
105. Hussain, M. M., Rava, P., Walsh, M., Rana, M. & Iqbal, J. Multiple functions of microsomal triglyceride transfer protein. *Nutr. Metab.* **9**, 14 (2012).
106. Zeissig, S. *et al.* Primary deficiency of microsomal triglyceride transfer protein in human abetalipoproteinemia is associated with loss of CD1 function. *J. Clin. Invest.* **120**, 2889–2899 (2010).
107. Kaser, A. *et al.* Microsomal triglyceride transfer protein regulates endogenous and exogenous antigen presentation by group 1 CD1 molecules. *Eur. J. Immunol.* **38**, 2351–2359 (2008).
108. Dougan, S. K. *et al.* Microsomal triglyceride transfer protein lipidation and control of CD1d on antigen-presenting cells. *J. Exp. Med.* **202**, 529–539 (2005).

109. Brozovic, S. *et al.* CD1d function is regulated by microsomal triglyceride transfer protein. *Nat. Med.* **10**, 535–539 (2004).
110. Sagiv, Y. *et al.* A distal effect of microsomal triglyceride transfer protein deficiency on the lysosomal recycling of CD1d. *J. Exp. Med.* **204**, 921–928 (2007).
111. Angénieux, C. *et al.* The cellular pathway of CD1e in immature and maturing dendritic cells. *Traffic Cph. Den.* **6**, 286–302 (2005).
112. Brigl, M. & Brenner, M. B. CD1: antigen presentation and T cell function. *Annu. Rev. Immunol.* **22**, 817–890 (2004).
113. Chiu, Y.-H. *et al.* Multiple defects in antigen presentation and T cell development by mice expressing cytoplasmic tail-truncated CD1d. *Nat. Immunol.* **3**, 55–60 (2002).
114. Cernadas, M. *et al.* Early recycling compartment trafficking of CD1a is essential for its intersection and presentation of lipid antigens. *J. Immunol. Baltim. Md 1950* **184**, 1235–1241 (2010).
115. Barral, D. C. & Brenner, M. B. CD1 antigen presentation: how it works. *Nat. Rev. Immunol.* **7**, 929–941 (2007).
116. Pereira, C. S. *et al.* Lipid Antigen Presentation by CD1b and CD1d in Lysosomal Storage Disease Patients. *Front. Immunol.* **10**, (2019).
117. Arora, P. *et al.* Endocytic pH regulates cell surface localization of glycolipid antigen loaded CD1d complexes. *Chem. Phys. Lipids* **194**, 49–57 (2016).
118. Self antigens. in *Rheumatology and Immunology Therapy* (eds. Abbott, J. D. et al.) 793–794 (Springer, 2004). doi:10.1007/3-540-29662-X_2408.
119. de Lalla, C. *et al.* High-frequency and adaptive-like dynamics of human CD1 self-reactive T cells. *Eur. J. Immunol.* **41**, 602–610 (2011).
120. de Jong, A. *et al.* CD1a-autoreactive T cells are a normal component of the human αβ T cell repertoire. *Nat. Immunol.* **11**, 1102–1109 (2010).
121. Kobayashi, E., Motoki, K., Uchida, T., Fukushima, H. & Koezuka, Y. KRN7000, a novel immunomodulator, and its antitumor activities. *Oncol. Res.* **7**, 529–534 (1995).
122. Kawano, T. *et al.* CD1d-Restricted and TCR-Mediated Activation of V $_{\alpha}$ 14 NKT Cells by Glycosylceramides. *Science* **278**, 1626–1629 (1997).
123. De Libero, G., Collmann, A. & Mori, L. The cellular and biochemical rules of lipid antigen presentation. *Eur. J. Immunol.* **39**, 2648–2656 (2009).
124. Relloso, M. *et al.* pH-dependent interdomain tethers of CD1b regulate its antigen capture. *Immunity* **28**, 774–786 (2008).
125. De Libero, G. & Mori, L. Novel insights into lipid antigen presentation. *Trends Immunol.* **33**, 103–111 (2012).
126. Pereira, C. S., Sa-Miranda, C., De Libero, G., Mori, L. & Macedo, M. F. Globotriaosylceramide inhibits iNKT-cell activation in a CD1d-dependent manner. *Eur. J. Immunol.* **46**, 147–153 (2016).
127. Godfrey, D. I., Uldrich, A. P., McCluskey, J., Rossjohn, J. & Moody, D. B. The burgeoning family of unconventional T cells. *Nat. Immunol.* **16**, 1114–1123 (2015).

128. Mori, L., Lepore, M. & De Libero, G. The Immunology of CD1- and MR1-Restricted T Cells. *Annu. Rev. Immunol.* **34**, 479–510 (2016).
129. Bendelac, A., Savage, P. B. & Teyton, L. The biology of NKT cells. *Annu. Rev. Immunol.* **25**, 297–336 (2007).
130. Schönrich, G. & Raftery, M. J. CD1-Restricted T Cells During Persistent Virus Infections: "Sympathy for the Devil". *Front. Immunol.* **9**, (2018).
131. Godfrey, D. I., Stankovic, S. & Baxter, A. G. Raising the NKT cell family. *Nat. Immunol.* **11**, 197–206 (2010).
132. Vincent, M. S., Xiong, X., Grant, E. P., Peng, W. & Brenner, M. B. CD1a-, b-, and c-Restricted TCRs Recognize Both Self and Foreign Antigens1. *J. Immunol.* **175**, 6344–6351 (2005).
133. Bagchi, S. *et al.* CD1b-autoreactive T cells contribute to hyperlipidemia-induced skin inflammation in mice. *J. Clin. Invest.* **127**, 2339–2352 (2017).
134. Vincent, M. S. *et al.* CD1-dependent dendritic cell instruction. *Nat. Immunol.* **3**, 1163–1168 (2002).
135. Bagchi, S., Li, S. & Wang, C.-R. CD1b-autoreactive T cells recognize phospholipid antigens and contribute to antitumor immunity against a CD1b+ T cell lymphoma. *Oncoimmunology* **5**, e1213932 (2016).
136. Raftery, M. J. *et al.* Inhibition of CD1 Antigen Presentation by Human Cytomegalovirus. *J. Virol.* **82**, 4308–4319 (2008).
137. Sieling, P. A. *et al.* Human double-negative T cells in systemic lupus erythematosus provide help for IgG and are restricted by CD1c. *J. Immunol. Baltim. Md 1950* **165**, 5338–5344 (2000).
138. Shissler, S. C. & Webb, T. J. The ins and outs of type I iNKT cell development. *Mol. Immunol.* **105**, 116–130 (2019).
139. Pellicci, D. G. *et al.* Differential recognition of CD1d-alpha-galactosyl ceramide by the V beta 8.2 and V beta 7 semi-invariant NKT T cell receptors. *Immunity* **31**, 47–59 (2009).
140. Godfrey, D. I., MacDonald, H. R., Kronenberg, M., Smyth, M. J. & Kaer, L. V. NKT cells: what's in a name? *Nat. Rev. Immunol.* **4**, 231–237 (2004).
141. Kumar, V. & Delovitch, T. L. Different subsets of natural killer T cells may vary in their roles in health and disease. *Immunology* **142**, 321–336 (2014).
142. Zhao, M. *et al.* Altered thymic differentiation and modulation of arthritis by invariant NKT cells expressing mutant ZAP70. *Nat. Commun.* **9**, 2627 (2018).
143. Guo, T. *et al.* Mouse and Human CD1d-Self-Lipid Complexes Are Recognized Differently by Murine Invariant Natural Killer T Cell Receptors. *PLOS ONE* **11**, e0156114 (2016).
144. Berzins, S. P., Smyth, M. J. & Baxter, A. G. Presumed guilty: natural killer T cell defects and human disease. *Nat. Rev. Immunol.* **11**, 131–142 (2011).
145. Look, A., Burns, D., Tews, I., Roghanian, A. & Mansour, S. Towards a better understanding of human iNKT cell subpopulations for improved clinical outcomes. *Front. Immunol.* **14**, (2023).

146. Montoya, C. J. *et al.* Characterization of human invariant natural killer T subsets in health and disease using a novel invariant natural killer T cell-clonotypic monoclonal antibody, 6B11. *Immunology* **122**, 1–14 (2007).
147. Gumperz, J. E., Miyake, S., Yamamura, T. & Brenner, M. B. Functionally Distinct Subsets of CD1d-restricted Natural Killer T Cells Revealed by CD1d Tetramer Staining. *J. Exp. Med.* **195**, 625–636 (2002).
148. Lantz, O. & Bendelac, A. An invariant T cell receptor alpha chain is used by a unique subset of major histocompatibility complex class I-specific CD4+ and CD4-8- T cells in mice and humans. *J. Exp. Med.* **180**, 1097–1106 (1994).
149. Crosby, C. M. & Kronenberg, M. Tissue-specific functions of invariant natural killer T cells. *Nat. Rev. Immunol.* **18**, 559–574 (2018).
150. Bernardo, D. *et al.* Decreased circulating iNKT cell numbers in refractory coeliac disease. *Clin. Immunol.* **126**, 172–179 (2008).
151. Bricard, G. *et al.* Enrichment of Human CD4+ Vα24/Vβ11 Invariant NKT Cells in Intrahepatic Malignant Tumors 1. *J. Immunol.* **182**, 5140–5151 (2009).
152. Dhodapkar, K. M. *et al.* Invariant natural killer T cells are preserved in patients with glioma and exhibit antitumor lytic activity following dendritic cell-mediated expansion. *Int. J. Cancer* **109**, 893–899 (2004).
153. Galante, N. Z. *et al.* Frequency of Valpha24+Vbeta11+ NKT cells in peripheral blood of human kidney transplantation recipients. *Int. Immunopharmacol.* **5**, 53–58 (2005).
154. Im, J. S. *et al.* Alteration of the relative levels of iNKT cell subsets is associated with chronic mycobacterial infections. *Clin. Immunol. Orlando Fla* **127**, 214–224 (2008).
155. Jing, Y. *et al.* Aging is associated with a rapid decline in frequency, alterations in subset composition, and enhanced Th2 response in CD1d-restricted NKT cells from human peripheral blood. *Exp. Gerontol.* **42**, 719–732 (2007).
156. Kis, J. *et al.* Reduced CD4+ subset and Th1 bias of the human iNKT cells in Type 1 diabetes mellitus. *J. Leukoc. Biol.* **81**, 654–662 (2007).
157. Montoya, C. J. *et al.* Invariant NKT cells from HIV-1 or Mycobacterium tuberculosis-infected patients express an activated phenotype. *Clin. Immunol. Orlando Fla* **127**, 1–6 (2008).
158. Peralbo, E. *et al.* Decreased frequency and proliferative response of invariant Valpha24Vbeta11 natural killer T (iNKT) cells in healthy elderly. *Biogerontology* **7**, 483–492 (2006).
159. Takahashi, T. *et al.* V alpha 24+ natural killer T cells are markedly decreased in atopic dermatitis patients. *Hum. Immunol.* **64**, 586–592 (2003).
160. Chen, G., Tang, Z. & Bai, X. Variation and significance of NKT cell and its subset in patients with severe multiple injuries. *Chin. J. Traumatol. Zhonghua Chuang Shang Za Zhi* **12**, 323–327 (2009).
161. Lee, Y. J., Holzapfel, K. L., Zhu, J., Jameson, S. C. & Hogquist, K. A. Steady-state production of IL-4 modulates immunity in mouse strains and is determined by lineage diversity of iNKT cells. *Nat. Immunol.* **14**, 1146–1154 (2013).

162. Kovalovsky, D. *et al.* The BTB–zinc finger transcriptional regulator PLZF controls the development of invariant natural killer T cell effector functions. *Nat. Immunol.* **9**, 1055–1064 (2008).
163. Savage, A. K. *et al.* The Transcription Factor PLZF Directs the Effector Program of the NKT Cell Lineage. *Immunity* **29**, 391–403 (2008).
164. Lee, M. *et al.* Single-cell RNA sequencing identifies shared differentiation paths of mouse thymic innate T cells. *Nat. Commun.* **11**, 4367 (2020).
165. Chang, P.-P. *et al.* Identification of Bcl-6-dependent follicular helper NKT cells that provide cognate help for B cell responses. *Nat. Immunol.* **13**, 35–43 (2012).
166. King, I. L. *et al.* Invariant natural killer T cells direct B cell responses to cognate lipid antigen in an IL-21-dependent manner. *Nat. Immunol.* **13**, 44–50 (2012).
167. Lynch, L. *et al.* Regulatory iNKT cells lack expression of the transcription factor PLZF and control the homeostasis of Treg cells and macrophages in adipose tissue. *Nat. Immunol.* **16**, 85–95 (2015).
168. Lee, P. T., Benlagha, K., Teyton, L. & Bendelac, A. Distinct Functional Lineages of Human Vα24 Natural Killer T Cells. *J. Exp. Med.* **195**, 637–641 (2002).
169. Krijgsman, D., Hokland, M. & Kuppen, P. J. K. The Role of Natural Killer T Cells in Cancer—A Phenotypical and Functional Approach. *Front. Immunol.* **9**, (2018).
170. Takahashi, T. *et al.* Cutting edge: analysis of human V alpha 24+CD8+ NK T cells activated by alpha-galactosylceramide-pulsed monocyte-derived dendritic cells. *J. Immunol. Baltim. Md 1950* **168**, 3140–3144 (2002).
171. Snyder-Cappione, J. E. *et al.* A Comprehensive Ex Vivo Functional Analysis of Human NKT Cells Reveals Production of MIP1-α and MIP1-β, a Lack of IL-17, and a Th1-Bias in Males. *PLOS ONE* **5**, e15412 (2010).
172. Moreira-Teixeira, L. *et al.* Rapamycin Combined with TGF-β Converts Human Invariant NKT Cells into Suppressive Foxp3+ Regulatory Cells. *J. Immunol.* **188**, 624–631 (2012).
173. Kim, C. H., Johnston, B. & Butcher, E. C. Trafficking machinery of NKT cells: shared and differential chemokine receptor expression among Vα24+Vβ11+ NKT cell subsets with distinct cytokine-producing capacity. *Blood* **100**, 11–16 (2002).
174. Mabrouk, N. *et al.* CXCR6 expressing T cells: Functions and role in the control of tumors. *Front. Immunol.* **13**, (2022).
175. Germanov, E. *et al.* Critical Role for the Chemokine Receptor CXCR6 in Homeostasis and Activation of CD1d-Restricted NKT Cells1. *J. Immunol.* **181**, 81–91 (2008).
176. Shimaoka, T. *et al.* Critical Role for CXC Chemokine Ligand 16 (SR-PSOX) in Th1 Response Mediated by NKT Cells1. *J. Immunol.* **179**, 8172–8179 (2007).
177. Tian, G. *et al.* $CD62L^+$ NKT cells have prolonged persistence and antitumor activity in vivo. *J. Clin. Invest.* **126**, 2341–2355 (2016).
178. Snyder-Cappione, J. E. *et al.* Evidence of Invariant Natural Killer T (iNKT) Cell Exhaustion in Sarcoidosis. *Eur. J. Immunol.* **43**, 10.1002/eji.201243185 (2013).
179. Tietscher, S. *et al.* A comprehensive single-cell map of T cell exhaustion-associated immune environments in human breast cancer. *Nat. Commun.* **14**, 98 (2023).

180. Erkers, T. *et al.* High-parametric evaluation of human invariant natural killer T cells to delineate heterogeneity in allo- and autoimmunity. *Blood* **135**, 814–825 (2020).
181. Cui, G. *et al.* A circulating subset of iNKT cells mediates antitumor and antiviral immunity. *Sci. Immunol.* **7**, eabj8760 (2022).
182. Dasgupta, S. & Kumar, V. Type II NKT cells: a distinct CD1d-restricted immune regulatory NKT cell subset. *Immunogenetics* **68**, 665–676 (2016).
183. Corbett, A. J., Awad, W., Wang, H. & Chen, Z. Antigen Recognition by MR1-Reactive T Cells; MAIT Cells, Metabolites, and Remaining Mysteries. *Front. Immunol.* **11**, (2020).
184. Treiner, E. *et al.* Selection of evolutionarily conserved mucosal-associated invariant T cells by MR1. *Nature* **422**, 164–169 (2003).
185. Huang, S. *et al.* Evidence for MR1 antigen presentation to mucosal-associated invariant T cells. *J. Biol. Chem.* **280**, 21183–21193 (2005).
186. Van Rhijn, I., Godfrey, D. I., Rossjohn, J. & Moody, D. B. Lipid and small-molecule display by CD1 and MR1. *Nat. Rev. Immunol.* **15**, 643–654 (2015).
187. Gherardin, N. A. *et al.* Human blood MAIT cell subsets defined using MR1 tetramers. *Immunol. Cell Biol.* **96**, 507–525 (2018).
188. Novak, J., Dobrovolny, J., Novakova, L. & Kozak, T. The Decrease in Number and Change in Phenotype of Mucosal-Associated Invariant T cells in the Elderly and Differences in Men and Women of Reproductive Age. *Scand. J. Immunol.* **80**, 271–275 (2014).
189. Kain, L. *et al.* The Identification of the Endogenous Ligands of Natural Killer T Cells Reveals the Presence of Mammalian α-Linked Glycosylceramides. *Immunity* **41**, 543–554 (2014).
190. Pereira, C. S., Ribeiro, H. & Macedo, M. F. From Lysosomal Storage Diseases to NKT Cell Activation and Back. *Int. J. Mol. Sci.* **18**, 502 (2017).
191. Macedo, M. F., Quinta, R., Pereira, C. S. & Sa Miranda, M. C. Enzyme replacement therapy partially prevents invariant Natural Killer T cell deficiency in the Fabry disease mouse model. *Mol. Genet. Metab.* **106**, 83–91 (2012).
192. Gadola, S. D. *et al.* Impaired selection of invariant natural killer T cells in diverse mouse models of glycosphingolipid lysosomal storage diseases. *J. Exp. Med.* **203**, 2293–2303 (2006).
193. Darmoise, A. *et al.* Lysosomal alpha-galactosidase controls the generation of self lipid antigens for natural killer T cells. *Immunity* **33**, 216–228 (2010).
194. Porubsky, S. *et al.* Globosides but not isoglobosides can impact the development of invariant NKT cells and their interaction with dendritic cells. *J. Immunol. Baltim. Md 1950* **189**, 3007–3017 (2012).
195. Pereira, C. S. *et al.* The GM2 ganglioside inhibits iNKT cell responses in a CD1d-dependent manner. *Mol. Genet. Metab.* **125**, 161–167 (2018).
196. Melum, E. *et al.* Control of CD1d-restricted antigen presentation and inflammation by sphingomyelin. *Nat. Immunol.* **20**, 1644–1655 (2019).
197. Pereira, C. S. *et al.* Invariant natural killer T cells are phenotypically and functionally altered in Fabry disease. *Mol. Genet. Metab.* **108**, 241–248 (2013).

198. Chen, H., Huang, H. & Paul, W. E. NK1.1+ CD4+ T cells lose NK1.1 expression upon in vitro activation. *J. Immunol. Baltim. Md 1950* **158**, 5112–5119 (1997).
199. Foster, B., Prussin, C., Liu, F., Whitmire, J. K. & Whitton, J. L. Detection of intracellular cytokines by flow cytometry. *Curr. Protoc. Immunol.* **Chapter 6**, 6.24.1-6.24.21 (2007).
200. Spurgeon, B. E. J. & Naseem, K. M. Platelet Flow Cytometry: Instrument Setup, Controls, and Panel Performance. *Cytometry B Clin. Cytom.* **98**, 19–27 (2020).
201. Sahir, F., Mateo, J. M., Steinhoff, M. & Siveen, K. S. Development of a 43 color panel for the characterization of conventional and unconventional T-cell subsets, B cells, NK cells, monocytes, dendritic cells, and innate lymphoid cells using spectral flow cytometry. *Cytometry A*
202. Bonilla, D. L., Reinin, G. & Chua, E. Full Spectrum Flow Cytometry as a Powerful Technology for Cancer Immunotherapy Research. *Front. Mol. Biosci.* **7**, (2021).
203. Ferrer-Font, L. *et al.* Panel Optimization for High-Dimensional Immunophenotyping Assays Using Full-Spectrum Flow Cytometry. *Curr. Protoc.* **1**, e222 (2021).
204. Kjer-Nielsen, L. *et al.* MR1 presents microbial vitamin B metabolites to MAIT cells. *Nature* **491**, 717–723 (2012).
205. Okada, H., Banchereau, J. & Lotze, M. T. CHAPTER 10 - Interleukin-4. in *The Cytokine Handbook (Fourth Edition)* (eds. Thomson, A. W. & Lotze, M. T.) 227–262 (Academic Press, 2003). doi:10.1016/B978-012689663-3/50014-4.
206. Nakagawa, R., Brayer, J., Restrepo, N., Mulé, J. J. & Mailloux, A. W. High-Dimensional Flow Cytometry Analysis of Regulatory Receptors on Human T Cells, NK Cells, and NKT Cells. in *Translational Bioinformatics for Therapeutic Development* (ed. Markowitz, J.) vol. 2194 255–290 (Springer US, 2021).
207. Liu, Y. *et al.* A modified α-galactosyl ceramide for staining and stimulating natural killer T cells. *J. Immunol. Methods* **312**, 34–39 (2006).
208. Kaneda, H. *et al.* ICOS costimulates invariant NKT cell activation. *Biochem. Biophys. Res. Commun.* **327**, 201–207 (2005).
209. Kurioka, A. *et al.* CD161 Defines a Functionally Distinct Subset of Pro-Inflammatory Natural Killer Cells. *Front. Immunol.* **9**, 486 (2018).
210. Corbett, A. J. *et al.* T-cell activation by transitory neo-antigens derived from distinct microbial pathways. *Nature* **509**, 361–365 (2014).
211. Human PBMC Isolation and Counting Using the Scepter™ 2.0 Handheld Automated Cell Counter. https://www.sigmaaldrich.com/PT/en/technical-documents/technical-article/cell-culture-and-cell-culture-analysis/cell-counting-and-health-analysis/human-pbmc-isolation-and-counting-using-scepter-cell-counter.
212. Thompson, J. Peripheral Blood Mononuclear Cells: A Brief Review – Caltag Medsystems. https://www.caltagmedsystems.co.uk/information/peripheral-blood-mononuclear-cells-a-brief-review/ (2020).
213. Buckner, C. M., Calderon, T. M., Willams, D. W., Belbin, T. J. & Berman, J. W. Characterization of monocyte maturation/differentiation that facilitates their

transmigration across the blood-brain barrier and infection by HIV: implications for NeuroAIDS. *Cell. Immunol.* **267**, 109–123 (2011).
214. Li, C. *et al.* A Higher Frequency of CD14+CD169+ Monocytes/Macrophages in Patients with Colorectal Cancer. *PLoS ONE* **10**, e0141817 (2015).
215. Alderson, M. R. *et al.* CD40 expression by human monocytes: regulation by cytokines and activation of monocytes by the ligand for CD40. *J. Exp. Med.* **178**, 669–674 (1993).
216. Pinto, B. F. *et al.* CD86 Expression by Monocytes Influences an Immunomodulatory Profile in Asymptomatic Patients with Chronic Chagas Disease. *Front. Immunol.* **9**, 454 (2018).
217. Fischer, K. *et al.* Isolation and characterization of human antigen-specific TCRαβ+ CD4-CD8- double-negative regulatory T cells. *Blood* **105**, 2828–2835 (2005).
218. Bohner, P. *et al.* Double Positive CD4+CD8+ T Cells Are Enriched in Urological Cancers and Favor T Helper-2 Polarization. *Front. Immunol.* **10**, (2019).
219. Overgaard, N. H., Jung, J.-W., Steptoe, R. J. & Wells, J. W. CD4+/CD8+ double-positive T cells: more than just a developmental stage? *J. Leukoc. Biol.* **97**, 31–38 (2015).
220. Cheroutre, H. & Lambolez, F. Doubting the TCR Coreceptor Function of CD8αα. *Immunity* **28**, 149–159 (2008).
221. Adachi, K. *et al.* Fabry disease associated with multiple myeloma: a case report. *CEN Case Rep.* **11**, 146–153 (2021).
222. The Innate Immune System - 1st Edition. https://shop.elsevier.com/books/the-innate-immune-system/monie/978-0-12-804464-3.
223. Rozenfeld, P., Agriello, E., De Francesco, N., Martinez, P. & Fossati, C. Leukocyte perturbation associated with Fabry disease. *J. Inherit. Metab. Dis.* **32**, S67–S77 (2009).
224. Cheroutre, H. Starting at the Beginning: New Perspectives on the Biology of Mucosal T Cells. *Annu. Rev. Immunol.* **22**, 217–246 (2004).
225. Zhang, N. & Bevan, M. J. CD8+ T Cells: Foot Soldiers of the Immune System. *Immunity* **35**, 161–168 (2011).
226. Gui, Y. *et al.* Development and function of natural TCR+ CD8αα+ intraepithelial lymphocytes. *Front. Immunol.* **13**, 1059042 (2022).

Appendix I

Approval of this project by the Ethical Committee of CHUSJ

SÃO JOÃO

DELIBERAÇÃO DO CONSELHO DE ADMINISTRAÇÃO

Após apreciação e pareceres favoráveis da Comissão de Ética e do Centro de Epidemiologia Hospitalar, considerando que se encontram reunidos os requisitos e demais trâmites previstos no circuito para submissão de projetos de investigação no Centro Hospitalar Universitário de S. João e em conformidade com as disposições legais em vigor, o Conselho de Administração – ao abrigo das competências previstas no Artigo 71.º dos Estatutos dos hospitais, centros hospitalares, institutos portugueses de oncologia e unidades locais de saúde, aprovados pelo Decreto-Lei n.º 52/2022, de 4 de agosto – delibera:

1. Aprovar a realização do projeto de investigação:
   - "Caracterização do fenótipo e função das células Natural Killer T na deficiência em alfa-Galactosidase A".
   - Serviço(s) onde decorrerá o projeto de investigação: Genética Humana, Imunohemoterapia e Patologia Clínica.
   - Investigador(a) principal: Maria de Fátima Macedo
2. Remeta-se à Comissão de Ética para os procedimentos adequados e demais trâmites convenientes.

CONSELHO DE ADMINISTRAÇÃO DO CENTRO HOSPITALAR UNIVERSITÁRIO DE S. JOÃO, EPE • REUNIÃO DE 18 DE MAIO DE 2023

Presidente do Conselho de Administração

Prof.ª Doutora Maria João Baptista

Diretor Clínico	Enfermeiro Diretor	Vogal Executiva	Vogal Executiva
Prof.º Doutor Roberto Roncon	Enfermeiro Paulo Emílio Mota	Dra. Sofia Leal	Dra. Fernanda Oliveira

) Comissão de Ética
) Centro de Epidemiologia Hospitalar
) Direção Clínica

□ CE 126/2023

REC-IN011-1

Appendix II

Approval of this project by the Data Protection Officer from CHUSJ

SÃO JOÃO

ENCARREGADO DE PROTEÇÃO DE DADOS (EPD)
CENTRO HOSPITALAR UNIVERSITÁRIO DE S. JOÃO, EPE
Paulo Alexandre Mota da Silva
Encarregado de Proteção de Dados do CHUSJ
epd@chsj.min-saude.pt

Ref.ª CES CHUSJ: **126 / 2023**

Título do Projeto	Caracterização do fenótipo e função das células Natural Killer T na deficiência em alfa-Galactosidase A
Responsável pelo tratamento	Maria de Fátima Macedo
Instituição	Centro Hospitalar Universitário São João (CHUSJ)
	Instituto de Investigação e Inovação em Saúde (i3S)
	Instituto de Biologia Molecular e Celular (IBMC)
Investigador	Interno **Externo**
Contacto telefónico	220408800 **Endereço Electrónico** fmacedo@ibmc.up.pt
Profissional de Ligação	Cristina Neves (Assistente Hospitalar Graduada de Imunohemoterapia)
	João Paulo Oliveira (Diretor de Serviço de Genética Médica)
Amostra	200

Análise de Risco: Tolerável **Baixo** Elevado Muito Elevado

Parecer do EPD: **Data:** 05/05/2023

Finalidade: caracterizar o fenótipo e função das células Natural Killer T invariantes (iNKT) em pacientes com a doença de Fabry, com base no que se conhece da sua reatividade a glicoesfingolípidos. Deste modo pretende-se aferir o efeito dos glicoesfingolípidos presentes nesta patologia na diferenciação, ativação e polarização das células iNKT. Com este projeto pretende-se também investigar se o fenótipo e função das células iNKT podem ser usadas como biomarcadores para a doença de Fabry.

Licitude: fundamento previsto no artigo **6(1)(a)** e **9(2)(a)** do **RGPD.**

Categorias de dados pessoais: variáveis identificadas com detalhe na AIPD, datada de 31/03/2023, **ponto 13**, tendo presente o **princípio da minimização dos dados.**

Conservação: os dados serão alvo de **pseudonimização**, armazenados em **local seguro**, em área restrita com acesso limitado ao profissional de ligação e Investigador Principal, com acesso a ficheiros protegido por **palavra-passe**, efetuando-se a conservação até a conclusão da investigação, durante o prazo máximo de **quinze (15) anos**. Os dados recolhidos **serão destruídos** após a finalização do estudo.

Comunicação de Dados: **há partilha** de dados pessoais (pseudonimizados).

Face ao exposto, e observadas as recomendações, entende-se que a presente AIPD apresenta os elementos necessários para assegurar que o **tratamento é realizado em conformidade com o RGPD.**

Recomendações:

1. Sempre que o consentimento do titular for o fundamento de legitimidade adequado para o tratamento de dados, dever-se-á assegurar que o mesmo é válido nas condições legalmente exigíveis: *uma manifestação de vontade livre, específica, informada e inequívoca*. Neste contexto, o consentimento deverá ser objeto de reflexão por parte do participante fora do ambiente hospitalar, devendo para tal, existir a possibilidade de o mesmo remeter o consentimento por correio em envelope RSF.
2. Reforçar as medidas de segurança previstas para a conservação dos documentos em formato de papel que impeçam o acesso à informação a pessoas não autorizadas, bem como o seu manuseamento indevido;
3. Garantir medidas de segurança adicionais no transporte dos dados com recurso a dispositivos electrónicos de armazenamento (Laptop), nomeadamente através de medidas de cifragem e autenticação;
4. Garantir medidas de segurança adicionais para o envio da informação por correio eletrónico, nomeadamente através de medidas de encriptação / codificação dos dados a tratar;
5. Em caso de necessidade de extensão de prazo e/ou de qualquer alteração dos pressupostos atinentes ao presente parecer o Investigador Principal deverá solicitar a reapreciação do projeto de investigação junto do EPD.

1 de 2

Revisão AIPD:

☐ Data da próxima revisão: ___ /___ / _____

☒ Não carece de revisão.

Anexos:

1. Processo CES n.º 126/2023
2. Parecer CES (24/03/2023)
3. AIPD (31/03/2023)
4. Consentimento Informado e Informação ao Participante
5. Protocolo de Investigação

Encarregado de Proteção de Dados
Assinado por: **PAULO ALEXANDRE MOTA DA SILVA**
Data: 2023.05.05 17:18:08+01'00'
Localização: CHUSJ

CARTÃO DE CIDADÃO